

Alma Mater Studiorum – Università di Bologna

DOTTORATO DI RICERCA IN

Scienze Chimiche

Ciclo XXVI

Settore Concorsuale di afferenza: 03/A2

Settore Scientifico disciplinare: CHIM/02

***Non-Covalent Interaction: Revealed by
Rotational Spectroscopy***

Presentata da: Qian Gou

Coordinatore Dottorato

Aldo Roda

Relatore

Walther Caminati

Esame finale anno 2014

Preface

Rotational spectroscopy is uniquely beautiful amongst the spectroscopic techniques, and the amount of rich chemical information we can gather from a simple microwave spectrum is often incredible.

Although rotational spectroscopy is traditionally associated with the determinations of molecular structures, today's microwave spectroscopy is addressing a wide variety of basic and applied key problems in physical chemistry, molecular physics, and related fields. Questions on molecular structure, conformational and tautomeric conversion, chemical bonding, charge transfer, and internal dynamics are elucidated not only for isolated molecules but also for molecular clusters. Over the years, the scope of rotational spectroscopy has widened from fundamental intramolecular observations to the interrogation of intermolecular interactions.

In this dissertation, the fundamental theories, spectroscopic techniques and non-covalent interactions have been briefly reviewed firstly. The pulsed jet Fourier transform microwave spectroscopy have been applied to several 1:1 molecular complexes involving H₂O, freons, methane, carboxylic acids, and rare gas. The obtained results showcase the suitability of the technique for the study of intermolecular interactions.

The rotational spectra of three water adducts of halogenated organic molecules, namely chlorotrifluoroethylene, isoflurane and α,α,α -trifluoroanisole, have been investigated. It has been found that, the halogenation of the partner molecules definitely changes the way in which water will link to the partner molecule.

Quadrupole hyperfine structures and/or the tunneling splittings have been observed in the rotational spectra of difluoromethane ··dichloromethane, chlorotrifluorometane ··fluoromethane, difluoromethane ··formaldehyde and trifluoromethane ··benzene. These features have been useful to describe their intermolecular interactions (weak hydrogen bonds or halogen bonds), and to size the potential energy surfaces of their internal motions. Further details will be given ahead in the section dedicated to the descriptions of each molecular system.

The rotational spectrum of pyridine ··methane pointed out that methane prefers to locate

above the ring and link to pyridine through a C-H $\cdots\pi$ weak hydrogen bond, rather than the C-H $\cdots n$ interaction. This behavior, typical of complexes of pyridine with rare gases, suggests classifying CH₄, in relation to his ability to form molecular complexes with aromatic molecules, as a pseudo rare gas.

With Fourier transform microwave technique, the conformational equilibria of three bi-molecules of carboxylic acids, acrylic acid \cdots trifluoroacetic acid, difluoroacetic acid \cdots formic acid and acrylic acid \cdots fluoroacetic acid have been studied. The increase of the hydrogen bond length upon H \rightarrow D isotopic substitution (Ubbelohde effect, see in the next sections) has been deduced from the elongation of the carboxylic carbons C \cdots C distance.

The van der Waals complex tetrahydrofuran \cdots krypton, revealed by the rotational spectrum, shows that the systematic doubling of the rotational lines has been attributed to the residual pseudo-rotation of tetrahydrofuran in the complex, based on the values of the Coriolis coupling constants, and on the type (μ_b) of the interstate transitions.

All the results presented here have been published in the international scientific journals of general interests. The details are available in the published papers. All the measured transition frequencies and *ab initio* geometries of the observed conformers with partial r_0 adjustment and other information can be found in the electronic supporting materials of the corresponding papers.

Catalogs

Preface	I
Abbreviations.....	VI
Chapter 1 Fundamental Theory	1
1.1 Moments of inertia	1
1.2 Rotational energy levels	3
1.3 Rotational transitions.....	4
1.4 Centrifugal distortion	5
1.5 Quadrupole coupling effect	6
1.6 Large amplitude motions.....	7
1.7 Theoretical calculations.....	7
1.8 Evaluation of molecular structure.....	8
1.9 Dissociation energy	10
1.10 Isotopic effect.....	10
Chapter 2 Spectroscopic Techniques.....	12
2.1 Resonator cavity.....	14
2.2 Time domain technique.....	14
2.3 Pulsed supersonic-jet expansion.....	15
2.4 Experimental cycle.....	16
Chapter 3 Non-covalent Interactions.....	18
3.1 Van der Waals interaction	18
3.2 Hydrogen bond.....	19
3.3 Weak hydrogen bond.....	19
3.4 Halogen bond	20
3.5 The other interactions.....	21
Chapter 4 Water Adducts	22

4.1 Introduction	22
4.2 Experimental	23
4.3 Chlorotrifluoroethylene ·Water	23
4.4 Isoflurane ·Water	28
4.5 Trifluoroanisole ·Water	34
4.6 Conclusions	39
Chapter 5 Complexes of Freons	41
5.1 Introduction	41
5.2 Experimental	42
5.3 Difluoromethane ·Dichloromethane	42
5.4 Chlorotrifluoromethane ·Fluoromethane	50
5.5 Difluoromethane ·Formaldehyde	55
5.6 Trifluoromethane ·Benzene	62
5.7 Conclusions	67
Chapter 6 Pyridine-CF_nH_{n-4}	69
6.1 Introduction	69
6.2 Experimental	70
6.3 Theoretical Calculations	71
6.4 Rotational spectra	71
6.5 Molecular structure	73
6.6 Dissociation energy	74
6.7 Internal Dynamics	75
6.8 Conclusions	76
Chapter 7 Bi-molecules of Carboxylic Acids	78
7.1 Introduction	78
7.2 Experimental	79
7.3 Acrylic acid ·Trifluoroacetic acid	80
7.4 Difluoroacetic acid ·Formic acid	83
7.5 Acrylic acid ·Fluoroacetic acid	90
7.6 Relative population of the conformers in the jet	93
7.7 Conclusions	94
Chapter 8 Complex of Rare Gas	95
8.1 Introduction	95
8.2 Experimental	95

8.3 Theoretical Calculations.....	96
8.4 Rotational Spectra.....	97
8.5 Location of the Kr atom in the complex.....	99
8.6 vdW vibrations.....	100
8.7 Conclusions.....	103
References.....	104
Acknowledgement.....	111
Appendices.....	112
Publications.....	112
Academic Congresses.....	114
Award.....	114

Abbreviations

AA: acrylic acid;

BSSE: basis set superposition error;

Bz: benzene;

CFC: chlorofluorocarbon;

COBRA: coaxially oriented beam resonator arrangement;

DFA: difluoroacetic acid;

DPM: the distributed polarizability model;

FA: formic acid;

FAA: fluoroacetic acid;

FT: Fourier transform;

HaB: Halogen bond;

HB: Hydrogen bond;

IR: infrared;

ISO: isoflurane;

lp: lone pair;

MW: microwave;

PES: potential energy surface;

PJ: pulsed jet;

PYR: pyridine;

RG: rare gas;

S/N: signal-to-noise;

TFA: trifluoroacetic acid;

TFANI: α,α,α -trifluoroanisole;

THF: tetrahydrofuran;

UV: ultraviolet;

vdW: van der Waals;

VIS: visible;

WHB: weak hydrogen bond;

Chapter 1 Fundamental Theory

The general strategy for discussing molecular spectra and the information they contain is to find expressions for the energy levels of molecules, to calculate the transition frequencies by applying selection rules, and to predict the appearance of the spectrum by taking into account the transition moments and the populations of the states.

It is such a long story about the theories of the rotational spectroscopy that one can refer to several monographs on such a topic for more details.^[1-3] For the most recent and innovative applications on microwave (MW) spectroscopy, some book chapters^[4] and reviews^[5-7] are available. In this chapter, only the basic theories, which are used to interpret the MW spectra of the molecular complexes studied through this dissertation, will be briefly introduced.

1.1 Moments of inertia

To derive the molecular structures from the rotational spectra, it requires the knowledge of classical mechanics of rotating bodies.

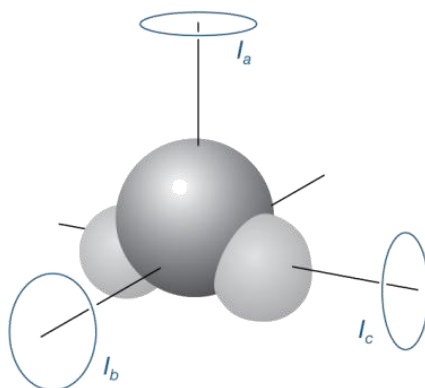


Figure 1.1 Asymmetry molecule with three moments of inertia

Depending on the symmetry of the molecule, one or more moments of inertia need to be specified to describe its rotational properties. For molecules with low symmetry, three moments of inertia relative to three perpendicular axes in the molecule have to be defined (see Figure 1.1). The three perpendicular axes are the principal axes when the origin of the coordinate system is chosen at the center of mass of the molecular system: this choice allows the total kinetic energy to be written as the sum of the kinetic energy of translational motion of the center of mass plus the kinetic energy of the motion relative to the center of mass. The translational and rotational motions can hence be treated separately.

As shown in Figure 1.2, the moment of inertia I of a system of particle (a molecule) is defined as:

$$I = \sum_i m_i r_i^2 \quad (1.1)$$

It depends on the mass distribution of the molecular system. The three principal axes of a particular molecule have been labeled by convention as a , b , c in such way that $I_a \leq I_b \leq I_c$, depending on its symmetry. For a symmetric top rotor, one of the principal axes of inertia must lie along the molecular symmetry axis. The principal moments of inertia which have their axes perpendicular to this axis are equal. If a -axis lies along the symmetry axis ($I_a < I_b = I_c$), the molecule is a prolate symmetric top. If c lies along the symmetric axis ($I_a = I_b < I_c$), the molecule is an oblate top.

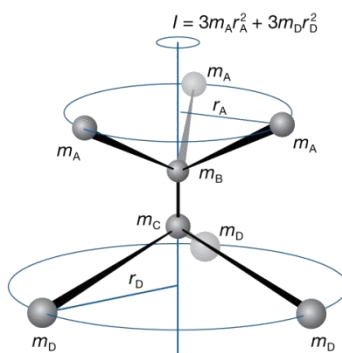


Fig.1.2 The moment of inertia of a rotor

We can identify the z axis with any of the three principal axes and depending on whether it is identified with a , b or c as I, II, III. We add a superscript r or l depending on whether a right or left (x, y, z) axis system is used.^[8]

In the principal axes system, the rotational constants can be written as:

$$A = \frac{h}{8\pi^2 c I_a}, \quad B = \frac{h}{8\pi^2 c I_b} \quad \text{and} \quad C = \frac{h}{8\pi^2 c I_c} \quad (1.2)$$

Therefore the rotational motion of a molecule can be accurately described when its moments of inertia are known.

From the rotational constants it is easy to calculate, for each species, the values of the planar moments of inertia, defined as (for example)

$$P_{aa} = \sum_i m_i a_i^2 \quad (1.3)$$

through the relation

$$P_{aa} = \frac{1}{2}(-I_a + I_b + I_c) = \frac{h}{16\pi^2} \left(-\frac{1}{A} + \frac{1}{B} + \frac{1}{C}\right) \quad (1.4)$$

The quantity gives a measure of the mass extension along the a -axis. The same, as well, applies to P_{bb} and P_{cc} .

An indication of accuracy in the calculated structure is the defect of inertia

$$\Delta_c = I_c - I_a - I_b = -2P_{cc} \quad (1.5)$$

which should be zero for an absolute planar molecule.

1.2 Rotational energy levels

In many cases, the rotational spectra of molecular systems can be described successfully with the assumption that they rotate as rigid rotors. In such ways the energies can be modeled in a manner parallel to the classical description of the rotational kinetic energy of rigid objects.

Energy calculations in quantum mechanics involve the solution of the Schrödinger equation with a properly formulated Hamiltonian to represent the energy operator. The form of the Hamiltonian can often be implied from the nature of the classical energy of such a physical system as:

$$E\Psi = \hat{H}\Psi \quad (1.6)$$

Supposing that molecules are rigid rotors (do not distort under the stress of rotation), the

potential energy may be set to zero since there is no change in bond length during the rotation. Taking the simplest molecules, spherical or linear top, the energy levels obtained from solving Schrödinger equation in terms of the rotational quantum number J are:

$$E_J = \frac{\hbar^2}{2I} J(J+1) \quad (1.7)$$

where $J = 0, 1, 2, \dots$

So that, according to Eq. (1.2), the solutions for the energy states of a rigid rotator can be expressed as

$$E_J = BhcJ(J+1) \quad (1.8)$$

1.3 Rotational transitions

MW radiation can induce the rotational transitions only in molecules or molecular systems with permanent dipole moments. Therefore, generally only the polar molecular system can give a pure rotational spectrum. As a consequence, *homo*-nuclear diatomic molecules and molecules with spherical symmetry are not directly observable with rotational spectroscopy.

In a practically symmetric top, any permanent dipole moment must lie along the symmetric axis. All matrix elements of this dipole moment resolved along a space-fixed axis vanish except those between states corresponding to $J \rightarrow J$ or $J \pm 1$, $K \rightarrow K$. The selection rules for the field free rotor are $\Delta J = 0, \pm 1$; $\Delta K = 0$. For absorption transition, the selection rule is $J \rightarrow J + 1$, $K \rightarrow K$. Applying these rules to Eq. (1.8) gives the relation of the absorption frequencies for a rigid symmetric top

$$\nu = 2B(J+1) \quad (1.9)$$

For a symmetric top, either a prolate or an oblate, the quantum number K determines the vector component of the angular momentum about the molecular symmetry axis, which is a -axis for a prolate top or c -axis for an oblate top. Its energies depend on K because the rotation about the symmetry axis and tumbling end over end are very different motions, so the relative amounts of the angular momentum about the different axes strongly affect the energy. The sign of K signifies the direction of the rotation about the z -axis. Energies are degenerated for $+K$ and $-K$, since a simple change of direction does not change the total energy.

When the molecular system is asymmetric, considerable complexity is encountered in its

pure rotational spectrum. The rotational transitions can no longer be expressed in convenient equations, as can be done for linear or symmetric top molecules. Only for certain low J values can the energy levels of the asymmetric rotor be expressed in closed form, even if centrifugal distortion effects are neglected.

1.4 Centrifugal distortion

It's very useful to take molecules as rigid rotors when interpreting the rotational spectra. However, the atomic structure cannot be absolutely rigid. Due to the centrifugal distortion, the molecular bond lengths and covalent angles will change along their rotation as a function of the states, which leads to changes in their rotational spectrum. Molecules of the smaller weight normally are obvious that the spectra usually include a set of constant rotation and a number of centrifugal distortion constants.

Taking account of this distortion, the moments of inertia cannot be considered as constant any longer, the values of which are dependent on the rotational states. Consequently, the rotational spectrum cannot be just treated as that of a rigid rotor characterized by a sequence of equilibrium moments of inertia. However the precision of MW measurements allows determining the centrifugal distortion constants even from the low-lying levels with relatively small rotational energies.

Centrifugal distortion effects only represent a small part of the rotational energies which are accounted for mainly by the rigid rotor term. Therefore in many cases this effect can be treated as a perturbation to the rigid rotor Hamiltonian (H_R). The total Hamiltonian can be written then as

$$H = H_R + H_D \quad (1.10)$$

where H_D is the contribution of the centrifugal distortion part. The first order perturbation treatment involves averaging the perturbing operator H_D over the asymmetric rigid rotor wave functions.

In the second order perturbation treatment of the term H_D , it's possible to transform the Hamiltonian H_R to an effective form H_{eff} which is diagonal in the vibrational quantum numbers transforming the Hamiltonian terms into the fourth degree in angular momentum P (quartic centrifugal distortion terms). By a second order treatment to an asymmetric top, the quartic centrifugal distortion coefficients $\tau_{\alpha\beta\gamma\delta}$ can be reduced to five independent constants as discussed in details in Watson's review.^[6] For the A - and S -reduction, the reduced quartic centrifugal distortion

Hamiltonian have the following forms:

$$H_4 = -\Delta_J J^4 - \Delta_{JK} J_z^2 J^2 - \Delta_K J_z^4 - 2\delta_J J_{xy}^2 J^2 - \delta K (J_z^2 J_{xy}^2 + J_{xy}^2 J_z^2) \quad (1.11)$$

where $J^2 = J \cdot J$, $J_{xy}^2 = J_x^2 - J_y^2$.

A least square fitting of the observed frequencies is carried out to obtain the rotational and centrifugal distortion constants. Particularly, the differences between the observed frequencies and the calculated rigid rotor frequencies are taken as the distortion effect.

1.5 Quadrupole coupling effect

When a nucleus has a spin quantum number, I , greater than $1/2$, it has a quadrupole moment. In that case, the coupling of the nuclear spin angular momentum with rotational angular momentum causes splittings of the rotational energy levels. If the quantum number J of a rotational level is greater than I , $2I+1$ levels are produced; but if J is less than I , $2J+1$ levels result. The effect is known as hyperfine splitting. For example, the rotational spectrum of the molecule with ^{14}N ($I = 1$), all levels with $J > 0$ are split into 3. The energies of the sub-levels are proportional to the nuclear quadrupole moment and as a function of F and J , where $F = J + I, J + I - 1, \dots, 0, \dots, |J - I|$. Thus, the observation of nuclear quadrupole splittings permits the magnitude of the nuclear quadrupole moment to be determined.^[9] This is an alternative method to use the nuclear quadrupole resonance spectroscopy. The selection rule for rotational transitions becomes $\Delta J = \pm 1$, $\Delta F = 0, \pm 1$.^[10]

There are only two independent coupling constants in the most general cases. These are usually expressed in terms of the coupling constants with the reference axis is chosen as the c axis, the two coupling constants would be χ_{cc} and

$$\eta = (\chi_{aa} - \chi_{bb}) / \chi_{cc}. \quad (1.12)$$

The reference axis is usually chosen as the one for which the coupling is most nearly symmetric, that is, for which η is the smallest. And according to the Laplace's equation, there's the relation

$$\chi_{aa} + \chi_{bb} + \chi_{cc} = 0. \quad (1.13)$$

It is evident that wherever the rotational transitions have resolved the hyperfine structure, one must measure the coupling constants in order to obtain the unperturbed frequency ν_0 and hence the rotational constants B_0 .

Generally speaking, with increasing J , the $F \rightarrow F - 1$ components become weaker and eventually undetectable; while the $F \rightarrow F + 1$ ones remain strong but converge in frequency and eventually become unresolvable as J continues to increase.

1.6 Large amplitude motions

The earliest MW studies of the rotational spectrum of ammonia concerned its inversion motion tunneling. Since then, the large amplitude internal motions of many molecular systems were characterized from the tunneling splittings observed in their rotational spectra. Typical motions are (i) internal rotation of symmetric (generally methyl) groups; (ii) inversion of amino or imino hydrogens; (iii) internal rotation of light asymmetric groups (OH, SH, NH₂); (iv) ring puckering of (saturated) four- or (near saturated) five membered rings; (v) pseudorotation. Even heavy atoms (or structural groups) can produce large splitting if their motions are characterized by low-barrier potential energy surfaces (PESs) as in many molecular complexes.

Potential barriers are presumably caused by the interactions of two groups of electrons and nuclei. In principle, it should be possible to determine the barrier heights from straightforward quantum-mechanical calculations. The mathematical complexity of such a treatment, however, is so great that a rigorous computation seems highly impractical at present. An alternative approach, which is perhaps somewhat empirical, is to try to describe the origin of the barriers in terms of the forces which appear in the study of intermolecular interactions, such as Van der Waals forces and resonance forces.

For most of the molecular complexes with the large amplitude motions in this dissertation, the PESs have been dealt with Meyer's flexible model, which provides energies and wave-functions for $J = 0, 1, 2$ in the ground and vibrational excited states.^[11] More details are given in the following sections for the particular molecular complexes studied.

1.7 Theoretical calculations

Modern theoretical *ab initio* quantum chemistry methods have been extremely successful in describing the electronic structure of isolated molecules to a degree of precision that in some cases comes very close to high-resolution spectroscopic results. The motivation for the application of theoretical *ab initio* methods to molecular clusters comes from the need to determine the structure of the cluster, its stabilization energy, its (intermolecular) vibrational frequencies and the potential energy and free energy surfaces.

The primary property of an isolated (rigid) system is its structure, and a main goal is to determine the equilibrium structure of such a system. The majorities of molecular clusters are non-rigid systems, and are dominated by large amplitude motions that make the concept of equilibrium structure meaningless. Structures of global and local minima of the surface are found by optimizing the stabilization energy and not the total energy. Stabilization energy thus plays a central role in non-covalent interactions. The geometry of a cluster is observable only by resolving rotational structure, which is not always possible. The key role in the world of non-covalent interactions is played by vibrational frequencies, which are more easily observable, and their detection is straightforward even for large clusters. Moreover, vibrational frequencies are very sensitive to the quality of the PES and can serve as a test of quality of the respective calculation procedure.

Ab initio and density functional theory (DFT) are used to assist the assignment of the rotational spectra. Geometry optimizations are used to predict the molecular equilibrium structure and conformational preferences from PES. The resulting information on rotational constants, dipole moment components, relative stabilized energies and quadrupole coupling constants are helpful indications for searching for rotational spectra and conformational assignment.

Since the studied molecular system is not large, high level calculations like MP2/6-311++G(d,p) level theory can be chosen. Frequency calculations are used to calculate the zero point energy and force constants. For molecular complexes, a counterpoise correction^[12] is used to remove the well-known basis set superposition error (BSSE). All theoretical calculations in this dissertation are performed with Gaussian 03^[13] or Gaussian 09^[14] program package.

Some molecular systems exist as a mixture of several conformers. With the computer program Maestro, it is also very useful to do the conformational search at the first step.^[15]

1.8 Evaluation of molecular structure

MW spectroscopy is very much at the heart of molecular physics. It is a method of very high resolution optical spectroscopy and has a sound foundation in molecular quantum mechanics. Once a rotational spectrum is obtained and assigned, it yields the three rotational constants A , B and C (assuming we are dealing with an asymmetric top), and from these rotational constants, the moments of inertia and hence the most probable structure can be obtained.

Different procedures have been introduced which correct various degrees for vibrational effects and which have led to different conceptions of interatomic distance. In particular, three

types of structures are frequently used in rotational studies.

r_e , the equilibrium structure for the hypothetical vibrationless state, evaluated by correction for the effects of vibration including zero-point vibrations. Particularly, in many cases, the geometries from *ab initio* can be treated as the equilibrium structure.

r_0 , the effective structure for the ground vibrational state could be calculated from the experimental rotational constants. A least squares fitting procedure has been used to evaluate the r_0 of the studied molecular systems. Several structural parameters could be chosen to fit the differences between experimental and theoretical values of rotational constants. The procedure of the fitting is based on the linearization of the following equation

$$B_i = B_i^0 + \sum_j (dB_i/dp_j) \Delta p_j \quad (1.14)$$

where B_i is the i th experimental rotational constant, B_i^0 is the i th rotational constant calculated from the initial assumed structure and p_i is the structural parameter chose for fitting, (dB_i/dp_i) is the changing of B_i^0 with respect to a small changing of p_i while all other structural parameters were kept constant. This procedure is repeated until the convergence has been achieved. However, normally the set of experimental data are not enough to determine the molecular structure completely. Only several bond lengths, valence angles, or valence dihedral angles can be evaluated from the structure fitting and thus only partial r_0 structure can be obtained. For non-covalent interaction bonded molecular complexes, this procedure is adoptable to determine the intermolecular bond length and angles while keeping the geometry of molecular moieties constants.

r_s , the substitution structure, is derived from the isotopic substitutions. Kraitchman^[16] method is applied to calculate the position of an atom in a molecule utilizing the changes of moments of inertia resulting from a single isotopic substitution of the atom. The molecule is assumed rigid so that the bond distances and angles are unchanged due to isotopic substitution. The I_x, I_y, I_z and I'_x, I'_y, I'_z are the moments of inertia along the principal axes for the parent and isotopically substituted molecule. The coordinates are measured from the center of mass principal axis system of the parent molecule. The mass of the isotopic atom can be denoted by $m+\Delta m$, with m the original mass of the atom. The moment of inertia in the parent center of mass principal axis system can be expressed as:

$$\begin{aligned} I'_{xx} &= I_x + \Delta m (y^2 + z^2) - (\Delta m y)^2 / (M + \Delta m) - (\Delta m z)^2 / (M + \Delta m) \\ &= I_x + \mu (y^2 + z^2) \end{aligned} \quad (1.15)$$

Similarly, that

$$I_{yy} = I_y + \mu (z^2 + x^2) \quad (1.16)$$

$$I_{zz} = I_z + \mu (x^2 + y^2) \quad (1.17)$$

where the μ is the reduced mass for the isotopic substitution, $\mu = M \Delta m / (M + \Delta m)$ with M is the total mass of the parent molecule. The I_x, I_y, I_z and I_x', I_y', I_z' can be determined experimentally, thus the coordinates $x, y,$ and z of the isotopic substituted atom can be obtained.

1.9 Dissociation energy

When the intermolecular stretching motion appears to be almost parallel to the a -axis of a complex, it is plausible to estimate its force constant (k_s) within the pseudo diatomic approximation to estimate by assuming such a motion to be separated from the other molecular vibrations. For an asymmetric complex, according to:^[17]

$$k_s = 16 \pi^4 (\mu_D R_{CM})^2 [4B^4 + 4C^4 - (B-C)^2(B+C)^2] / (hD_J), \quad (1.18)$$

while for a symmetric complex, according to:

$$k_s = 128 \pi^4 (\mu_D R_{CM})^2 B^4 / hD_J \quad (1.19)$$

B and C are the experimental rotational constants. μ_D is the pseudo diatomic reduced mass, for the two subunits 1 and 2,

$$\mu_D = m_1 m_2 / (m_1 + m_2) \quad (1.20)$$

and R_{CM} is the distance between the centers of the mass of the two subunits; D_J is the centrifugal distortion constant.

The dissociation energy (E_D) can be then evaluated by assuming a Lennard-Jones type potential function and applying the approximate expression:^[18]

$$E_D = 1/72 k_s R_{CM}^2 \quad (1.21)$$

1.10 Isotopic effect

Isotopic substitution is generally considered not to perturb the structure of a molecular system. It

affects, however, the molecular spectroscopy of the system, especially the frequencies of rotational transitions, which depend on moments of inertia. Differences in moments of inertia among isotopomers represent, in turn, the best tool for the determination of molecular structure.^[1] Furthermore, changes in chemical properties, such as kinetics^[19] and equilibrium constants,^[20] are well known, and it has been observed that the temperature of spontaneous phase transitions can vary,^[21] sometimes by as much as 25 K.^[22] A smaller modification (relative to that described herein) of the structure of a system through the so-called geometric isotope effect was outlined by Ichikawa.^[23] However, when isotopically labeled substances are used, the usually justified assumption is made that they do not alter the fundamental nature of the material under study.

Reasonable information on the geometric changes of molecular complexes, for example, complexes of water with ethers, has been obtained upon deuteration of the water moiety. It is well known that the H→D isotopic substitution of hydrogen atoms involved in relatively strong hydrogen bonds (e.g. O-H ···O) produces an increase (Ubbelohde effect^[24]) or a decrease (inverse Ubbelohde effect^[25]) of the distance between the heavy atoms participating in the hydrogen bonds. However, generally both effects are called “Ubbelohde effect”. The effect is related to the fact that the ν_0 fundamental frequency of a R-H stretching (R is a generic heavy group attached to a hydrogen atom) is reduced by a factor $\approx 1.4 \approx (m_{\text{H}}/m_{\text{D}})^{1/2}$ in the R-D deuterated form. When the proton transfer connects two equivalent forms (such as in malonaldehyde or in the dimers of carboxylic acids) we have the Ubbelohde effect; when the proton transfer leads to the dissociation (like in dimers of alcohols), we have the reverse effect. The Ubbelohde effect is mentioned also in recent paper on the quantum nature of the hydrogen bond,^[26] but no distinction is given between the two cases mentioned above.

In the 1:1 complex anisole-water, a novel isotopic effect has been described: water moiety acts mainly as proton donor forming a strong bifurcated HB, but the deuteration of water produces a conformational change. Two qualitative hypotheses are plausible: 1) a small change, upon deuteration, in the potential-energy surface; 2) a substantial change, upon deuteration, in some of the frequencies of the six low-frequency normal vibrational modes of water with respect to anisole, and therefore in the relative r_0 energies of the two $\text{O}_{\text{water}} \cdots \text{H}_{\text{Me}}$ and $\text{O}_{\text{water}} \cdots \text{H}_{\text{Ph}}$ conformations, even in the case of two nearly equivalent wells in PES.^[27]

Chapter 2 Spectroscopic Techniques

For decades until now, MW spectroscopy is progressing impressively: this is partially by the virtue of the experimental developments that combine jet-expansion sources with specific means of sample preparation for new chemical systems.



Figure 2.1 Pulsed jet Fourier transform microwave spectrometer built in University of Bologna

All the rotational spectra in this dissertation were measured using the pulsed-jet Fourier transform microwave spectrometer with a coaxially oriented beam resonator arrangement (COBRA) built in University of Bologna, which covers the frequency range 6.5-18 GHz.^[28] The photo of the spectrometer is shown in Figure 2.1, while the block diagram of this entire instrument is shown in Figure 2.2. The design of the spectrometer follows the guidelines given by Stahl and Grabow^[29-30] and most of the details are taken from the Valladolid spectrometer.^[31]

Basically, there are two parts, the mechanic system and the electrician part. In this chapter, the spectroscopic techniques will be briefly introduced.

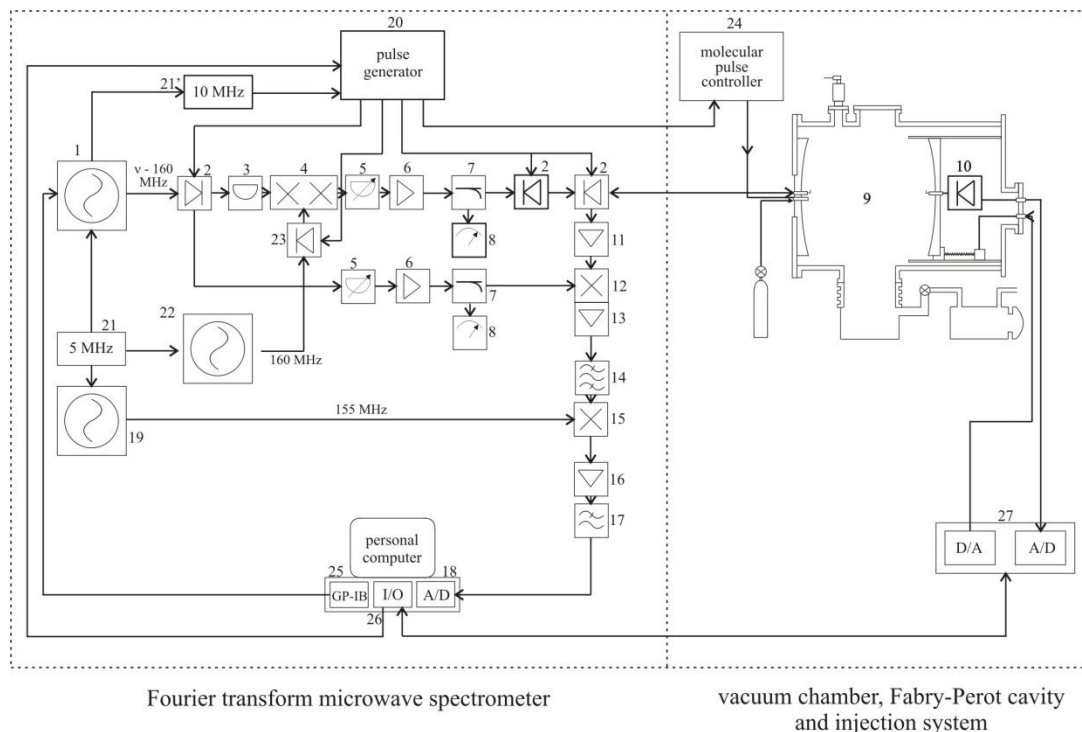


Figure 2.2 Block diagram of the MB-FTMW spectrometer

MW = Micro Wave; RF = Radio Frequency; P = output power, IF = intermediate frequency, IL = insertion losses, G = gain, NF = noise figure, IS = isolation, IR = image rejection: **1.** MW synthesizer, HP 8672 A. **2.** MW switch SPDT, SMT SFD0526-001S. **3.** Fixed attenuator MCL BW-S3W2. **4.** Single side band modulator, MITEQ MN0226LC1C. **5.** Variable attenuator, NARDA 4798. **6.** MW amplifier ALC Microwave ALS0618-30-20. **7.** Directional coupler NARDA 4203-16. **8.** Power meter, HP 435 B + Power sensor 8485A. **9.** Fabry-Perot resonator, see text. **10.** MW crystal detector HP8470B. **11.** MW low noise amplifier, MITEQ JSD4-0600-1800-16-8P. **12.** Image rejection mixer, MITEQ IR0226LC1C. **13.** 160 MHz RF amplifier, MITEQ AU-1466-140. **14.** BAndpass filter, TTE KC6-160M-20M. **17.** RF mixer, HP 10514A. **16.** RF amplifier, MCL MAN 1LN. **17.** Lowpass Filter, TTE LC5-25M-50-7135. **18.** Transient recorder, SPECTRUM PAD 82A, modified following the design of the Kiel University. **19.** RF synthesizer, PTS 160-M7020. **20.** Pulse Sequencer TTL, made at the University of Valladolid, based on a PCB card from the University of Kiel. **21.** Reference signal, Rb oscillator 5 MHz, Ball-Efraton FRK-LLN. **22.** RF synthesizer, MARCONI 2019A. **23.** RF switch MCL 7MSW-1111. **24.** Pulse controller General Valve IOTA ONE. **25.** IEEE 488 interface, NI GP-IB-488 PCII. **26.** I/O card, NI PC-DIO-96. **27.** A/D and D/A converter for Stepper motor control made in Valladolid.

2.1 Resonator cavity

The schematic diagram of the mechanic part is shown in Figure 2.3. The resonator, of the Balle-Flygare type, is made by two aluminum mirrors with a curvature radius of 60 cm and with a diameter of 35 cm and placed in a stainless steel high vacuum chamber of cylindrical shape (built by HVP, Parma, Italy). The diameter of the chamber is 40 cm while the length is 85 cm. The chamber is evacuated with an 8000 s^{-1} diffusion pump driven by a block of two Leybold mechanical pumps (D65B and Ruvac WAU 251, rotary and booster pumps, respectively).

The mirrors are situated in a near-confocal arrangement with one of them fixed in one flange of the vacuum chamber and the other one mounted on a motorized slide rack. A computer program which can control the stepping motor, allows tuning the resonator to the right polarization frequency.

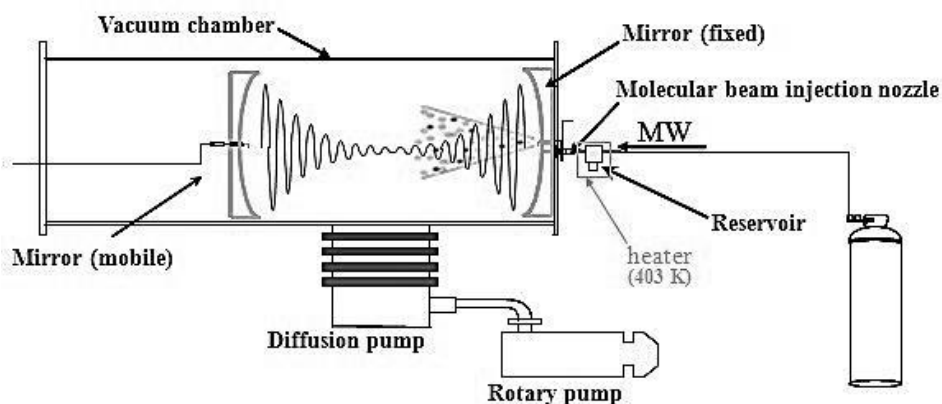


Figure 2.3 Schematic diagram of the mechanic part.

2.2 Time domain technique

Instead of continuously passing monochromatic radiation through cell and detecting the transmitted signal as a function of frequency, contemporary MW spectrometers apply the radiation for a short period of time. In the presence of a sample, a radiative response is induced. To obtain the spectrum, the response signal is recorded as a function of time and subjected to Fourier transformation (FT).

The time-dependent behavior of absorption and emission of two-level quantum mechanical systems makes it possible to measure rotational transitions in the time domain, analogous to the pioneering development of pulsed nuclear magnetic resonance experiments.

The interaction of the MW radiation and the molecular beam results in rotational coherence. The molecular signal power is relative to the fraction of the total energy stored by the field within the resonator volume. Due to the coaxially of the jet expansion and the MW radiation, the amplitude of the molecular signal is approximated by

$$S_{ab}(t) \propto s' \exp(i(\omega_{ab}-k v_{\infty})t+\theta_{ab}') + s'' \exp(i(\omega_{ab}+k v_{\infty})t+\theta_{ab}'') \quad (2.1)$$

where ω_{ab} is the angular resonance frequency and $k = \omega/c$ is the wavenumber of the radiation. The Doppler doublet consisting of frequency components at $v_{ab} (1-v_{\infty}/c)$ and $v_{ab} (1+v_{\infty}/c)$ is observed in the frequency domain. The molecular resonance frequency is then recovered as the arithmetic mean of the components separated by $\Delta v_{ab} = 2v_{ab}v_{\infty}/c$. The line width of the individual components is on the order of 1.5 kHz; at an appreciable S/N ratio, a frequency accuracy of 150 Hz, is achieved for unblended lines. The sensitivity allows for the routine observation of mono-deuterated asymmetric-top molecules in natural abundance.

2.3 Pulsed supersonic-jet expansion

Progress of the supersonic jet systems has enabled experiments of molecular clusters much easier. In order to explain the jet-cooled abundances we considered how equilibrium populations evolve kinetically in the expansion. Conformational populations may be particularly affected by collisional relaxations transferring population to lower energy species so the supersonic expansion will preserve the preexisting equilibrium conformational distribution only in the cases of large inter-conversion barriers.

It is well known that the supersonic expansion of molecular systems seeded in rare gas is rich in molecules of low rotational temperature. It's stated that normally rotational temperature about 1 K can be reached. Thus supersonic expansion provides significantly sensitivity advantage for transitions originating from low energy rotational levels in the vibrational states. This expansion can be generated by using an electromagnetic valve and provide a sample of high number density. The COBRA can significantly increase the resolution and sensitivity than the orientation that molecular beam is perpendicular to MW pulsed excitation.

To ensure optimal expansion conditions also at higher stagnation pressure, *i.e.* maintain the low background pressure for a given pump capacity, the nozzle diameters can become impractically small. Therefore, in many cases, a pulsed jet (PJ) expansion is favorable for the observation of molecular complexes.^[32]

In our FTMW spectrometer, the solenoid valve (General Valve, Series 9) is used to generate the supersonic expansion (nozzle diameter 0.5 mm), which is located above the antenna in the fixed mirror in a coaxial arrangement with the MW radiation.

Typically, ~1% sample seeded in rare gas at a total pressure in range of 0.1~0.6 MPa is expanded into the high evacuated resonator chamber. The process is a rapid adiabatic expansion rather than effusive, which cools the molecular systems to very low vibrational temperature and generates molecules traveling along radial path without collision. Thus the transition lines are very narrow and the broadening of transitions is only due to that natural line width, which corresponds to a very high resolution.

2.4 Experimental cycle

An experimental cycle (as shown in Figure 2.4) starts with a pulse of a rare gas carrying the sample molecules (the stagnation pressures 0.1~0.6 MPa). Later on, after a certain delay, a MW pulse is applied to produce a macroscopic polarization of the species in the jet. Once the excitation stops with a very short delay, molecular relaxation gives rise to a transient emission signal. Finally, the molecular signal in the time domain (coherent emission) is processed by a fast FT giving the frequency domain spectrum. A new experimental cycle can start once the vacuum cavity has been evacuated. A repetition rate of 2 Hz is normally employed. For very weak signals thousands of cycles must be added coherently to obtain a better signal-to-noise (S/N) ratio.

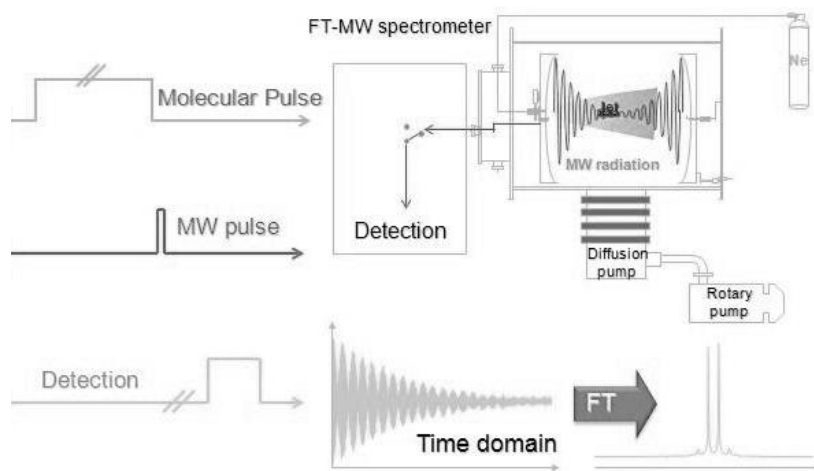


Figure 2.4 Pulse sequence for a single experimental cycle.

The duration of the pulse, computer controlled, can be optimized depending on the

particular molecular systems of interest. The delay between the molecular and MW pulses is critical and must be optimized by taking account the character of the gas expansion such that the main body of the gas mixture is present in the cavity during the MW pulse. The delay between the MW pulse and the recording of the molecular decay is necessary to allow polarizing radiation to dissipate.

The frequencies were determined after FT of the 8k data points time domain signal, recorded with 100 ns sample interval. The pulsed nozzle valve is mounted near the center of one of the mirrors in such a way that the supersonic beam propagates parallel to the resonator axis. In this set-up, all lines appear as enhanced by Doppler effect. The line position is the arithmetic mean of both Doppler component lines. The estimated accuracy of the frequency measurements is better than 3 kHz, resolution is better than 7 kHz.

Chapter 3 Non-covalent Interactions

Atoms and molecules can interact together leading to the formation of either a new molecule (reactive channel) or a molecular cluster (non-reactive channel). The former is clearly a covalent interaction; the latter one in which a covalent bond is neither formed nor broken is termed a non-covalent interaction.

Non-covalent interactions are known to act at distances of several angstroms or even tens of angstroms and overlap is thus unnecessary (in fact overlap between occupied orbitals leads only to repulsion). The reason for the attraction between interacting subsystems must be sought elsewhere and it can lie only in the electrical properties of the subsystems. Non-covalent interactions originate from interaction between permanent multipoles, between a permanent multipole and an induced multipole, and finally, between an instantaneous time variable multipole and an induced multipole.

Various types of molecular complexes, stabilized by non-covalent interactions, have been studied by gas phase high resolution spectroscopy, which provides a wealth of data on their shapes, structures, intermolecular interactions and internal dynamics.

In this chapter, the molecular non-covalent interactions have been classified. Their properties, mainly for rotational spectroscopy, have been briefly reviewed.

3.1 Van der Waals interaction

In the last decades, high resolution rotational spectroscopic technique has revealed itself to be particularly efficient in studying the nature of van der Waals (vdW) interactions which dominates the formation of the molecular complexes of rare gas (RG) atoms with organic molecules. Rotational spectra can give precise information on the large-amplitude motions typical of this kind of adducts,^[4] especially in conjunction with the observation of even small vibrational splitting.

Generally, complexes with aromatic molecules have the RG atom firmly linked to one side of the ring and the vdW motions do not generate observable inversion splittings. This is the case, for example, of the complexes of pyridine with all RG atoms, that is RG = He,^[33] Ne,^[34-35] Ar,^[36-38] Kr,^[36] Xe.^[39] Vice versa, when a RG atom is linked to an open chain molecule, such as, for example, dimethylether, all the rotational spectra of its complexes, with RG = Ne,^[40] Ar,^[41-44] Kr,^[45] and Xe,^[28, 46] display rotational transitions characterized by inversion splittings. From centrifugal distortion effects it has been possible to estimate the dissociation energies of the complexes, which are higher for the aromatic molecules complexes, and which increase with the atomic number of RG. The tunneling splittings have been useful to determine the barrier to inversion along the tunneling motion.

3.2 Hydrogen bond

Hydrogen bond (HB), which involves many research areas, is the most important and attractive non-covalent interaction, and is often invoked to explain the energetic and structural features of inorganic, organic and biological chemical systems.

Complexes with HBs are stabilized by electrostatic, induction (charge transfer), and dispersion energy terms. The electrostatic term, with its mainly dipole-charge and dipole-dipole contributions, is the most important and gives HBs their typical (and very important) directionality. In a HB X-H \cdots Y-Z, an electropositive H atom intercedes between two electronegative species X and Y and brings them closer together. The HB is strong and orientational enough to hold two molecules together at normal temperature but weak enough to resemble the hydrophobic interaction.

The physical forces involved in the HB must include electrostatic and inductive forces in addition to London dispersion forces. Forming a HB, the lengths of X-H bonds and, to a lesser extent, of the Y-Z bonds deviate from their equilibrium values. Generally, the stronger the HB, the more nearly linear is the H \cdots Y-Z arrangement and the shorter the H \cdots Y distance. The interaction energy per one HB is greater than at least a few times kT , where T is the temperature of the observation, in order to ensure its stability.

3.3 Weak hydrogen bond

Weak hydrogen bonds (WHB) such as C-H \cdots O, C-H \cdots F, CH \cdots S, C-H \cdots π represent often the linkages which hold together small molecules constituting a molecular complex. WHB's

interaction energies are quite low, a few $\text{kJ}\cdot\text{mol}^{-1}$, and similar in value to those of vdW forces. Although a book is available, reviewing this kind of interaction, there are still some controversies on the justification to classify it as a hydrogen bond. A recent IUPAC meeting promotes a redefinition of “hydrogen bonding”, and it has even been suggested to consider these interactions only as contacts, in view of the fact that hydrogen atoms are generally in the external part of a molecular system.^[47]

A vast literature based on X-rays investigations has shown that it has the same directional properties of “classical” HB.^[48] Another technique which supplied plenty of information on WHBs is IR spectroscopy in rare gas solutions of molecular adducts,^[49] which leads also to a probably not so appropriate nomenclatures, such as “anti-hydrogen bond”^[50] or “improper blue shifted hydrogen bond”.^[51] We believe, however, that the investigations of the MW spectra of several molecular adducts generated in supersonic jets have provided the most precise information on the energies, structures and dynamics of such kind of interactions, obtaining in an environment free from the intermolecular interaction which takes place in the condensed phases.^[4]

3.4 Halogen bond

Several of the investigated complexes were stabilized by a halogen bond (HaB), and these studies result in qualitative and quantitative details of non-covalent interactions. It has been found that in some cases the HaB is competitive or preferred to the HB. According to IUPAC, “a HaB occurs when there is evidence of a net attractive interaction between an electrophilic region associated with a halogen atom in a molecular entity and a nucleophilic region in another, or the same, molecular entity”.^[52]

The importance of the HaB in supramolecular chemistry and in crystal engineering has been outlined in several papers.^[53] Reviews on the HaB are available,^[54] as well as its parallels with the HB.^[55] Most of the investigations dedicated to the HaB are based on solid-state X-ray diffraction.^[56] However, more precise information on the HaB, neat of solvent effects or solid state linkages, comes from studies of an isolated complex of two subunits created by this interaction. Such studies have been performed by vibrational spectroscopy on HaB bonded complexes in cryo solutions by van der Veken and collaborators.^[57]

Accurate details of the nature of the HaB in the gas phase can be obtained by rotational spectroscopy of molecular complexes, as shown in an overview by Legon.^[58] There, FTMW spectroscopy studies of a series of $\text{B}\cdots\text{XY}$ complexes, where B is the electron donor and XY is

the dihalogen molecule, are reviewed, to reveal some properties of the HaB interaction. For example, information on radial and angular geometry, on the intermolecular stretching forces and on the extent of charge redistribution upon formation of the HaB have been reported.^[59] These studies also proved that HaB is more linear than WHB, with B ···X-Y angles close to 180°.

3.5 The other interactions

Besides aforementioned interactions, some other interactions such as dipole-dipole interactions, charge transfer interactions, ion-mediated interactions have been also found to be of interest, which could be in competition with the prevalent interactions in the molecular systems.

Chapter 4 Water Adducts

4.1 Introduction

Water is ubiquitous in chemical, physical and biological systems, and the knowledge of the ways it interacts with the various kinds of molecules would be helpful to understand the solvation processes in aqueous environments and its effects on gas-phase reactions.^[60-63] When we were studying the water adducts, two interesting points caught our attentions: 1) How the halogenation of the partner molecule affects the linkages between the two subunits, the internal dynamics of water and even the isotopic effect upon the deuteration of the water hydrogens; 2) the orientations of water in its complexes.

The typology of the complexes that water forms with organic molecules has been described and classified.^[7] Generally, water links to alcohols, ethers, amines, amides or N containing aromatics through relatively strong (15–25 kJ mol⁻¹) O–H ···O, O–H ···N or N–H ···O HBs. With ethers,^[27, 64-67] aliphatic amines,^[68] diazines,^[69-71] alcohols,^[7, 72] water acts as a proton donor. However, when forming adducts with phenols^[73] or NH groups inserted in an aromatic ring,^[74] water takes the role of a proton acceptor. With amides^[75] and amino acids,^[76] water forms a two HBs ring structure with the double roles of proton donor and proton acceptor.

With the freons containing hydrogens, water forms O–H ···X relatively weak (X = F, Cl) HBs (4–6 kJ mol⁻¹), such as O–H ···F or O–H ···Cl interactions.^[77-80] When both Cl and F atoms are present in a freon molecule, sometimes the O–H ···Cl linkage is favorite,^[77] but the O–H ···F one is preferred in other cases.^[78] However, when an aliphatic freon molecule is perhalogenated, then a HaB (6–10 kJ mol⁻¹), rather than a HB is formed.^[81-82] One should notice that, the properties of the partner molecules would definitely change the ways in which water will interact with them.

In this chapter, the rotational results concerning on how halogenation affects the way of the partner molecules interacting with water will be discussed in detail, including three water adducts, perhalogenated ethylene (chlorotrifluoroethylene),^[83] halogenated ethyl methyl ether

(isoflurane)^[84] and trifluorinated anisole (α,α,α -trifluoroanisole).^[85]

4.2 Experimental

Molecular clusters were generated in a supersonic expansion, under conditions optimized for the formation of the adducts.

The gas mixture of ca. 1% of chlorotrifluoroethylene or isoflurane (commercial sample used without any further purification) in Helium at a stagnation pressure of ~ 0.25 MPa was passed over a sample of H₂O (or H₂¹⁸O, or D₂O) and expanded through into the Fabry-Pérot cavity.

Helium at a stagnation pressure of ~ 0.3 MPa was passed over a 1:1 mixture of α,α,α -trifluoroanisole (commercial sample, cooled to 0 °C) and H₂O (or H₂¹⁸O, or D₂O) and expanded into the Fabry-Pérot cavity.

4.3 Chlorotrifluoroethylene···Water

The geometries of the water-aromatic complexes are found to be dependent on their electronic structure that water may form two types of molecular complexes with aromatic ring structure.^[86] The one stabilized due to H·· π interactions with the OH bond pointing to the aromatic molecular plane has been well studied both theoretically^[87] and experimentally^[88-89]. However, a stabilizing effect of the interaction between a lone pair of electrons in oxygen atom and the face of the π system (*lone pair*·· π interaction, *lp*·· π interaction) appears counter intuition.^[90] *Ab initio* calculations (BSSE counterpoise-corrected, cc, MP2(full)/6-31G(d,p)) revealed the *lp*·· π interaction with energy 8.8 kJ mol⁻¹ in the water–hexafluorobenzene complex.^[91] Compared with the H·· π interaction between water and benzene^[86, 88], the presence of electron-withdrawing fluorine atoms should be the reason of the higher stability of the *lp*·· π interaction between water and hexafluorobenzene.

As a comparison of aromatic molecules, the unsaturated aliphatic molecules are easy to be taken into consideration. The simplest one in this case is ethylene (C₂H₄). The rotational spectrum of C₂H₄··H₂O complex was firstly investigated by Peterson and Klempner using the molecular-beam electric resonance technique.^[92] Latter, Andrews and Kuczkowski restudied the rotational spectrum of this complex with FTMW spectroscopy.^[93] It indicated that the complex would have a structure with the water hydrogen bonded to the C=C bond center forming an H·· π bond.

We are interested in the effect of the electric withdrawing of the halogen atoms in the

ethylene derivants. Chlorotrifluoroethylene (C_2ClF_3 , Freon-1113) is a fully halogenated freon with a π -electrons system. The rotational spectrum of C_2ClF_3 has been reported previously.^[94] Its spectrum appeared very intense and then the assignment of the rotational spectrum of $C_2ClF_3-H_2O$ seems promising. No rotational investigations of an adduct of water with a molecule fully halogenated and with a π -electrons system has been reported.

4.3.1 Theoretical calculations

Before collecting the spectra, the full geometry optimization of the complex has been done with *ab initio* calculation at the MP2/6-311++G(d,p) level.^[13] Six plausible conformers were found. The shapes, the relative energies, the rotational constants and the values of the dipole moment components were obtained and collected in Table 4.1.

Table 4.1 MP2/6-311++G(d,p) shapes and spectroscopic parameters of the six more stable forms of the complex $C_2ClF_3-H_2O$

	I	II	III
<i>A/B/C</i> (MHz)	2356/1352/1234	3948/876/717	3327/1057/802
$\chi_{aa}/\chi_{bb}/\chi_{cc}/\chi_{ab}$ (MHz)	-24.4/-49.9/54.6	-71.1/-4.2/19.6	9.1/-84.1/48.9
$\mu_a/\mu_b/\mu_c$ (D)	1.9/1.4/0.6	3.2/0.8/0.0	0.3/1.2/0.0
$\Delta E/\Delta E_{BSSSE}(cm^{-1})$	0/0 ^[a]	476/18	645/214
	IV	V	VI
<i>A/B/C</i> (MHz)	2705/1145/804	3146/1027/774	3319/889/701
$\chi_{aa}/\chi_{bb}/\chi_{cc}/\chi_{ab}$ (MHz)	-62.2/129.2/35.1	15.0/-90.7/43.2	11.8/-86.0/46.4
$\mu_a/\mu_b/\mu_c$ (D)	2.8/1.4/0.0	2.4/1.0/0.0	1.3/2.4/0.2
$\Delta E/\Delta E_{BSSSE}(cm^{-1})$	667/261	773/355	903/373

[a] Absolute energies: -910.8993341 and -910.8957242 E_h, respectively.

In order to have a better estimate of the energy differences, all intermolecular binding energy values were counterpoise corrected for BSSE.^[12] The most stable conformer, rather than to be stabilized by a HB or a HaB, is characterized by a *lp* ··· π interaction.

4.3.2 Rotational spectra

We searched first for the μ_a -type transition of species I, which were expected to be the most intense ones. The $J\ 2\leftarrow 1$ μ_a -band was assigned first, and then many more μ_a - and μ_b - transitions have been measured. Only transitions corresponding to conformer I of Table 4.1 were observed and assigned. Each of them appeared as a multiplet of lines (see Figure 4.1) because of the nuclear quadrupole moment of the ^{35}Cl (or ^{37}Cl) nucleus.

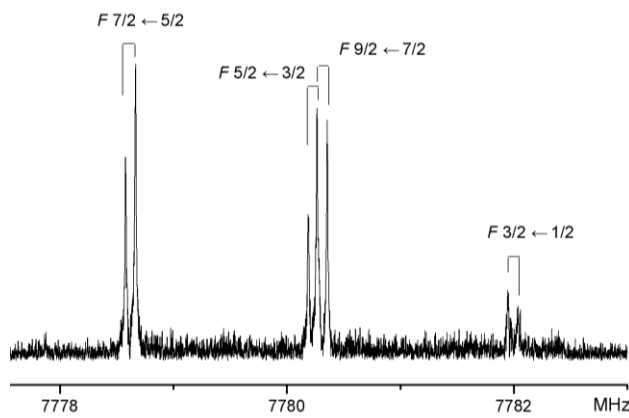


Figure 4.1 Recorded $3_{1,2}\leftarrow 2_{1,1}$ transition of the observed conformer of $\text{C}_2\text{ClF}_3\text{-H}_2\text{O}$ showing the ^{35}Cl hyperfine structure. Each line exhibits the Doppler doubling.

The transition frequencies were fitted to the spectroscopic constants with Pickett's SPFIT computer program,^[95] according to the following Hamiltonian:

$$H = H_R + H_{\text{CD}} + H_Q \quad (4.1)$$

where H_R represents the rigid rotational parts of the Hamiltonian. The centrifugal distortion contributions (analyzed using the S reduction and I' representation)^[8] are represented by H_{CD} . H_Q is the operator associated with the ^{35}Cl (or ^{37}Cl) quadrupolar interaction. The obtained spectroscopic parameters are reported in the first column of Table 4.2.

After partial structural adjustments, the spectra of the ^{37}Cl , H_2^{18}O , D_2O and DOH isotopologues were searched and assigned. The rotational transition frequencies were fitted with the same procedures as described for the normal species, and the spectroscopic parameters are also shown in Table 4.2.

The conformational assignment is straightforward: comparing the experimental values of the rotational and quadrupole coupling constants of Table 4.2 to the theoretical values of Table 4.1, one can see that the match is acceptable only for conformer I.

Table 4.2 Spectroscopic constants of all measured isotopologues of C₂ClF₃-H₂O

	C ₂ ³⁵ ClF ₃ -H ₂ O	C ₂ ³⁷ ClF ₃ -H ₂ O	C ₂ ClF ₃ -H ₂ ¹⁸ O	C ₂ ClF ₃ -D ₂ O	C ₂ ClF ₃ -DOH
A/MHz	2265.0902(5) ^[a]	2254.829(2)	2218.789(1)	2182.9360(6)	2235.4866(6)
B/MHz	1321.8363(4)	1298.3329(4)	1282.8122(4)	1263.5962(5)	1292.4213(4)
C/MHz	1224.4208(2)	1201.2806(4)	1189.0918(4)	1171.0099(5)	1199.7660(4)
D _J /kHz	3.103(6)	2.972(9)	3.146(6)	3.282(8)	3.473(7)
D _{JK} /kHz	-6.46(3)	[-6.46] ^[b]	-8.69(6)	-8.41(6)	-8.71(5)
D _K /kHz	17.55(4)	[17.55]	21.4(1)	20.84(8)	22.58(7)
d ₁ /kHz	-0.482(5)	[-0.482]	-0.546(5)	-0.723(6)	-0.714(6)
d ₂ /kHz	-0.185(7)	[-0.185]	-0.164(8)	-0.216(8)	-0.248(6)
χ _{aa} /MHz	-24.14(1)	-20.51(3)	-20.03(1)	-19.40(2)	-21.36(1)
χ _{bb} /MHz	-13.57(1)	-9.22(1)	-16.24(1)	-17.10(2)	-15.48(1)
χ _{cc} /MHz	37.71(1)	29.73(1)	36.27(1)	36.50(2)	36.84(1)
χ _{ab} /MHz	-54.8(4)	-43(1)	-46.6(6)	-50.1(8)	-49.8(4)
N ^[c]	86	44	80	72	92
σ ^[d] /kHz	3.1	2.5	3.4	3.9	4.1

[a] Uncertainties (in parentheses) are expressed in units of the last digit. [b] Fixed to the value obtained for normal species. [c] Number of transitions in the fit. [d] Standard deviation of the fit.

It is presumable that water undergoes a nearly free rotation in the complex. Only one spectrum was observed, indeed, for the mono-deuterated species, but the intensities of its rotational transitions are the double of those of the di-hydrogenated and of the bi-deuterated species when the ratio H/D is about 1:1. This indicates that the spectra of the two mono-deuterated species are not distinguishable, in accord a nearly free internal rotation of water about its symmetry axis. In none of the isotopologues, splittings attributable to the torsional motion of water were observed. That means what transitions we measured were only belonging to the $m = 0$ torsional state.

4.3.3 Molecular structure

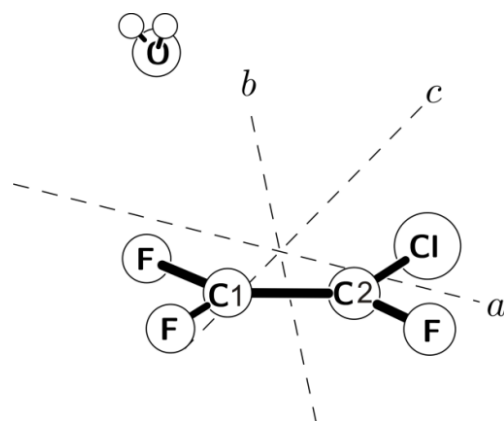
According to what mentioned above, the angular position of water cannot be determined from the isotopic substitution, although it is possible to estimate that the hydrogen atoms are oriented far away from the C₂ClF₃ unit. The r_s substitution coordinates^[16] can be reliably determined, however, for the Cl and O atoms. The obtained values are shown in Table 4.3, and there compared to the values calculated with a partial r_0 geometry. In such a r_0 geometry, the parameters defining the position of the O atom have been modified from the *ab initio* values ($r_{O-C1} = 2.8286$ Å, OC1C2 = 101.8°, OC1-C2Cl = 87.8°) to the empirically corrected values ($r_{O-C1} = 2.947$ Å, OC1C2 = 100.5°, OC1-C2Cl = 88.4°) which best reproduce the rotational constants of the C₂³⁵ClF₃-H₂O, C₂³⁷ClF₃-H₂O and C₂ClF₃-H₂¹⁸O isotopologues.

Table 4.3 r_s coordinates (Å) of the Cl and O atoms

	<i>a</i>		<i>B</i>		<i>c</i>	
	Exptl.	Calc.	Exptl.	Calc.	Exptl.	Calc.
O	$\pm 2.177(1)^{[a]}$	2.135	$\pm 1.152(1)$	-1.223	$\pm 1.079(1)$	1.329
Cl	$\pm 1.870(1)$	-1.874	$\pm 0.736(2)$	-0.735	$[0]^{[b]}$	-0.014

[a] Uncertainties (in parentheses) are expressed in units of the last digit. [b] Slightly imaginary value: set to zero.

One can note that the *c*-coordinate of the oxygen atom is not satisfactorily reproduced, probably due to the large amplitude bending motions of the full molecule of water with respect to C_2ClF_3 .

**Figure 4.2** Conformation and principal axis of the observed species (conformer I) of $C_2ClF_3-H_2O$.

The shape and atom numbering of the observed conformer are shown in Figure 4.2. The observed $lp-\pi$ interaction can be explained in terms of an electron-withdrawing from the π -electronic system towards the halogen atoms (especially the F atoms) generating a positive potential above the carbon atom C1. This effect has been theoretically described, and the region of low electronic density is called “ π -hole”.^[96]

MP2/6-311++G(d,p) counterpoise-corrected *ab initio* calculations supplied for the dissociation energy of the complex a value of 6.6 kJ mol^{-1} , which can be considered, in a first approximation, the energy of the $lp \cdot \pi$ interaction.

4.4 Isoflurane···Water

The molecular mechanism describing the interactions of anesthetics with biological substrates has been the subject of several investigations. Most evidences suggest that anesthesia may affect the organization of fat molecules, or lipids, in a cell's outer membrane — potentially altering the ability to send signals along nerve cell membranes.^[97-98] The full-scale experimental descriptions of anesthetic mechanisms are usually ascertained using large-scale molecular modeling.^[99]

The inhaled anesthetic isoflurane (1-chloro-2,2,2-trifluoroethyl difluoromethyl ether, C₃H₂ClF₅O, ISO since now on), contains several different sites for stereospecific interaction, which might imply the interaction through WHB or HaB with neuronal ion channels and on the protein binding in the central nervous system.^[98] The intrinsic structural properties of bare ISO have been revealed in the isolation conditions of a supersonic expansion using FTMW spectroscopy,^[100] and two conformers (*trans* and *gauche*) distinguished by the orientation of the difluoromethyl group have been identified. These spectroscopic data allow the study on the intermolecular complex or hydration aggregates involving ISO.

When forming the complex with water, ISO has several active sites which could bind with the solvent molecule through different interactions: (1) the ether oxygen could act as proton acceptor binding with water through O-H···O HB; (2) thanks to the electron withdrawing effect of the halogen atoms, the aliphatic hydrogen atoms could act as proton donors linking water with C-H···O WHBs; (3) HaBs could be formed between the halogen atoms and the negative site of water oxygen, resulting from the “ σ -hole”.^[59, 101] In order to figure out what kind of interaction dominates the hydration aggregates of ISO, herein we conduct the investigation of 1:1 complex of ISO-H₂O with FTMW spectroscopy.

4.4.1 Theoretical calculations

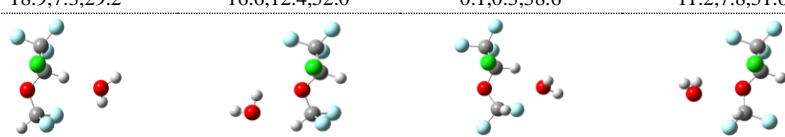
We preliminarily explored the conformational space of the complex by Molecular Mechanics, using conformational search algorithms implemented in MacroModel 9.2 within the MMFFs force field.^[15] We found 88 different geometries within an energy window of 800 cm⁻¹ which, at the MP2/6-311++G(d,p) level^[14] converged to five plausible conformers. Further vibrational frequency calculations at the same level proved four conformers, shown in Table 4.4, to be real minima.

These calculations provided, besides the relative energies, the rotational, quadrupole coupling and first order centrifugal distortion constants. Also the components of the electric

dipole moments have been estimated. Two structural families, corresponding to the *trans* and *gauche* (T and G, respectively) monomers, can be distinguished by the orientation of the $-\text{CHF}_2$ group with respect to the ether group of ISO. In each family, there are two different ways to link the two subunits together, labeled as “1” (C-H \cdots O WHB, water acting as proton acceptor) and “2” (O-H \cdots O hydrogen bond, water acting as proton donor). The calculations indicate that in the global minimum (G2) the configuration adopted by the ISO is apparently the less stable one (G) in the isolated monomer.^[100] However, when BSSE^[12] are taken into account, the *trans* form T2 turns out to be the global minimum. Anyway, the theoretical values are very close and predicting three structures (T2, G2 and T1) almost iso-energetics, these differences are within the error of the theoretical method (Table 4.4).

Table 4.4 MP2/6-311++G(d,p) spectroscopic parameters of the plausible conformers of ISO-H₂O.

	T1	T2	G1	G2
$\Delta E/\text{cm}^{-1}$	40	235	791	0 ^[a]
$\Delta E_{\text{BSSE}}/\text{cm}^{-1}$	99	0 ^[b]	789	11
$A, B, C/\text{MHz}$	1055,670,626	1014,625,584	1116,617,566	1058,638,553
$ \mu_a , \mu_b , \mu_c /\text{D}$	3.4, 0.2, 0.8	0.4, 1.1, 0.8	0.7, 1.7, 0.7	2.0, 4.3, 1.9
D_J/kHz	0.12	0.17	0.09	0.05
D_{JK}/kHz	0.14	0.06	-0.16	0.20
D_K/kHz	0.07	0.04	0.27	0.02
d_1/kHz	-0.04	-0.04	0.03	-0.02
d_2/kHz	-0.01	-0.04	-0.01	-0.01
χ_{aa}/MHz	32.5	31.8	33.9	32.1
$\chi_{bb}-\chi_{cc}/\text{MHz}$	-86.05	-20.82	-75.2	-15.2
$\chi_{ab}-\chi_{ac}-\chi_{bc}/\text{MHz}$	18.9,7.3,29.2	16.6,12.4,52.0	0.1,0.3,38.6	11.2,7.8,51.6



[a] $E/E_h = -1224.604444$. [b] $E/E_h = -1224.600173$.

4.4.2 Rotational spectra

The rotational spectra of ISO-H₂O were predicted from the theoretical values of the rotational and quadrupole coupling constants of the four forms of the complex. After scanning wide frequency ranges, the spectrum of only one rotamer was detected and assigned in the supersonic expansion. 13 transitions (K_a from 0 to 6) of the μ_a -R branch with $J = 7 \leftarrow 6$ were assigned in the first stage. Three more μ_a -R bands with J_{upper} from 6 to 9 were then measured. Finally, we could measure six weaker μ_c -R transitions. No μ_b - type lines were observed possibly because of the quite small dipole moment component. Each transition is split into several component lines due

to the quadrupole effect of the ^{35}Cl (or ^{37}Cl) nuclei, as shown, for example, in Figure 4.3 for the $7_{07}\leftarrow 6_{06}$ transition of the ^{35}Cl isotopologue.

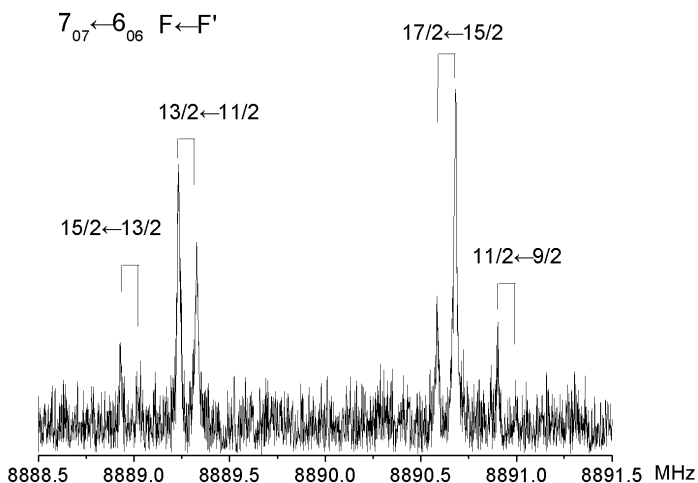


Figure 4.3 Recorded $7_{07}\leftarrow 6_{06}$ rotational transition of the observed conformer of ISO- H_2O showing the ^{35}Cl hyperfine structure. Each component line exhibits the Doppler doubling.

The frequencies were fitted to the Watson’s “S” reduced semi-rigid rotor Hamiltonian^[8] within the I' representation, according to the Hamiltonian Eq. (4.1). The spectroscopic constants were derived by direct diagonalization using Pickett’s SPFIT program.^[95]

Table 4.5 Spectroscopic parameters of the three isotopologues of ISO- H_2O

	ISO(^{35}Cl)- H_2O	ISO(^{37}Cl)- H_2O	ISO- H_2^{18}O
A/MHz	1034.7187(4) ^[a]	1018.05(2)	1007.4568(6)
B/MHz	668.9313(3)	667.506(1)	654.782(2)
C/MHz	624.0039(3)	618.1093(6)	618.1754(7)
D_J/kHz	0.785(1)	0.8320(5)	0.95(1)
D_K/kHz	0.608(6)	[0.608]	[0.608]
d_1/kHz	-0.310(1)	-0.335(4)	-0.46(1)
d_2/kHz	-0.0121(5)	[-0.0121] ^[b]	-0.16(1)
χ_{aa}/MHz	33.00(2)	25.60(7)	33.01(2)
$\chi_{bb}-\chi_{cc}/\text{MHz}$	-77.92(8)	-66.24(8)	-57.32(8)
$N^{[c]}$	139	36	43
$\sigma/\text{kHz}^{[d]}$	3.3	3.7	4.1

[a] Uncertainties (in parentheses) are expressed in units of the last digit. [b] Fixed to the value obtained for normal species. [c] Number of transitions in the fit. [d] Standard deviation of the fit.

Following the same procedure, the μ_a -type spectrum of the ^{37}Cl isotopomer has been measured and assigned in natural abundance. The determined parameters of both isotopologues are listed in Table 4.5.

Later on, the rotational spectra of three additional heavy water isotopologues (ISO- H_2^{18}O , ISO-DOH, ISO- D_2O) have been successfully assigned. The rotational assignment of ISO- H_2^{18}O was straightforward, and its spectroscopic constants obtained are reported in the third column of Table 4.5.

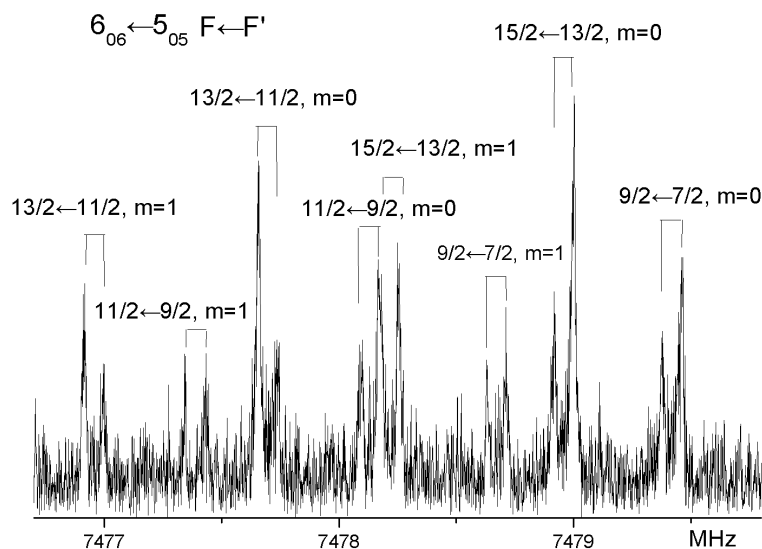


Figure 4.4 The internal rotation of water is apparent in the doubling of all hyperfine components of the $6_{06} \leftarrow 5_{05}$ rotational transition of ISO- D_2O . Each component is further split by an instrumental Doppler effect.

The rotational spectra of the deuterated species displayed some unexpected features, which raised some interpretation problems. On one hand, the rotational transitions of ISO- D_2O are split, apart from the quadrupole hyperfine structure, into doublets with component lines separated by about 1 MHz (see Figure 4.4), indicating a finite V_2 barrier hindering the internal rotation of the D_2O moiety in the complex. On the other hand, a single rotational spectrum of the ISO-DOH species could be assigned, suggesting the two water hydrogens to be equivalent to each other; an experimental evidence compatible with a near free or low V_2 barrier. Although it appears difficult to estimate relative populations from intensity measurements, it seems, from intensity measurements of some nearby transitions, that the mono-deuterated species is almost as twice intense than the bi-deuterated and the normal species in appropriate H/D abundance ratio conditions. Probably the mass effects related to the considerable heavier top when we have D_2O rather than H_2O in the complex, makes the internal rotation effects observable in the first case,

even within a low V_2 barrier. Similar effects have been observed previously in some complexes of water with organic molecules.^[7]

Table 4.6 Spectroscopic parameters of the isotopologues with deuterated water.^[a]

	ISO(³⁵ Cl)-D ₂ O		ISO(³⁵ Cl)-HDO
	$m = 0$	$m = 1$	
A/MHz	999.55(2) ^[b]	999.28(2)	1022.25(2)
B/MHz	655.740(1)	655.870(2)	665.106(1)
C/MHz	610.4737(6)	610.3869(7)	615.3569(5)
D_J/kHz	0.698(5)	0.705(7)	0.637(6)
d_1/kHz	-0.268(4)	-0.266(6)	-0.242(4)
χ_{aa}/MHz		32.1(2)	32.0(2)
$\chi_{bb}-\chi_{cc}/\text{MHz}$		-48.4(8)	-65.36(8)
$N^{[c]}$		62	37
$\sigma/\text{kHz}^{[d]}$		6.4	5.8

[a]The D_K and d_2 centrifugal distortion parameters have been fixed to the values of the parent species. [b] Uncertainties (in parentheses) are expressed in units of the last digit. [c] Number of transitions in the fit. [d] Standard deviation of the fit.

The noticeable low values of the quadrupole coupling parameter $\chi_{bb}-\chi_{cc}$ for the ISO-H₂¹⁸O and ISO-D₂O species with respect to that of the normal species are interpretable in terms of a considerable rotation of the principal inertial axes system upon isotopic substitution.

The transitions frequencies of the two states of the bideuterated species have been fitted with a common set of centrifugal distortion constants. The spectroscopic parameters are shown in Table 4.6 for the two deuterated water isotopologues.

4.4.3 Conformational assignment

Concerning the conformational assignment, the comparison of Tables 4.5 and 4.4 shows that the experimental rotational and quadrupole coupling constants match the theoretical values only for conformer T1. In addition, μ_b and μ_c type spectra could not be observed, confirming the assignment to T1. This result is apparently in contrast with the theoretical conformational energies. However, the presence of T2 in the jet cannot be excluded totally due to its low μ_a dipole moment component, which is about 1/10 of the μ_a value of T1, the observed conformer. Since the spectrum is relatively weak, we cannot exclude the T2 conformer to be as much abundant as T1. Also for conformer G2 we could not observe any line, in spite of its high μ_a value. In this case, we can state that its abundance should not exceed 1/10 of that of T1.

4.4.4 Structural information.

In the observed conformer, T1, water is linked to ISO through a C-H \cdots O WHB (see Figure 4.5), and plausibly undergoes a near free internal rotation around its C_2 axis.

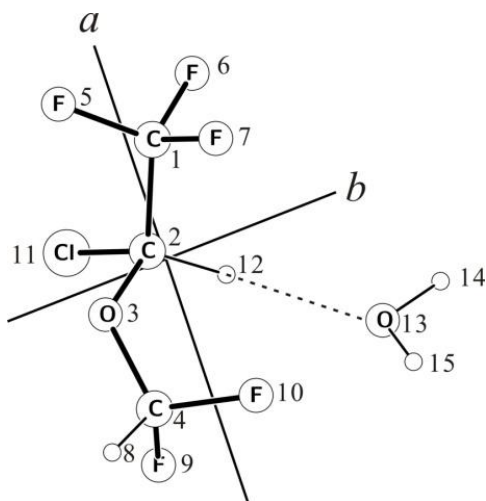


Figure 4.5 Sketch of the observed conformer of ISO-H₂O with atom numbering

Within this hypothesis, the position of the water hydrogens is undetermined, and a tentative determination of their substitution coordinates^[16] gave meaningless (imaginary) values. However, reliable values of the r_s substitution coordinates of the Cl and O_{H₂O} atoms have been obtained, as shown in Table 4.7.

Table 4.7 The r_s coordinates of substituted atoms of ISO-H₂O compared with calculated values

	$a/\text{Å}$		$b/\text{Å}$		$c/\text{Å}$	
	Exptl.	Calc. ^[a]	Exptl.	Calc.	Exptl.	Calc.
Cl	$\pm 0.573(3)^{[b]}$	-0.601	$\pm 1.874(1)$	-1.874	$\pm 0.739(2)$	-0.728
O _{H₂O}	$\pm 1.611(1)$	1.535	$\pm 0.960(2)$	1.320	$\pm 2.419(1)$	-2.312

[a] Deduced from the partial r_0 structure (see text). [b] Uncertainties (in parentheses) are expressed in units of the last digit.

The r_s values are in a good accord with the values calculated with an effective partial r_0 structure, in which the WHB parameters have been fitted to the values $r_{\text{O13H12}} = 2.153(3)$ Å and $\angle \text{O13H12C2} = 180.0(4)^\circ$, respectively. Their *ab initio* values are: $r_{\text{O13H12}} = 2.084$ Å and $\angle \text{O13H12C2} = 175.9^\circ$, respectively.

4.5 Trifluoroanisole...Water

α,α,α -trifluoroanisole (trifluoromethoxybenzene, $C_6H_5OCF_3$, TFANI from now on) is a halogenated ether with an electronic π system. Water could then interact with this molecule in several ways. It has been found that in the isolated molecule the substitution of the three methyl hydrogens with fluorine atoms change the position of the side chain from the in-plane configuration of anisole^[102] to a perpendicular shape.^[103] In the 1:1 complex anisole-water, water acts mainly as proton donor, but the deuteration of water produces a conformational change, as shown in Figure 4.6. The value of the θ angle decreases from 138° to 128° , while the secondary interaction $O \cdots H_{Me}$ is replaced by the $O \cdots H_{Ph}$ one.^[27]

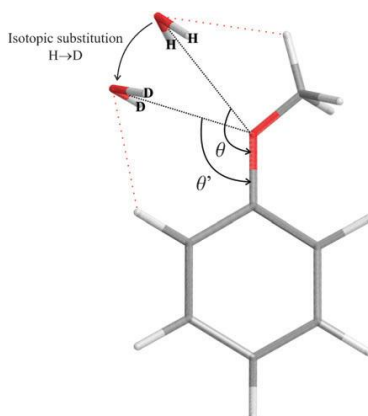


Figure 4.6 The deuteration of water produces a conformational change in the anisole-water complex.^[7, 27]

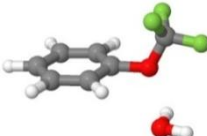
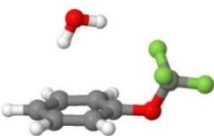
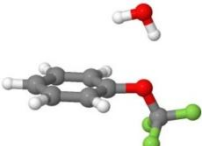
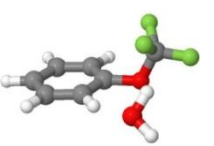
It is interesting to investigate how the fluorination of the CH_3 group of anisole will change these features of the complex with water. Herein we studied the rotational spectrum of the adduct TFANI-water with PJ-FTMW technique. The results are presented below.

4.5.1 Theoretical calculation

We preliminarily explored the conformational space of the complex by Molecular Mechanics, using conformational search algorithms implemented in MacroModel 9.2 within the MMFFs force field.^[15] We found 100 different geometries within an energy window of 13 kJ mol^{-1} which, at the MP2/6-311++G(d,p) level^[14] converged to six plausible conformers. Further vibrational frequency calculations at the same level proved the four conformers, shown in Table 4.8, to be real minima and provide additional centrifugal distortion constants. All these conformers are characterized by hydrogen bonds, with water acting as a proton donor (conformer II and III) or

having the double role of proton donor and proton acceptor (conformer I and IV).

Table 4.8 MP2/6-311++G(d,p) calculated energies and spectroscopic parameters of the plausible conformers of TFANI-water

	I	II
		
<i>A,B,C</i> /MHz	1309,662,505	1502,620,571
μ_a, μ_b, μ_c /D	1.1,-0.6,-0.3	-2.1,-2.4,-0.6
<i>D_J</i> /kHz	34.98	53.18
<i>D_{JK}, D_K</i> /MHz	0.62,0.53	0.64, 0.10
<i>d₁, d₂</i> /kHz	-2.65,-6.17	1.87,3.90
$\Delta E, \Delta(E+ZPE), \Delta E_{BSSE}$ /kJ mol ⁻¹	0.0, ^[a] 0.5,0.0 ^[b]	0.5,0.0, ^[c] 3.4
<i>E_D</i> ^[d] /kJ mol ⁻¹	12.2	8.8
	III	IV
		
<i>A,B,C</i> /MHz	1224,627,531	1239,673,482
μ_a, μ_b, μ_c /D	2.8,-2.9,0.0	0.6,0.3,-0.3
<i>D_J</i> /kHz	48.78	53.09
<i>D_{JK}, D_K</i> /MHz	1.70,-1.08	0.18,1.41
<i>d₁, d₂</i> /kHz	-2.37,10.07	-10.33,0.78
$\Delta E, \Delta(E+ZPE), \Delta E_{BSSE}$ /kJ mol ⁻¹	2.0,0.1,3.7	2.7,2.3,2.1
<i>E_D</i> /kJ mol ⁻¹	8.5	10.1

[a] Absolute energy: -719.396479 E_h; [b] Absolute energy: -719.3754723 E_h; [c] Absolute energy: -719.267205 E_h; [d] Calculated dissociation energy with BSSE correction

All intermolecular binding energy values were counterpoise corrected for BSSE.^[12] It resulted the conformer I, with O-H···O and C-H···O hydrogen bonds, to be the global minimum. Therefore the dissociation energies have been estimated, inclusive of BSSE corrections. All the theoretical parameters are reported in Table 4.8.

4.5.2 Rotational Spectra

We started our search with frequency scans for μ_a -type R -branch transitions belonging to conformer I, which, according to the theoretical calculations is the most stable species. We could first identify the $J = 8 \leftarrow 7$, $K_{-1} = 0$ and $K_{-1} = 1$ transitions. Then the assignment was extended to many R -type transitions with J_{upper} from 7 to 11 and with K_{-1} up to 5. Later on, some much weaker μ_b and μ_c transitions could be measured.

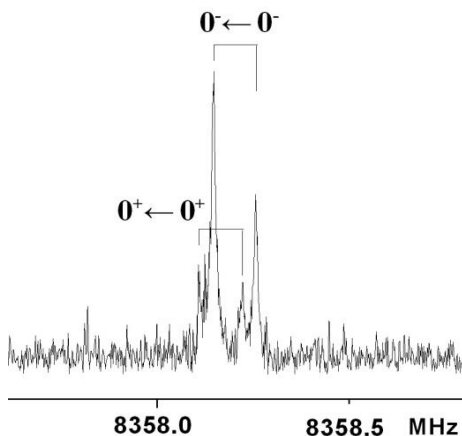


Figure 4.7 0^+ and 0^- component lines of the $8_{18} \leftarrow 7_{17}$ transition of TFANI- H_2O . Each component is further split by an instrumental Doppler effect.

Each transition appeared as a doublet, with a relative intensity ratio of the two component lines about 1:3, as in Figure 4.7 for the μ_a^- type transition $8_{18} \leftarrow 7_{17}$. This ratio corresponds to the statistical weight expected for the internal rotation of water around its C_{2v} axis, which implies the exchange of a pair of equivalent hydrogen atoms (fermions with $I = 1/2$). According to this, we could assign the weaker line of the two components to the ground state (0^+). The splitting space is quite smaller than that of anisole-water, outlining a higher barrier to internal rotation.

Using Pickett's SPFIT program,^[95] the 96 rotational transition frequencies were fitted by the Hamiltonian:

$$H = H_R(0^+) + H_R(0^-) + H_{\text{CD}} \quad (4.2)$$

$H_R(0^+)$ and $H_R(0^-)$ represent the rigid rotational parts of the Hamiltonian for the 0^+ and 0^- states, respectively. The centrifugal distortion contributions are represented by H_{CD} . Watson S -reduction and I' -representation have been adopted.^[8]

The transition frequencies of the two tunneling components did not show any appreciable

interaction between the two states, so that it was not possible to determine parameters such as ΔE (the energy difference between the two states), or Coriolis' coupling terms. The fitted rotational and centrifugal distortion constants are reported in the first two columns of Table 4.9, where the centrifugal distortion constants for both sub-states are fixed to be the same. The differences between the rotational constants of the 0^+ and 0^- states would, in principle, allow estimating the barrier to internal rotation of water, as in the cases, for example, of phenol-water^[73] or chlorofluoromethane-water.^[77] A knowledge of the associate structural relaxations is required for this purpose, because it strongly affect the reduce mass of the motion. However, in the case TFANI-H₂O we could not determine these structural relaxations because we did not succeed in finding, by *ab initio* calculations, the pathway of the motion.

Table 4.9 Spectroscopic parameters of the 0^+ and 0^- sub-states of the parent species and its H₂¹⁸O isotopologue of the observed conformer of TFANI-water.

	TFANI-H ₂ O		TFANI-H ₂ ¹⁸ O	
	0^+	0^-	0^+	0^-
<i>A</i> /MHz	1291.6717(6) ^[a]	1292.6534(6)	1233.72(1)	1233.70(1)
<i>B</i> /MHz	656.3183(2)	656.3193(2)	652.709(4)	652.713(4)
<i>C</i> /MHz	500.8509(2)	500.8532(2)	490.0453(2)	490.0479(2)
<i>D_J</i> /kHz	0.0385(7)		[0.0385] ^[b]	
<i>D_{JK}</i> /kHz	0.901(8)		[0.901]	
<i>D_K</i> /kHz	0.64(2)		[0.64]	
<i>d₁</i> /Hz	-5.0(3)		[-5.0]	
<i>d₂</i> /Hz	-8.2(2)		[-8.2]	
$\sigma^{\text{[c]}}$ /kHz	2.5		2.7	
<i>N</i> ^[d]	96		18	

[a] Error in parentheses in units of the last digit. [b] Fixed at the values of the parent species.[c] RMS error of the fit. [d] Number of lines in the fit.

After the empirical adjustment to the molecular structure (applying the difference between the calculated and experimental values to the rotational constants), the spectra of four additional isotopologues, the ones with H₂¹⁸O, HOD, DOH and DOD, have been assigned. The transitions of the H₂¹⁸O, whose spectroscopic parameters are listed in the last columns of Table 4.10, display the same splitting features observed for the parent species. For the three deuterated species the water internal rotation splittings have not been observed according to a heavier reduced mass of the

motion.^[7] The obtained rotational constants are listed in Table 4.10. For the isotopically substituted species the centrifugal distortion constants have been fixed at the values of the parent (all protonated) species.

Table 4.10. Spectroscopic parameters of the three deuterated isotopologues of TFANI-water^[a]

	TFANI-HOD	TFANI-DOH	TFANI-DOD
<i>A</i> /MHz	1252.33(1) ^[b]	1274.47(1)	1236.158(1)
<i>B</i> /MHz	652.523(3)	653.994(3)	650.161(4)
<i>C</i> /MHz	493.0183(2)	498.1981(2)	490.4597(2)
$\sigma^{[c]}$ /kHz	3.7	2.6	4.0
<i>N</i> ^[d]	9	9	9

[a] The quartic centrifugal distortion parameters have been fixed at the values of the parent species. [b] Error in parentheses in units of the last digit. [c] RMS error of the fit. [d] Number of lines in the fit.

The obtained rotational constants match only the calculated values of species I, making the conformational assignment straightforward. No lines belonging to the other conformer could be identified. This could be due to the conformational relaxation to the most stable conformer upon supersonic expansion. It has, indeed, been shown that this kind of relaxation takes place easily when the inter-conversion barrier is smaller than $2kT$.^[104]

4.5.3 Molecular Structure

An $O_w-H \cdots O_{eth}$ hydrogen bond and a weaker $C-H \cdots O_w$ interaction hold the two units together in the observed conformer of the complex, as shown in Figure 4.8.

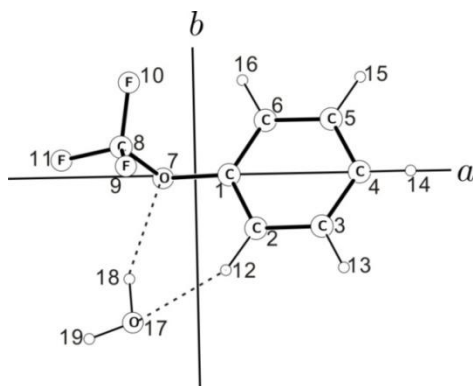


Figure 4.8 Sketch of the observed conformer of TFANI-water with atom numbering

Due to the internal rotation of water and, plausibly, to the Ubbelohde effect^[24] upon the H→D substitution, the position of the water hydrogens is undetermined. Therefore, a tentative determination of the substitution coordinates^[16] of the water hydrogens gave meaningless (imaginary) values. However, reliable values of the r_s substitution coordinates of the O_{H2O} atom have been obtained, as shown in Table 4.11, where the values from the partial r_0 structure are also given as comparison.

Table 4.11 r_s coordinates of the water oxygen atom in TFANI-water.

	a/Å	b/Å	c/Å
Exptl.	±1.397(1) ^[b]	±3.0439(5)	±0.325(5)
Calc. ^[a]	1.371	3.058	-0.500

[a] Calculated with the r_0 structure in Table 4.12; [b] Error in parentheses in units of the last digit.

The partial r_0 structure, was obtained by adjusting three structural parameters (R_{H12O17} , $\angle\text{C2H12} \cdot\cdot\text{O17}$ and $\angle\text{O17} \cdot\cdot\text{C2H12C1}$), whilst keeping the remaining parameters fixed to their *ab initio* values, in order to reproduce the experimental rotational constants of TFANI-H₂O and TFANI-H₂¹⁸O. The fitted and derived hydrogen bond parameters are reported in Table 4.12, and there compared to the *ab initio* values.

Table 4.12 r_0 and r_e hydrogen bond parameters of TFANI-water.

Fitted parameters			
	R _{H12O17} /Å	∠C2H12 ··O17/°	∠O17 ··C2-H12C1/°
r_0	2.574(5) ^[a]	130.8(5)	-36.6(3)
r_e	2.447	132.0	-36.4
Derived parameters			
	R _{O7H18} /Å	∠O7 ··H18O17/°	
r_0	2.294(5)	140.5(5)	
r_e	2.170	143.1	

[a] Uncertainties (in parentheses) are expressed in units of the last digit.

4.6 Conclusions

The rotational spectra of the water adducts of the three halogenated molecules have indeed shown how halogenations affect the way of the partner molecules to interact with water. When

the ethylene is full halogenated, as C_2ClF_3 , a $lp \cdots \pi$ interaction is favorite rather than WHB or HaB. This is, to our knowledge, the first time that this interaction is observed and described through a rotational study in a molecular complex.

Although water still links with the halogenated ether, like ISO and TFANI here, through WHB or HB, the role of water to act as proton donor or acceptor could be different with respect to that of water to act with the non-halogenated ether. For ISO- H_2O , the water is thus linked to ISO, as a proton acceptor, through a linear C-H $\cdots O$ WHB. Besides the normal species, four more isotopologues of the complex were also observed and assigned, consistent with this interpretation. The observed splittings in the bideuterated species and the indistinguishability of the two monodeuterated species, though apparently puzzling, could indicate an almost free internal rotation of water. Thus only the position of the water oxygen is determinable. Instead, the observed conformer of TFANI- H_2O is stabilized an $O_w-H \cdots O_{eth}$ interaction while the secondary C-H $\cdots O_w$ HB is also contributable to the stability of the complex, where water has the double role as the proton donor and proton acceptor which is different with that in the complex anisole-water, water acts as proton donor forms a strong hydrogen bridge – bifurcated – with the ether oxygen atom.

For the water adducts, there's another effect also deserving attentions. As outlined in many cases, the large amplitude motions of water and the possible Ubbelohde effect associated to the deuterations in the HBs do not allow a reliable determination of the position of the water hydrogens.^[7, 67-69, 71, 79] This is mostly because that the orientation of the water molecule in the complex is not precisely determined. It brings to mind the fact that in the complexes of organic molecules with ammonia, the effective orientation of NH_3 with respect to the partner molecule has been often obtained from the values of the ^{14}N quadrupole coupling constants.^[105-106] This kind of information is not available, however, in complexes of organic molecules with water involving the two most common oxygen isotopes, ^{16}O and ^{18}O , which have nuclear spin quantum number $I = 0$. The nucleus ^{17}O has $I = 5/2$, so that the rotational transitions of molecular complexes containing $H_2^{17}O$ are split in several quadrupole component lines. From such a hyperfine structure it is possible to determine the ^{17}O quadrupole coupling constants, whose values are related to the average orientation of the water subunit in a complex, like the 1:1 complexes of water with ethylene^[93] and *p*-difluorobenzene.^[107]

The average orientations of water in its complexes with difluoromethane,^[108] tetrafluoromethane^[109] and 1,4-dioxane have been obtained from the rotational studies of the ^{17}O isotopologues, and the details are available in the corresponding published papers.

Chapter 5 Complexes of Freons

5.1 Introduction

Freon is the family of a number of halocarbon products which are stable, nonflammable, and moderately toxic gases or liquids which have typically been used as refrigerants and as aerosol propellants. In chemistry, some of them are also frequently used as the solvent.

Considerable attention has been dedicated during the last years to chlorofluorocarbons (CFCs) and to their impact on the atmospheric processes, in relation to both the role in ozone reduction and in the greenhouse effect. The complexation of CFCs with atmospheric water and pollutants of the atmosphere affects their reactivity and it seems to accelerate, for example, the decomposition rate of freons in the atmosphere.^[110]

In the rotational spectroscopic studies, CFCs are usually used as the prototype molecules involving in the complexes of WHB or HaB. Generally speaking, in the hydrogenated CFCs, the C-H group can be act as the proton donor, enhanced by the electron withdrawing of the halogen atoms, to form the WHBs with the negative sites of the partner molecules.^[78, 111] However HaBs are favorable for the cases of fully halogenated CFCs.^[82, 112-113] due to the so called “ σ -hole”.^[59, 101] If a perhalogenated CFC has a π -electron system as well, the electron withdrawing of halogens will generate a positive region above the π system (π -hole) which is ready to interact with the negative sites, that is the case what has been discussed in Chapter 4 for the complex C_2F_3Cl -water.^[83]

A lot of our rotational studies were dedicated to the 1:1 complex between different CFCs or between CFCs with other organic molecules. An amount of information on the interactions between the two subunits and on the internal dynamics from the rotational spectra with or without the nuclear hyperfine structures has been gathered and is available in the corresponding published papers.

Here in this chapter, I will present the most interesting results we have obtained from the

FTMW studies of 1:1 complexes involving CFCs to showcase the abilities to extract the rich informations of the molecular systems: 1) difluoromethane ··dichloromethane concerning the hyperfine structure in the rotational spectrum; 2) chlorotrifluoromethane ··fluoromethane concerning the contribution of the free internal rotation of the $-CF_3$ group to the rotational constants. 3) difluoromethane ··formaldehyde concerning the internal rotation of formaldehyde around its symmetric axis;^[111] and 4) trifluoromethane ··benzene concerning the Ubbelohde effect in WHB.^[114]

5.2 Experimental

Molecular clusters were generated in a supersonic expansion, under conditions optimized for the dimer formation

A mixture of 2% difluoromethane and dichloromethane in helium at a stagnation pressure of ~ 0.5 MPa was allowed to expand into the Fabry-Pérot cavity.

A mixture of 2% chlorotrifluoromethane and fluoromethane in helium at a stagnation pressure of ~ 0.5 MPa was allowed to expand into the Fabry-Pérot cavity.

A mixture of 2% difluoromethane in helium a stagnation pressure of ~ 0.3 MPa was allowed to flow over formaldehyde (heated up to 60 °C) and expanded into the Fabry-Pérot cavity.

A mixture of 2% trifluoromethane-(*d*) (CDN Isotopes) in Helium a stagnation pressure of ~ 0.3 MPa was allowed to flow over benzene (cooled to 0 °C) and expanded into the Fabry-Pérot cavity.

5.3 Difluoromethane··Dichloromethane

Hydrogenated CFCs have sites which can act as weak proton donors or weak proton acceptors, leading to an easy formation of their oligomers or hetero adducts, with the subunits held together by a net of WHBs. The aliphatic hydrogen atoms have, indeed, been found to act as proton donors, enhanced by the electron withdrawing effect of the halogen atoms. Difluoromethane (CH_2F_2) can be regarded as the prototype for this kind of ambivalent molecules. Its oligomers, $(CH_2F_2)_n$, with $n = 2-4$, have been recently characterized by rotational spectroscopy, which pointed out that the dimer,^[115] trimer^[116] and tetramer^[117] of CH_2F_2 are stabilized by a network of 3, 9, and 16 C-H ··F-C WHBs, respectively. In the hetero adduct CH_3F-CHF_3 , the two subunits are linked together by three weak C-H ··F-C WHBs, while the two subunits rotate through low V_3

barriers around their symmetry axes.^[118]

Only one adduct between freon molecules containing halogen atoms other than fluorine has been investigated by rotational spectroscopy, *i. e.* CH₂ClF with FHC=CH₂, which presents a combination of C-H ··F-C and C-H ··Cl-C WHBs.^[119] No complexes between freons with two heavy halogen (Cl, Br, I) have been investigated. This because unlike the F atom, whose nuclear spin quantum number is $I = 1/2$, the other halogens have $I = 3/2$ or $5/2$ resulting in complicated quadrupolar hyperfine structures in the rotational spectra of the multi-halogenated molecular systems. From a spectroscopic point of view, especially for a system with multiple quadrupolar nuclei, the interpretation of the rotational spectra can be a challenging task. For example, the rotational spectra of even very simple molecules with two heavy halogen atoms have been reported only in a few cases. Accurate information of the methylene di-halide series, CH₂Cl₂,^[15] CH₂Br₂,^[16] and CH₂I₂,^[120-121] became available only in recent two decades. But, as far as we know, no information on their complexes is available.

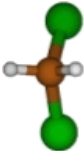
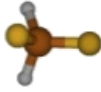
Herein, we decide to investigate the rotational spectrum of the 1:1 complex between CH₂Cl₂ and CH₂F₂, (Freon 30 and Freon 32) with the aim of determining the orientation of the subunits in the complex and ascertaining which WHB, C-H ··Cl-C or C-H ··F-C is more favorable.

5.3.1 Theoretical calculations

Two conformers, both stabilized by three WHBs are, by chemical intuition, expected to be the most stable forms of the title complex. They are shown in Table 5.1. MP2/6-311++G(d,p) calculations, performed by using the Gaussian03 Program^[13] confirmed this hypothesis. Table 5.1 also reports their relative energies (ΔE) and the spectroscopic parameters useful for the investigation of the microwave spectrum. In order to obtain a better estimate of the energy differences, the intermolecular binding energy values were counterpoise corrected for BSSE.^[12] It turned out that conformer **I**, with two C-H ··Cl-C and one C-H ··F-C WHBs is slightly more stable than conformer **II**, with two C-H ··F-C and one C-H ··Cl-C WHBs. We also evaluated the dissociation energies, inclusive of the BSSE corrections, $E_{D(BSSE)}$. We did not calculate the zero-point-energy corrections.

Conformer **I** was calculated to be slightly distorted with respect to a C_s configuration with the two F atoms in the plane of symmetry. However, it is well known that in similar cases the vibrational ground state wave-function is symmetric with respect to the “near”-symmetry plane. Herein we fixed the complex to be symmetric, and as consequence, the quadrupole coupling constants of the two Cl atoms to be the same. This is consistent, as shown below, with the experimental evidence.

Table 5.1 Shapes and spectroscopic parameters of the two most stable forms of CH₂F₂-CH₂Cl₂.

	I	II
		
$\Delta E, \Delta E_{\text{BSSE}}^{[\text{a}]}/\text{cm}^{-1}$	0,0 ^[b]	72,12
$E_{\text{D(BSSE)}}^{[\text{c}]}/\text{kJ mol}^{-1}$	7.0	6.9
$A, B, C/\text{MHz}$	2706,976,792	3313,870,794
$\chi_{aa}, \chi_{bb}, \chi_{cc}(1)/\text{MHz}$	36.25, -45.14	-61.90, -8.14
$\chi_{ab}, \chi_{ac}, \chi_{bc}(1)/\text{MHz}$	-10.34, 7.84, 47.22 ^[d]	-27.11, -17.04, -3.53
$\chi_{aa}, \chi_{bb}, \chi_{cc}(2)/\text{MHz}$		29.69, -96.32
$\chi_{ab}, \chi_{ac}, \chi_{bc}(2)/\text{MHz}$		-20.42, 3.43, 20.42
$\mu_a, \mu_b, \mu_c/\text{D}$	-1.5, -0.0, 0.0	2.9, 0, 3, 0, 4

[a] ΔE and ΔE_{BSSE} are the energy difference with respect to the most stable isomer, without and with BSSE corrections. [b] Absolute values are -1197.020145 E_h and -1197.016320 E_h, respectively. [c] Dissociation energy. [d] For this isomer the quadrupole coupling constants of Cl2 are the same as for Cl1, except for the sign of χ_{bc} .

5.3.2 Rotational spectra

The spectrum was expected to be quite complicated for two reasons: (i) the presence of several abundant isotopologues (³⁵Cl/³⁵Cl, ³⁵Cl/³⁷Cl, ³⁷Cl/³⁷Cl, in the ratio 10/6/1, according to the 75 and 25% natural abundance of ³⁵Cl and ³⁷Cl, respectively); (ii) the presence of two quadrupolar nuclei (³⁵Cl or ³⁷Cl) with a nuclear spin $I = 3/2$ and with a relatively large nuclear electric quadrupole moment (Q).

Following the prediction from the computations, which show the μ_a dipole moment component to be the largest one, we searched first for the $J = 5 \leftarrow 4$ μ_a -R band. We could identify the intense $K = 0, 1$ transitions of the parent species of conformer I. Each of them was split into several quadrupole component lines, as illustrated in Figure 5.1 for the $5_{15} \leftarrow 4_{14}$ transition.

Later on, many additional μ_a -type transitions, with J_{upper} and K_a up to 8 and 3, respectively, have been measured. Then, about 100 MHz below each transition of the observed $J = 5-4$ band, a weaker set of transitions was observed, belonging to the ³⁵Cl/³⁷Cl isotopologue. The intensities of these transitions were about 2/3 of those of the parent species, in consistency with the natural

relative abundance of the two isotopes and the existence of two equivalent $^{35}\text{Cl}/^{37}\text{Cl}$ isotopologues. This confirmed the equivalence of the two Cl atoms, and consequently the C_s symmetry of the complex.

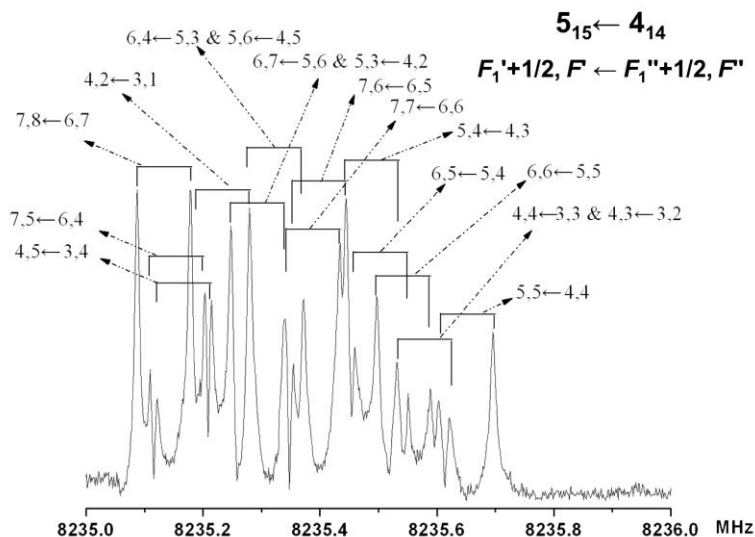


Figure 5.1 The recorded $5_{15} \leftarrow 4_{14}$ rotational transition of the parent species of the observed conformer of $\text{CH}_2\text{F}_2\text{-CH}_2\text{Cl}_2$, showing hyperfine structure originated by the two ^{35}Cl nuclei. Each component line exhibits Doppler doubling.

The frequencies were fitted with Pickett's SPFIT program.^[95] by direct diagonalization of the Hamiltonian consisting of Watson's "S" reduced semi-rigid rotor Hamiltonian^[8] in the I' representation, augmented by the hyperfine Hamiltonian which has been described in Chapter 4 (Eq. (4.1)). The obtained spectroscopic constants are summarized in Table 5.2.

No μ_b -type transitions have been observed in accordance with the C_s symmetry of the conformer. The C_s symmetry makes the two ^{35}Cl atoms of the parent species equivalent to each other, and correspondingly, their quadrupole coupling constants have the same values. As mentioned above, also for the $^{35}\text{Cl}/^{37}\text{Cl}$ isotopologue the μ_a -type spectrum has been assigned and measured in natural abundance. Its spectroscopic parameters are listed in the second column of Table 5.2. Here, the ^{35}Cl and ^{37}Cl nuclei are different from each other, and, in addition, the geometrical symmetry of the complex is destroyed, so that two different sets of quadrupole coupling constants are required. Since a smaller number of lines have been measured for this isotopologue, the d_1 and d_2 centrifugal distortion parameters are fixed at the values for the parent species, while the off-diagonal quadrupolar coupling constants χ_{ab} and χ_{ac} have been fixed at the theoretical values. We did not succeed in measuring at least four transitions of the $^{37}\text{Cl}/^{37}\text{Cl}$

isotopologue since its abundance is only ~10% of that of the parent species.

Table 5.2 Spectroscopic parameters of the two isotopologues of CH₂F₂-CH₂Cl₂.

	³⁵ Cl/ ³⁵ Cl	³⁵ Cl/ ³⁷ Cl
<i>A</i> /MHz	2663.073(3) ^[a]	2604.320(3)
<i>B</i> /MHz	958.4016(2)	951.1963(1)
<i>C</i> /MHz	785.1948(1)	775.4507(1)
<i>D</i> _{<i>J</i>} /kHz	0.7171(7)	0.710(1)
<i>D</i> _{<i>JK</i>} /kHz	10.813(6)	9.88(7)
<i>d</i> ₁ /kHz	-0.1604(7)	[-0.1604] ^[b]
<i>d</i> ₂ /kHz	-0.0613(4)	[-0.0613] ^[b]
χ_{aa} (³⁵ Cl)/MHz	37.399(5)	37.17(3)
$\chi_{bb}-\chi_{cc}$ (³⁵ Cl)/MHz	-43.68(2)	-42.34(3)
χ_{ab} (³⁵ Cl)/MHz	±9.00(7)	11.16 ^[c]
χ_{ac} (³⁵ Cl)/MHz	7.0(1)	8.43 ^[c]
χ_{bc} (³⁵ Cl)/MHz	∓49.71(6)	-50.03(2)
χ_{aa} (³⁷ Cl)/MHz		29.62(2)
$\chi_{bb}-\chi_{cc}$ (³⁷ Cl)/MHz		-35.44(2)
χ_{ab} (³⁷ Cl)/MHz		-7.52 ^[c]
χ_{ac} (³⁷ Cl)/MHz		6.19 ^[c]
χ_{bc} (³⁷ Cl)/MHz		39.23(1)
<i>N</i> ^[d]	349	160
σ ^[e] /kHz	2.9	3.1

[a] Uncertainties (in parentheses) are standard deviations expressed in units of the last digit. [b] Numbers in the brackets are fixed to the values obtained for the parent species. [c] Fixed to the values obtained from the theoretical calculation. [d] Number of lines in the fit. [e] Standard deviation of the fit.

The comparison of the experimental spectroscopic parameters with the theoretical values for the two conformations of Table 1, leads to a straightforward assignment of the observed spectrum to conformer **I**, the one stabilized by two C-H ···Cl-C and one C-H ···F-C WHBs.

We could not observe any lines belonging to conformer **II**, despite the very small complexation energy difference. This could be due to the conformational relaxation to the most stable conformer upon supersonic expansion. It has, indeed, been shown that this kind of relaxation takes place easily when the inter-conversion barrier is smaller than $2kT$.^[104]

5.3.3 Structural information

The C_s configuration of the observed conformer of $\text{CH}_2\text{F}_2\text{-CH}_2\text{Cl}_2$ is shown in Figure 5.2.

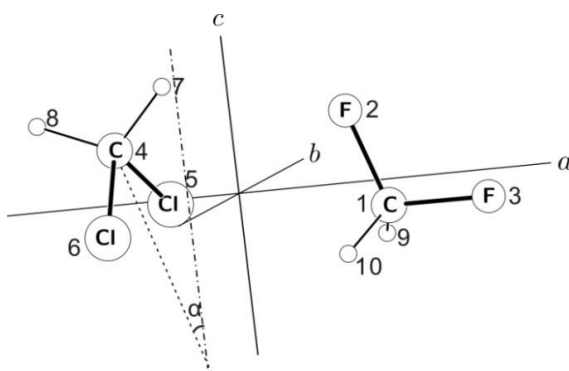


Figure 5.2 The observed conformer of $\text{CH}_2\text{F}_2\text{-CH}_2\text{Cl}_2$, with indicated atom numbering and the positions of the principal axes. α is the angle between the bisector of the ClCCl valence angle and the bc -plane.

Table 5.3 The experimental coordinates of the chlorine atoms in $\text{CH}_2\text{F}_2\text{-CH}_2\text{Cl}_2$.

	$a/\text{\AA}$	$b/\text{\AA}$	$c/\text{\AA}$
r_s	$\pm 1.399(1)^{[b]}$	$\pm 1.466(1)$	$0.223(7)$
$r_0^{[a]}$	-1.404	± 1.473	-0.239

[a] Calculated with the r_0 structure in Table 5.4, the signs of the b coordinates depend on the specific Cl atom due to the symmetry.

Table 5.4 Partial r_0 and r_e structures of $\text{CH}_2\text{F}_2\text{-CH}_2\text{Cl}_2$.

Fitted parameters			
	$R_{\text{ClC4}}/\text{\AA}$	$\angle \text{H7C4} \cdot \text{Cl} / ^\circ$	$\angle \text{F2C1} \cdot \text{C4} / ^\circ$
r_0	$3.755(1)^{[a]}$	$62.5(1)$	$55.7(1)$
r_e	3.751	63.5	50.4
Derived parameters			
	$R_{\text{F2H7}}/\text{\AA}$	$R_{\text{Cl5H9}}/\text{\AA}$	$(a/\sigma)^{[b]}$
r_0	$2.489(2)$	$3.147(2)$	$11.8(1)$
r_e	2.421	3.139	13.8

[a] Uncertainties (in parentheses) are expressed in units of the last digit. [b] The angle between the ClCCl plane and the bc inertial plane.

From the rotational constants of the two isotopologues, it is possible to calculate the substitution, r_s , coordinates^[16] of the Cl in the principal axes of the parent species. The obtained values are shown in Table 5.3, and are compared there with the values of a partial r_0 structure according to the adjustments in Table 5.4.

The partial r_0 structure, was obtained by adjusting three structural parameters (R_{C1C4} , $\angle H7C4 \cdots C1$ and $\angle F2C1 \cdots C4$), while keeping the remaining parameters fixed to their *ab initio* values (while preserving the C_s symmetry), in order to reproduce the six experimental rotational constants. The obtained parameters are reported in Table 5.4, and there compared to the *ab initio* values. From this partial r_0 structure, the lengths of the three WHBs have been derived, and reported in Table 5.4.

5.3.4 Quadrupole coupling constants

The nuclear quadrupole hyperfine structure considerably complicates the rotational spectrum but its analysis can provide useful information on the structure and internal dynamics in the complex. This becomes possible if the principal nuclear quadrupole tensor can be determined since for hyperfine nuclei terminal to a bond this tensor is known to be usually oriented to within 1 degree of the direction the relevant bond axis.^[122] The only three non-zero components of the principal hyperfine tensor, $\chi_g = eQq_g$, with $g = x, y, z$, can be obtained from the quadrupole tensor determined experimentally in the principal inertial axes. The latter consists of the diagonal χ_{aa} , χ_{bb} and χ_{cc} quadrupole coupling constants, and the off-diagonal χ_{ab} , χ_{bc} and χ_{ac} constants. Diagonalization of the corresponding 3x3 matrix results in three principal hyperfine tensor components χ_{zz} , χ_{xx} and χ_{yy} , conventionally labeled in such a way that χ_{zz} describes the molecular field gradient around the axis close to the bond axis, which is in this case the CCl axis.

We made the transformation by using the program QDIAG available on the PROSPE website,^[123-124] which also provides the rotation angles between the two axis systems. One of the more useful of these angles is θ_{zb} , which allows an estimate of the $\angle ClCCl$ valence angle from the relation $\angle ClCCl = (180 - 2 \theta_{zb})^\circ$. The quadrupole asymmetry parameter $\eta = (\chi_{xx} - \chi_{yy})/\chi_{zz}$ is also evaluated. These parameters are compared in Table 5.5 with those for the CH_2Cl_2 monomer. The differences do not appear to be significant, suggesting that vibrational averaging in the cluster has little effect on the chlorine nuclear quadrupole hyperfine splitting.

We can therefore use the quadrupole orientation to work out how much the ClCCl plane in the complex is tilted away from the bc -plane. This is quantified by means of the tilt angle α as defined in Figure 5.2. The hyperfine estimate of this angle obtained from QDIAG of $\alpha = 10.6(1)^\circ$ is close to the values from the *ab initio* geometry and from the partial r_0 structure providing

additional independent confirmation for the determined structure.

Table 5.5 The principal quadrupole tensors, η , θ and $\angle\text{ClCCl}$ of CH_2Cl_2 and $\text{CH}_2\text{F}_2\text{-CH}_2\text{Cl}_2$.

	CH_2Cl_2 ^[a]	$\text{CH}_2\text{F}_2\text{-CH}_2\text{Cl}_2$
χ_{zz}/MHz	-75.4(2)	-74.16(6)
χ_{xx}/MHz	33.4(2)	35.31(8)
χ_{yy}/MHz	39.9414(2)	38.85(7)
η ^[b]	0.060(3)	0.048(1)
θ ^[c] / °	33.43(5)	33.6(1)
$(\angle\text{ClCCl})$ ^[d]	113.1	112.7

[a] see Ref.[15]. [b] $\eta = (\chi_{xx} - \chi_{yy})/\chi_{zz}$. [c] This angle corresponds to θ_{za} for CH_2Cl_2 and θ_{zb} for $\text{CH}_2\text{F}_2\text{-CH}_2\text{Cl}_2$. [d] Estimate obtained from $180-2\theta$, comparing with $\angle\text{ClCCl}=111.8^\circ$ from the structural analysis for the monomer [15].

5.3.5 Dissociation energy

The intermolecular stretching motion which leads to the dissociation appears to be almost parallel to the a -axis of the complex. By assuming that such a motion is separated from the other molecular vibrations, it is possible in this case, within the pseudo diatomic approximation, to estimate the stretching force constant through Eq. (1.18)^[17] Then the intermolecular dissociation (Eq. (1.19)) has been evaluated to be $E_D = 7.6 \text{ kJ mol}^{-1}$.^[18]

Table 5.6 Binding energies of the investigated dimers of freons.

	WHBs	$E_D/\text{kJ mol}^{-1}$	Ref.
$\text{CH}_3\text{F} \cdots \text{CHF}_3$	three C-H \cdots F-C	5.3	13
$\text{CH}_2\text{F}_2 \cdots \text{CH}_2\text{F}_2$	three C-H \cdots F-C	8.7	10
$\text{CH}_2\text{ClF} \cdots \text{FHC}=\text{CH}_2$	one C-H \cdots Cl-C	8.7	14
	one C-H ₂ \cdots F-C		
$\text{CH}_2\text{F}_2 \cdots \text{CH}_2\text{Cl}_2$	two C-H \cdots Cl-C	7.6	this work
	one C-H \cdots F-C		

In Table 5.6, we compare the dissociation energy of $\text{CH}_2\text{F}_2\text{-CH}_2\text{Cl}_2$ to those of some related adducts among freon molecules. It appears, on the average, that the C-H \cdots Cl interaction is stronger than the C-H \cdots F one.

5.4 Chlorotrifluorometane...Fluoromethane

It has been found, for example, that CF_4 forms a trifurcated HaB with water ($\text{CF}_3 \cdots \text{O}$)^[81] and with pyridine ($\text{CF}_3 \cdots \text{N}$),^[113] while strong dynamic effects considerably alter the values of the “rigid rotor limit” rotational constants. In addition, $\text{CF}_4\text{-H}_2\text{O}$, which is expected to be a classical asymmetric top, is found to be a quantum-mechanical symmetric top, instead. A good, somehow prototype molecule, to investigate HaB has been found to be CF_3Cl , which Cl atom forms very easily HaBs. CF_3Cl forms, indeed, a C-Cl $\cdots \text{O}$ HaB with H_2O ^[82] and dimethyl ether^[125] and the C-Cl $\cdots \text{N}$ HaB with NH_3 .^[112] Also in the cases of $\text{CF}_3\text{Cl-H}_2\text{O}$ and $\text{CF}_3\text{Cl-NH}_3$, strong dynamic effects have been observed: water and ammonia undergo effective free rotations with respect to the CF_3Cl , making the complex $\text{CF}_3\text{Cl-H}_2\text{O}$ an effective symmetric top. In the case of $\text{CF}_3\text{Cl-dimethylether}$, the free internal rotation of the CF_3 group causes an unexpectedly large value of the rotational constant A .

After having characterized the C-Cl $\cdots \text{O}$ and the C-Cl $\cdots \text{N}$ HaBs using CF_3Cl as “halogen donor”, we decided to describe the C-Cl $\cdots \text{F}$ halogen-halogen bond by studying the rotational spectrum of $\text{CF}_3\text{Cl-FCH}_3$, that is the molecular adduct formed by Freon-13 and Freon-41. This 1:1 complex has been recently investigated using FTIR and Raman spectroscopy in the liquid krypton.^[126] The authors discussed the existence of the C-Cl $\cdots \text{F}$ HaB, mainly based on their *ab initio* calculations. We believe that precise experimental information on the structure and internal dynamics can be supplied by the rotational spectrum. Below we report the obtained results.

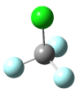
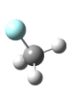
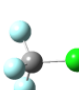
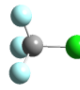
5.4.1 Theoretical calculations

MP2/aug-cc-pVDZ(-PP) *ab initio* calculations of $\text{CF}_3\text{Cl-FCH}_3$, is reported in ref.^[126]. The authors present only one conformation, and do not report any spectroscopic constant useful for the MW investigation. For this reason, we performed our own calculations. We preliminarily explored the conformational space of the complex by Molecular Mechanics, using conformational search algorithms implemented in MacroModel 9.2 within the MMFFs force field.^[15] We found about 100 different geometries within an energy window of about 15 kJ mol^{-1} which, at the MP2/6-311++G(d,p) level^[14] converged to 4 most stable conformers (relative energies $\Delta E < 2 \text{ kJ mol}^{-1}$). All these four conformers are characterized by the C-X $\cdots \text{F}$ (X = F or Cl) HaBs.

Also C-H $\cdots \text{F}$ WHBs contribute to the stabilities of conformer I and II. Vibrational frequency calculations at the same level of theory proved conformer I, II and III to be real

minima while a negative frequency was found for conformer IV. However, when taking account BSSE corrections,^[12] conformer IV becomes – surprisingly – the one with the lowest energy. Shapes, relative energies, BSSE dissociation energies (E_D), calculated rotational constants, dipole moment components and ^{35}Cl quadrupole coupling constants of the four conformers are summarized in Table 5.7.

Table 5.7 MP2/6-311++G(d,p) shapes and spectroscopic parameters of the four most stable conformers of $\text{CF}_3\text{Cl}-\text{CH}_3\text{F}$

	I	II	III	IV
				
$\Delta E/\text{kJ mol}^{-1}$	0.0 ^[a]	0.9	1.0	1.3
$\Delta E_0/\text{kJ mol}^{-1}$	0.0 ^[b]	1.2	0.7	0.5
$\Delta E_{\text{BSSE}}/\text{kJ mol}^{-1}$	2.7	3.6	0.3	0.0 ^[c]
$E_D/\text{kJ mol}^{-1}$	1.8	0.8	4.2	4.5
A/MHz	3028	4708	4788	5512
B/MHz	1256	976	691	611
C/MHz	1058	948	678	611
μ_a/D	-0.9	0.2	-1.6	-3.2
μ_b/D	-0.1	-1.2	-1.8	0.0
μ_c/D	1.2	1.4	1.0	0.0
χ_{aa}/MHz	37.4	-69.9	-70.2	-74.3
$(\chi_{bb}-\chi_{cc})/\text{MHz}$	-109.9	-0.7	-4.2	0.0
χ_{ab}/MHz	-10.2	-18.2	20.3	0.0
χ_{ac}/MHz	0.1	-0.5	-0.4	0.0
χ_{bc}/MHz	1.7	-0.1	0.0	0.0

[a] Absolute energy: -936.076714 E_h . [b] Absolute energy: -936.113783 E_h . [c] Absolute energy: -936.130914 E_h .

5.4.2 Rotational spectra

Following extensive spectral searches for the various conformers, we could identify, based on their ^{35}Cl quadrupole pattern, the $6_{06}\leftarrow 5_{05}$, $7_{07}\leftarrow 6_{06}$, and $8_{08}\leftarrow 7_{07}$ transitions of conformer III. After that, we had some difficulties with the assignment of the corresponding $K_1 = 1$ transitions. We could finally identify these six transitions, still again from the ^{35}Cl quadrupole pattern, which is shown in Figure 5.3 for the $6_{15}\leftarrow 5_{14}$ transition. However, their insertion in the fitting produced

an unexpectedly high value of the rotational constant A . We will see in a following section that this effect is due to the almost free internal rotations of the CF_3 and CH_3 tops.

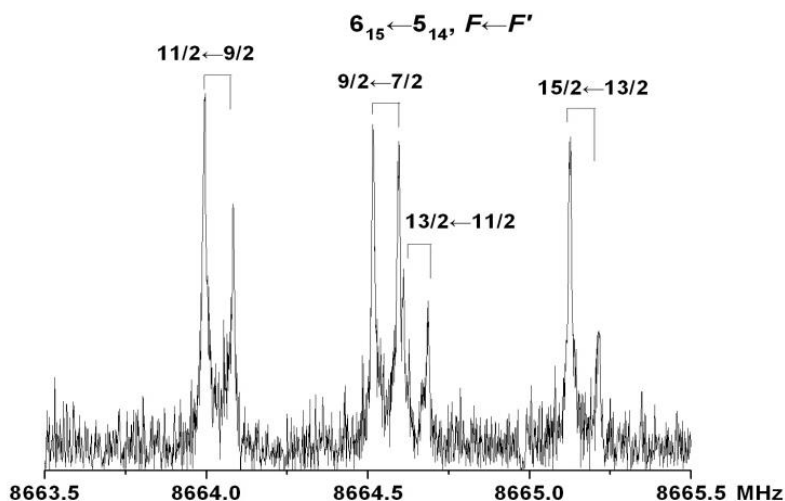


Figure 5.3 ^{35}Cl quadrupole hyperfine structure of the $6_{15} \leftarrow 5_{14}$ transition of $\text{CF}_3^{35}\text{Cl}-\text{CH}_3\text{F}$. Each line appears as a doublet (□) due to the Doppler effect.

It was then possible to assign the $K_{-1} = 0, 1$ transitions for all the J values from 5 to 12. The observed transition lines were fitted using Pickett's SPFIT program^[95] (with the S reduction and I' representation^[8]) according to the Hamiltonian Eq. (4.1). The obtained spectroscopic parameters are summarized in the first column of Table 5.8.

As one can see, the rotational constants B and C as well as the quadrupole coupling constants match best the corresponding theoretical values of conformer III. Vice versa, as previously outlined, the rotational constant A is 4-5 times larger than the theoretical value.

We could then assign the rotational spectrum of the ^{37}Cl isotopologue in natural abundance. Its transitions are just a few MHz lower in frequency than those of the parent species. This is in agreement with the fact that the Cl lies very close to the adduct's centre of mass. The assignment of the spectrum was facilitated by two factors: (i) the quadrupolar splittings, which are about 80% of those of the ^{35}Cl isotopologue (according to the ratio of the electric nuclear quadrupole moments Q); (ii) the intensity of the lines, which is about one third of that of the parent species. The obtained spectroscopic constants are listed in the second column of Table 5.8.

Finally, we measured the rotational spectra of the two isotopologues (^{35}Cl and ^{37}Cl) in which CH_3F is replaced by CD_3F . The results of the fittings are reported in the two right columns

of Table 5.8. The rotational constants A for both deuterated isotopologues are much smaller than those of the CH_3F species.

Table 5.8 Experimental spectroscopic constants of $\text{CF}_3\text{Cl}-\text{CH}_3\text{F}$

	$\text{CF}_3^{35}\text{Cl}-\text{CH}_3\text{F}$	$\text{CF}_3^{37}\text{Cl}-\text{CH}_3\text{F}$	$\text{CF}_3^{35}\text{Cl}-\text{CD}_3\text{F}$	$\text{CF}_3^{37}\text{Cl}-\text{CD}_3\text{F}$
A/MHz	21826(28) ^[a]	21573(64)	17264(35)	17079(39)
B/MHz	728.2164(3)	728.1154(2)	685.7804(4)	685.7554(4)
C/MHz	702.9987(3)	702.7130(3)	658.9718(4)	658.7455(4)
D_y/kHz	0.9363(8)	0.929(3)	0.961(1)	0.956(2)
D_{JK}/MHz	-0.2376(2)	-0.2360(3)	-0.1483(3)	-0.1469(4)
d_1/kHz	-0.1052(6)	[-0.1052] ^[b]	-0.1279(9)	[-0.1279] ^[b]
χ_{aa}/MHz	-73.3(1)	-58.1(2)	-72.3(2)	-57.1(2)
$\chi_{bb}-\chi_{cc}/\text{MHz}$	-5.2(3)	-4.3(4)	-6.4(4)	-5.2(4)
χ_{ab}/MHz	29.0(7)	22(1)	26(1)	18.7(9)
$N^{[c]}$	80	52	64	56
$\sigma^{[d]}/\text{kHz}$	2.9	1.7	1.9	2.4

[a] Error in parenthesis is expressed in units of the last digit. [b] Fixed at the value of the ^{35}Cl isotopologue. [c] Number of transitions in the fit. [d] Standard deviation of the fit.

5.4.3. Molecular structure

In the observed conformer (see Figure 5.4, where the inertial principle axes system and the atom numbering are also shown), the angles $\angle\text{C1Cl2F6}$ and $\angle\text{Cl2F6C7}$ have the *ab initio* values, 173.8° and 118.7° , respectively. By adjusting the value of $\angle\text{Cl2F6C7}$ to 105.7° , we could satisfactorily reproduce the rotational constants B and C of all isotopologues.

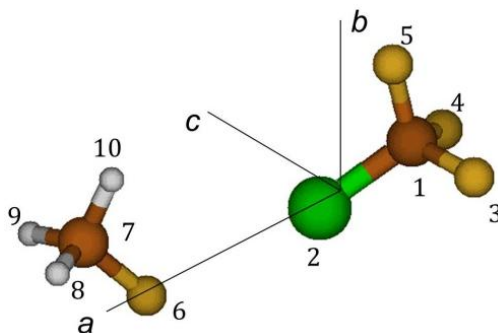


Figure 5.4 Shape, atomic numbering, and principal axes of the observed configuration of $\text{CF}_3\text{Cl}-\text{CH}_3\text{F}$.

5.4.4 Internal dynamics

Back to the aforementioned disagreement of the rotational constant A between the fitted values and the calculated values, the enormously large discrepancies can be, as in CF_3Cl -dimethyl ether,^[125] accounted by the effects of a free (or almost free) internal rotation of the CF_3 and CH_3 groups about their symmetry axes. We could explain it qualitatively if we take into account the effective rotational constants of the ground state ($\nu = 0$, $\sigma = 0$) and assuming no perturbation between the two free internal motions, according to:^[127]

$$\begin{aligned} A_{00} &= A_r + [W_{00}^{(2)} F\rho_a^2]_{\text{CF}_3} + [W_{00}^{(2)} F\rho_a^2]_{\text{CH}_3} \\ B_{00} &= B_r + [W_{00}^{(2)} F\rho_b^2]_{\text{CF}_3} + [W_{00}^{(2)} F\rho_b^2]_{\text{CH}_3} \\ C_{00} &= C_r + [W_{00}^{(2)} F\rho_c^2]_{\text{CF}_3} + [W_{00}^{(2)} F\rho_c^2]_{\text{CH}_3} \end{aligned} \quad (5.1)$$

where A_r , B_r and C_r are the “rigid” rotational constants in the limit of both infinite barriers. The $W_{00}^{(2)}$ are the Hersbach's barrier-dependent perturbation sums relative to the sublevels of the A-symmetry ($\sigma = 0$) species of the torsional ground state ($\nu = 0$) with $\rho_g = \lambda_g I_\alpha / I_g$ depending on the moments of inertia along the symmetry axis α of the internal rotor and the principal axis g and their directional cosine λ_g . $F = \hbar / [2 (1 - \sum_g \lambda_g I_\alpha / I_g) I_\alpha]$ is the reduced constant of the motion. Tables of the $W_{00}^{(n)}$ as a function of the reduced barrier s are available.^[127] The parameter s is, in turn, related to the V_3 barrier according to: $V_3 = 0.215 s F$.

Table 5.9 Values of the $F\rho_g^2$ parameters for the CF_3 and $-\text{CH}_3$ (or CD_3) tops of the four isotopologues of $\text{CF}_3\text{Cl-CH}_3\text{F}$

		$\text{CF}_3^{35}\text{Cl-CH}_3\text{F}$	$\text{CF}_3^{37}\text{Cl-CH}_3\text{F}$	$\text{CF}_3^{35}\text{Cl-CD}_3\text{F}$	$\text{CF}_3^{37}\text{Cl-CD}_3\text{F}$
CF ₃	$F\rho_a^2/\text{MHz}$	17074.0	16932.5	13082.5	12973.4
	$F\rho_b^2/\text{MHz}$	16.7	16.6	14.7	14.6
CH ₃	$F\rho_a^2/\text{MHz}$	17.6	17.6	35.7	35.5
	$F\rho_b^2/\text{MHz}$	3.0	3.0	5.2	5.2

In Table 5.9 we report the values of the $F\rho_g^2$ parameters ($g = a, b$) of the two tops for the four isotopologues. By inspection of Figure 5.4, the c -axis of the complex is perpendicular to the internal rotation axis of both the CH_3 and CF_3 tops. Then λ_c , ρ_c and $F\rho_c^2$ are zero, and the rotational constant C is not affected by the internal rotations of the two tops. On the other hand, one can see that the $F\rho_a^2$ values for the CF_3 groups, which alter the rotational constants A with respect to their “rigid” values, are three orders of magnitude larger than any other term. In

addition, their magnitudes, decreasing from $\text{CF}_3^{35}\text{Cl}-\text{CH}_3\text{F}$ to $\text{CF}_3^{37}\text{Cl}-\text{CD}_3\text{F}$ follow the magnitudes of the A rotational constants.

Since $-\text{CF}_3$ has a much larger reduced mass than $-\text{CH}_3$, with much larger value of the term $F\rho_g^2$, the contribution to the rotational constants from the internal rotation of $-\text{CH}_3$ becomes negligible. Similar situation applies to the rotational constant B , where the angle between the internal rotation axis of CF_3 and the principal axis b are almost 90° according to the *ab initio* geometry. The rotational constants A are much more strongly affected by the free internal rotation of CF_3 due to the near linearity of a -axis with the internal rotation axis of CF_3 .

By applying the differences between the model calculated (after the above mentioned structural adjustment, $A_r = 4647, 4639, 4444$ and 4436 MHz, for the four isotopologues, respectively) and the experimental values of A (see Table 5.8) to Eq (2), one could calculate the barrier to the internal rotation of CF_3 . All four isotopologues give $W_{00}^{(2)}$ a value of 1.0 which corresponding a very small internal rotational barrier, $V_3 \approx 7 \text{ cal mol}^{-1}$.

This value of $W_{00}^{(2)}$ can also interpret the near zero values of the inertial defects, which should be, in the rigid approximation $\Delta_c = -91.7$ or $-95.0 \text{ u}\text{\AA}^2$, for the CH_3 and CD_3 forms, respectively.

5.5 Difluoromethane...Formaldehyde

As mentioned in Section 5.3, CH_2F_2 has two sites which can act as weak proton acceptor and two sites which are weak proton donors. 3, 9 and 16 C-H...F-C WHBs have been found to stabilize the dimer^[115], the trimer^[116] and the tetramer^[117] of CH_2F_2 , respectively. The complex $\text{CH}_2\text{F}_2 \cdots \text{H}_2\text{O}$ has been investigated by free jet millimeter wave spectroscopy^[79] and FTMW spectroscopy.^[80] Besides a main O-H...F H-bond, it is stabilized by a bifurcated O...H₂C WHB. In the case of $\text{CH}_2\text{F}_2 \cdots \text{oxirane}$, the rotational spectrum of the complex corresponds to a configuration with one O...H₂C and one F...H₂C₂ WHBs.^[128] A single C-H...O WHB characterizes the shape of $\text{CH}_2\text{F}_2 \cdots \text{OCS}$, while the S atom embraces the two F atoms, reminding the HaB interactions.^[129]

Apart from the examples mentioned above, concerning CH_2F_2 , this kind of WHB appears every time we consider adducts involving partially halogenated hydrocarbons. Three C-H...F-C WHBs characterize $\text{CHF}_3 \cdots \text{CH}_3\text{F}$,^[118] while two C-H...F-C and one C-H...O WHBs constitute small cages in $\text{CHF}_3 \cdots \text{oxirane}$,^[130] $\text{CHF}_3 \cdots \text{cyclobutanone}$ ^[131] and $\text{CHF}_3 \cdots \text{dioxane}$.^[132] A $\text{CHF}_3 \cdots \pi$ WHB stabilizes $\text{CHF}_3 \cdots \text{benzene}$.^[133] However, when perhalogenated hydrocarbons are involved, only HaB linkages have been observed.^[7] This is the case, for example, of $\text{CF}_4 \cdots \text{H}_2\text{O}$,^[81]

CClF₃ ··H₂O^[82] and CClF₃ ··NH₃.^[78]

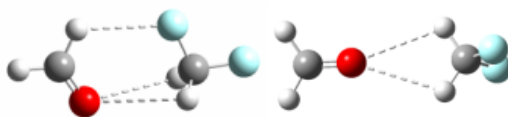
Coming back to the adducts of CH₂F₂ with small molecules, in the case of CH₂F₂ ··H₂O, a doubling of the rotational transitions was observed, due to the internal rotation of water around its symmetry axis, which allowed for the determination of the corresponding potential energy function. The replacement in such a complex of water with formaldehyde (H₂CO) rises two interesting points: (i) will H₂CO form the same network of WHBs as water? (ii) if yes, will the internal rotation of H₂CO (heavier than H₂O) still generate measurable splittings? Here we present the results of the rotational investigation of the complex of CH₂F₂ with formaldehyde, CH₂F₂ ··H₂CO.

5.5.1 Theoretical calculations

Some theoretical calculations were performed to have a clue on the configurations of the complex. According to the conformational search with the program MacroModel 9.2,^[15] four plausible stationary points have been found for CH₂F₂ ··H₂CO.

Table 5.10 MP2/6-311++G(d,p) spectroscopic parameters of the plausible conformers of CH₂F₂ ··H₂CO.

	I	II
<i>contacts</i>	C-H ··F-C & CH ₂ ··O	2 CH ₂ ··O
$\Delta E/\text{cm}^{-1}$	0 ^[a]	293
$\Delta E_{\text{BSSE}}/\text{cm}^{-1}$	0 ^[b]	128
<i>A, B, C /MHz</i>	13898, 1766, 1584	10168, 1307, 1176
$ \mu_a , \mu_b , \mu_c /\text{D}$	2.5, 0.4, 0.0	4.9, 0.0, 0.0
D_J/kHz	1.86	1.97
D_{JK}/MHz	0.013	1.44
D_K/MHz	-0.39	1.35
d_1/kHz	-0.20 ^[c]	0.21 ^[d]
d_2/kHz	-0.02 ^[c]	709 ^[d]
$P_{\text{cc}}/\text{u}\text{\AA}^2$	1.74	3.31



[a] Absolute energy: -352.782020 E_h . [b] Counterpoise corrected energy: the absolute value is -352.780316 E_h . [c] S-reduction. [d] A-reduction.

Full geometry optimizations of these configurations were carried out at the MP2/6-311++G(d,p) level.^[13] Frequency calculations proved only two conformers to be real minima, and provided the spectroscopic constants given in Table 5.10. Counterpoise corrections^[12] were calculated in order to remove the well-known BSSE. The global minimum (configuration *I*) formed through three WHBs is about 128 cm⁻¹ lower in energy than configuration *II*, with two WHBs. The calculated values of the dipole moment components suggest that μ_a -type lines should be very intense. The values of the planar moment of inertia P_{cc} which give an indication on the degree of the planarity of the conformations are also reported in Table 5.10.

5.5.2 Rotational spectra

Following the *ab initio* indications, we started our spectral scans searching for the μ_a -type *R* branch transitions of conformer I, which were rapidly identified. After a first refinement of the spectroscopic constants, we were able to measure some μ_b -type lines. Each transition appeared as a doublet, with relative intensity of the two component lines of about 1:3. This ratio corresponds to the statistical weight expected for the internal rotation around the C_{2v} axis of a top like H₂CO, with the exchange of a pair of equivalent fermions with spin $I = 1/2$.

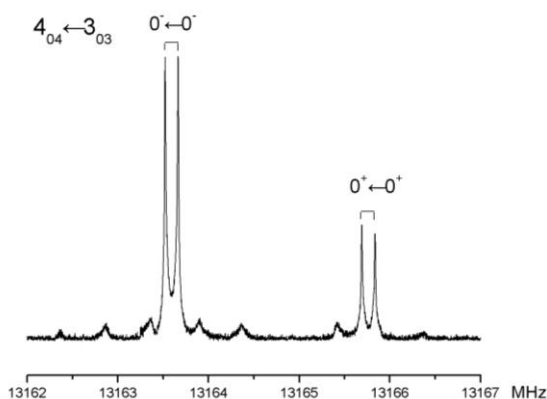


Figure 5.5 0^+ and 0^- component lines of the $4_{04} \leftarrow 3_{03}$ transition of CH₂F₂ · H₂CO.

Using Pickett's SPFIT computer program,^[95] the rotational transition frequencies were fitted by the Hamiltonian (Eq. (4.2)). Watson *S*-reduction and *I'*-representation have been adopted.^[8] The transition frequencies of the two tunneling components did not show any appreciable interaction between the two states, so that it was not possible to determine parameters such as ΔE (the energy difference between the two states), or Coriolis' coupling terms.

The fitted rotational constants, centrifugal distortional constants, and planar moment of inertia P_{cc} , listed in Table 5.11, match the theoretical values only for configuration I. In addition, the observation of μ_b -type lines discards the assignment to conformer II, by symmetry reasons. So the conformation assignment is straightforward. The two component lines, due to the internal rotation of H_2CO , are shown in Figure 5.5 for the $4_{04} \leftarrow 3_{03}$ transition.

After a first structural adjustment, it has been possible to assign the spectra of the two ^{13}C isotopologues in natural abundance. However, only the most intense lines belonging to the 0^- state could be measured for both isotopologues. The determined parameters of the ^{13}C species are listed in the right columns of Table 5.11. In spite of a careful search, no transitions corresponding to conformer II were detected.

Table 5.11 Spectroscopic constants of three isotopologues of $\text{CH}_2\text{F}_2 \cdot \text{H}_2\text{CO}$ (S -reduction, F representation).

	$\text{CH}_2\text{F}_2\text{-H}_2\text{CO}$ (0^+)	$\text{CH}_2\text{F}_2\text{-H}_2\text{CO}$ (0^-)	$^{13}\text{CH}_2\text{F}_2\text{-H}_2\text{CO}$ (0^-)	$\text{CH}_2\text{F}_2\text{-H}_2^{13}\text{CO}$ (0^-)
A/MHz	13725.398(3) ^[a]	13719.351(3)	13675(2)	13671(2)
B/MHz	1737.258(1)	1736.720(1)	1731.0654(8)	1698.7766(8)
C/MHz	1559.247(1)	1559.218(1)	1554.1606(8)	1528.0736(8)
D_J/kHz	2.33(1)	2.33(1)	2.29(2)	2.22(2)
D_{JK}/kHz	21.25(5)	20.78(5)	[20.78] ^[b]	[20.78]
d_1/kHz	-0.24(1)	-0.23(1)	[-0.23]	[-0.23]
d_2/kHz	0.029(6)	0.022(6)	[0.022]	[0.022]
$P_{cc}/\text{u}\text{\AA}^2$	1.69	1.93	1.86	1.87
$\sigma^{\text{[c]}}/\text{kHz}$	2.6	2.1	4.9	3.0
$N^{\text{[d]}}$	23	23	9	9

[a] Errors in parenthesis are expressed in units of the last digit. [b] Values in brackets have been fixed to the values of the 0^- state of the “normal” (i.e. most abundant) species. [c] Standard deviation of the fit. [d] Number of fitted lines.

5.5.3. Molecular structure

The observed configuration is schematically shown in Figure 5.6, together with the parameters defining the WHB interaction. The P_{cc} values of the three isotopic species, reported in Table 5.11, are quite close to that of isolated CH_2F_2 corresponding to the two out-of-plane methylenic hydrogens of CH_2F_2 ($P_{cc} = 1.652 \text{ u}\text{\AA}^2$).^[134] The H_2CO moiety lies in the FCF plane of CH_2F_2 , similarly to water in $\text{CH}_2\text{F}_2 \cdot \text{H}_2\text{O}$.^[80] The two subunits are linked through a C-H $\cdot \cdot$ F-C bond and a bifurcated $\text{CH}_2 \cdot \cdot$ O bond.

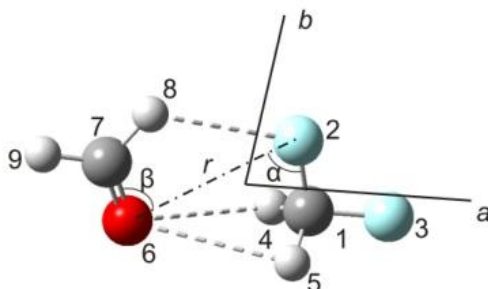


Figure 5.6 Sketch of the observed conformer of $\text{CH}_2\text{F}_2 \cdots \text{H}_2\text{CO}$ with atom numbering, some structural parameters used through the text, and principal axes of inertia.

From the rotational constants of the parent and of the two ^{13}C - species, we obtained the r_s substitution coordinates^[16] of the carbon atoms, which are shown in Table 5.12. The c -coordinates have been fixed to zero by symmetry.

Table 5.12 r_s coordinates of the carbon atoms of $\text{CH}_2\text{F}_2 \cdots \text{H}_2\text{CO}$.

		$a/\text{\AA}$	$b/\text{\AA}^a$
$\text{C}_{\text{CH}_2\text{F}_2}$	exptl.	$\pm 0.965(3)^{[a]}$	$\pm 0.370(8)$
	calc. ^[b]	-0.982	-0.324
$\text{C}_{\text{H}_2\text{CO}}$	exptl.	2.551(1)	0.389(8)
	calc.	2.572	0.320

[a] Uncertainties (in parentheses) are expressed in units of the last digit. [b] Calculated with the r_0 structure of Table 5.13.

Table 5.13 Partial r_0 geometry of $\text{CH}_2\text{F}_2 \cdots \text{H}_2\text{CO}$.

Fitted parameters			
	$r_{\text{H8} \cdots \text{F2}}/\text{\AA}$	$\angle \text{C7H8} \cdots \text{F2}/^\circ$	$\angle \text{H8} \cdots \text{F2C1}/^\circ$
r_0	2.658(1)	113.6(1)	113.4(1)
r_e	2.583	114.3	114.6
Derived parameters (see Figure 1)			
	$r/\text{\AA}$	$\alpha/^\circ$	$\beta/^\circ$
r_0	3.132(1)	73.6(1)	85.0(1)
r_e	3.096	74.1	83.6

They are in good accord with the calculated values of conformer I. In order to have a structure able to satisfactorily reproduce the experimental rotational constants, we modified some

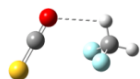
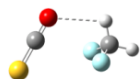
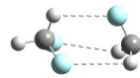
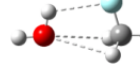
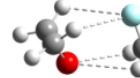
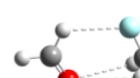
structural parameters involving the WHBs. The optimized parameters can be considered as constituting a partial r_0 structure, and are reported in Table 5.13.

5.5.4 Dissociation energy

The intermolecular stretching motion appears to be almost parallel to the a -axis of the complex (see Fig. 5.6). In this case, assuming such a motion to be separated from the other molecular vibrations, its force constant (k_s) can be estimated with Eq. (1.18).^[17] The R_{CM} is determined to be 3.65 Å from the r_0 structure. The value $k_s = 9.3 \text{ Nm}^{-1}$ corresponding to a harmonic stretching frequency of 88 cm^{-1} has been obtained. The dissociation energy (E_D) has been, according to Eq. (1.21), evaluated to be 10.4 kJ mol^{-1} .^[18]

The dissociation energies of the above mentioned complexes of CH_2F_2 , calculated with the same approximation, are given in Table 5.14.

Table 5.14 Pseudo-diatomic binding energies of some complexes of CH_2F_2

Molecular complex		$E_D/\text{kJ mol}^{-1}$	Ref.
$\text{CH}_2\text{F}_2 \cdots \text{OCS}$		2.1	8
$(\text{CH}_2\text{F}_2)_2$		6.6	3
$\text{CH}_2\text{F}_2 \cdots \text{H}_2\text{O}$		7.5	5
$\text{CH}_2\text{F}_2 \cdots \text{C}_2\text{H}_4\text{O}$		9.6	7
$\text{CH}_2\text{F}_2 \cdots \text{H}_2\text{CO}$		10.4	This work

The dissociation energy appears to be roughly proportional to the number of WHB interactions present in the complex: $\text{CH}_2\text{F}_2 \cdots \text{OCS}$, with a single WHB, is considerably more labile than the remaining adducts.

5.5.5 Internal rotation of H_2CO in the complex

The vibrational energy spacing between the two tunneling states (ΔE) is a key parameter to picture the potential pathway for a tunneling motion. But, as mentioned above, it is not possible

to determine ΔE from the fitting to the measured rotational transitions. However, the shifts of the planar moments of inertia ΔP_{aa} , ΔP_{bb} and ΔP_{cc} between the 0^+ and 0^- states can be utilized for this purpose, as shown, for example, in the case of $\text{CH}_2\text{F}_2 \cdot \text{H}_2\text{O}$.^[80]

Meyer's one dimensional flexible model^[11] provides energies and wave-functions for $J = 0, 1, 2$ in the ground and vibrational excited states. From these data the rotational and centrifugal distortion constants can be calculated. The following potential energy function, which is suitable for two equivalent periodic minima, has been adopted,

$$V(\tau) = 1/2 V_2 [1 - \cos(2 \tau)] \quad (5.2)$$

Here V_2 and τ are the potential barrier and the dihedral angle, $\tau = \text{H8C7-O6F2}$. $\tau = 0^\circ$ corresponds to the equilibrium value with H_2CO lying in the FCF plane.

Table 5.15 Flexible model results and potential energy parameters for the internal rotation of formaldehyde in $\text{CH}_2\text{F}_2 \cdot \text{H}_2\text{CO}$.

1) Experimental and calculated data		
	Exptl.	Calc.
$\Delta P_{aa}/\text{u}\text{\AA}^2$	0.040	0.039
$\Delta P_{bb}/\text{u}\text{\AA}^2$	-0.034	-0.030
$\Delta P_{cc}/\text{u}\text{\AA}^2$	0.050	0.050
$\Delta E/\text{MHz}$	-	3411
2) Model parameters		
	$V_2 = 180(10)^{[a]} \text{ cm}^{-1}$	$\Delta\beta = 2.6(5)^\circ$
	$\Delta r(\text{O6} \cdot \text{F2}) = 0.027\text{\AA}^{[b]}$	$\Delta\alpha = -1.4^{\text{ob}}$

[a] Uncertainties in parentheses are given in units of the last digit. [b] Fixed to the *ab initio* values.

The structural relaxations of the $r_{\text{O6} \cdot \text{F2}}$ distance and of the $\angle \text{C7O6} \cdot \text{F2}$ and $\angle \text{O6} \cdot \text{F2C1}$ angles (abbreviated below as β and α) as functions of τ were also required for the model, according to the following relations:

$$\beta(\tau) = 85.0 + \Delta\beta/2 [1 - \cos(2 \tau)] \quad (5.3)$$

$$r(\tau)/\text{\AA} = 3.132 + \Delta r/2 [1 - \cos(2 \tau)] \quad (5.3')$$

$$\alpha(\tau) = 73.6 + 1/2 \Delta\alpha [1 - \cos(2 \tau)] \quad (5.3'')$$

However, due to the lack of experimental data, Δr and $\Delta\alpha$ have been fixed at the theoretical

values (0.027 Å and -1.4 °, respectively). Eight vibrational states were calculated from the model potential optimization on a grid of 67 mesh points in the range $0 \leq \tau \leq 2\pi$ with the results for the fitted shifts in the planar moments reported in Table 5.15.

The experimental value of the barrier ($V_2 = 180 \text{ cm}^{-1}$) is very close to the *ab initio* predicted value (192 cm^{-1}). And the energy splitting between the two vibrational states has been calculated as 3411 MHz.

5.6 Trifluoromethane···Benzene

Rotational spectroscopy is especially suitable to quantitatively describe these fine structural effects. Already in 1961 Constain and Srivastava, from the low resolution microwave spectrum of formic acid-trifluoroacetic acid,^[135] observed an increase of the O···O distances upon H→D isotopic substitution of the hydrogen atoms involved in the HB. Precise quantitative values of this effect effects have been supplied this year in a PJFTMW investigation of the conformers of the bimolecule formic acid-acrylic acid.^[136]

As to the reverse Ubbelohde effect, several MW investigations are available. In 1976 Penn and Olsen showed, with the investigation of many isotopologues of 2-aminoethanol, that the O···N distance between the two heavy atoms involved in the O-H···N intramolecular hydrogen bond decreases of 0.0057 Å upon H→D substitution of the hydroxyl group.^[137] Analogous shrinkages have been evaluated from the rotational spectra of molecular complexes with the two subunits held together by a O-H···O hydrogen bond, such as the dimer of *tert*-butyl alcohol,^[138] the dimer of isopropanol,^[139] and the adducts of some alcohols with some ethers.^[140-143]

No data are available on the effects of the H→D isotopic substitution of the hydrogen atom involved in a WHB. A C-H··· π interaction links the trifluoromethane (HCF₃) and benzene (Bz) units in the Bz-CHF₃ complex, as proved by its rotational spectrum.^[133] To verify the appearance of the Ubbelohde effect within WHB linkages, we decided to investigate the rotational spectrum of its Bz-DCF₃ isotopologue, and of the ¹³C species of both Bz-HCF₃ and Bz-DCF₃ forms. The obtained data are reported below, and we will see that they prove the existence of the Ubbelohde effect also in the case of WHB's.

5.5.1 Rotational spectrum

After we applied empirical corrections to the rotational constants calculated with the geometry reported in the previous study on the most abundant species,¹² five evenly spaced bands with the features of a symmetric top were observed.

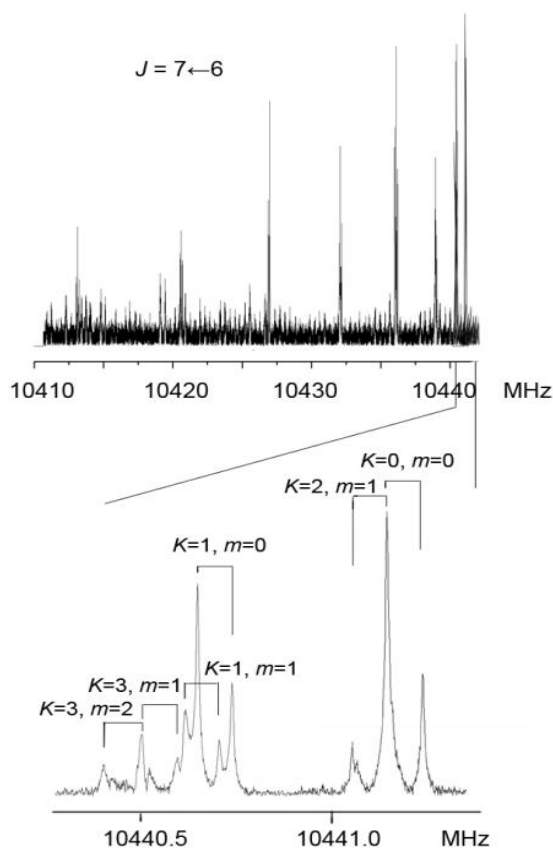


Figure 5.7 The $J = 7 \leftarrow 6$ band of Bz-DCF_3 (upper trace). The high-resolution details (lower trace) show the complex patterns due to free internal rotation. Each rotational transition, split by the Doppler effect (\square), is labeled with the quantum numbers K and m .

In Figure 5.7 we report the $J = 7 \leftarrow 6$ band, which, similarly to the case of parent species, shows the complex pattern that arises from the free internal rotation of DCF_3 with respect to Bz . Each rotational transition resulted to lie at a frequency higher than that of the corresponding transition of the parent species (see Figure 5.8), so immediately showing the presence of the Ubbelohde effect.

The measured transition frequencies could easily be fitted with Eq. (5.4), which is valid for a symmetric top with a free internal rotation.^[133, 144-145]

$$\begin{aligned} \nu = & 2(J+1)[B-D_{JK}K^2-D_{Jm}m^2+H_{mJ}m^4-D_{JKm}Km] \\ & -4(J+1)^3[D_J-H_{JK}K^2-H_{Jm}m^2-H_{JKm}Km] \end{aligned} \quad (5.4)$$

where D_J , D_{JK} , D_{Jm} and D_{JKm} are the quartic centrifugal distortion constants. Higher order

centrifugal distortion parameters, such as H_{mJ} , H_{JK} , H_{Jm} and H_{JKm} were required to fit the data, in agreement with the high flexibility of the adduct. The parameters obtained from the least-squares fit of the 97 measured lines are provided in the second column of Table 5.16. In the first column, we report, for comparison, the molecular parameters of the parent species.

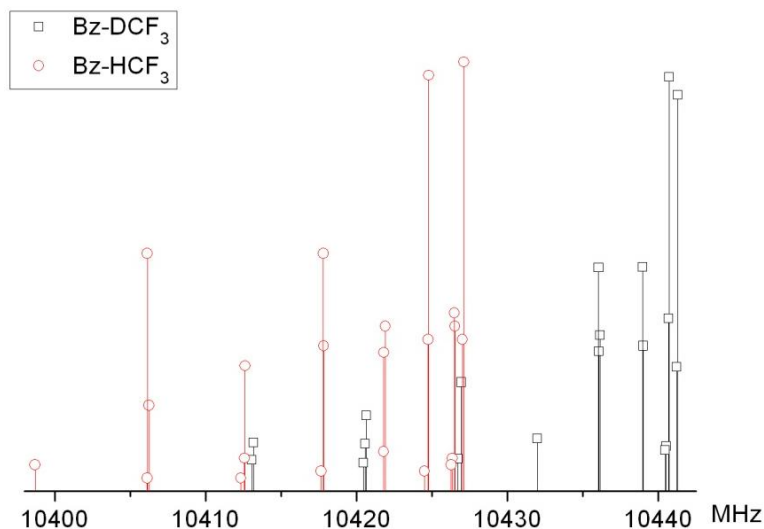


Figure 5.8 The $J = 7 \leftarrow 6$ band of Bz-DCF₃ (black) lies at higher frequency than the corresponding band of Bz-HCF₃ (red), contrarily to what expected for a heavier isotopologues within a rigid rotor approximation.

After the assignment of the most abundant species, it was possible to assign some weak transitions ($m = 0$ state) belonging to the ^{13}C isotopologues in natural abundance (*ca.* 1%) with further signal accumulation. The spectrum of the Bz(^{13}C)-DCF₃ species in natural abundance is expected to be intense about 6% of that of Bz-DCF₃, because the benzene ring contains six equivalent carbon atoms. In addition, its spectral features are completely different with respect to those of the parent species, because the asymmetric isotopic substitution breaks down the C_{3v} symmetry of complex, leading to a slightly near prolate asymmetric top. The measured transitions of this ^{13}C species have been fitted with Watson's semi-rigid Hamiltonian (S -reduction; I^r -representation).^[17] The obtained parameters are reported in the fourth column of Table 1, and there compared to the values of the Bz(^{13}C)-HCF₃ species.¹² One should note that the A rotational constant is much larger than the value expected for a rigid molecule, because for $m = 0$ the top does not rotate. The value of $(B+C)$ of the F₃CD species is quite larger than that of the F₃CH species, thus confirming the Ubbelohde effect.

Later on, a few very weak transition lines of the Bz-D ^{13}C F₃ isotopologue (only $K = 0, 1$) have

been identified. After the assignment of this weak spectrum, we searched for the spectrum of the Bz-H¹³CF₃ isotopologue, which was not observed in the previous investigation,^[133] and fulfilled its assignment. Due to the very few measured transitions, we needed to fix the centrifugal distortion constant D_J to the values of the respective parent species. The parameters obtained for these two last isotopologues, with a reduced form of Eq. (5.4), are shown in the two last columns of Table 5.16.

Table 5.16 Spectroscopic parameters of all measured isotopologues of benzene-trifluoromethane

	Bz-HCF ₃ ^[a]	Bz-DCF ₃	Bz(¹³ C)-HCF ₃ ^[a]	Bz(¹³ C)-DCF ₃	Bz-D ¹³ CF ₃	Bz-H ¹³ CF ₃
A/MHz	-	-	2837(6)	2700(76)	-	-
B/MHz	744.84012(6)	745.8548(9) ^[b]	741.33150(6)	742.3282(6)	742.9132(2)	741.8858(2)
C/MHz			739.19544(6)	740.1868(6)		
D_J/kHz	0.4700(5)	0.475(3)	0.4640(4)	0.458(6)	[0.475] ^f	[0.4700] ^f
D_{JK}/kHz	42.392(7)	41.90(1)	41.792(8)	41.27(6)	40.7(3)	41.73(3)
D_{Jm}/kHz	166.82(2)	165.70(4)	-	-	-	-
D_{JKm}/kHz	-164.70(2)	-162.89(3) ^[c]	-	-	-	-
H_{JK}/Hz	1.78(6)	2.3(1)	1.49(6)	-	-	-
H_{KJ}/Hz	-1.0(2)	-	-	-	-	-
H_{Jm}/Hz	7.3(1)	8.3(3)	-	-	-	-
H_{mj}/Hz	-37.2(8)	-39(3)	-	-	-	-
H_{JKm}/Hz	7.5(1)	-6.6(3) ^c	-	-	-	-
$L_{JK}^3 m^3/\text{Hz}$	2.0(4)	-	-	-	-	-
$\sigma^{[d]}/\text{kHz}$	1.9	3.4	0.9	3.5	4.1	2.2
$N^{[e]}$	125	97	34	17	6	7

[a] From Ref. 12. [b] Standard errors in parentheses are given in units of the last digit. [c] The sign given for these constants is arbitrary. The sign given here corresponding to the choice of the sign of m . [d] Root-mean-square deviation of the fit. [e] Number of fitted transitions. [f] Fixed to the values of parent species.

5.5.2 Structural information and quantitative estimate of the Ubbelohde effect

As a consequence of the Ubbelohde effect, the Kraitchman's equations^[16] are not suitable to evaluate the position of the H_{HCF₃} hydrogen, because the H→D mass change is overwhelmed by the shortening of the CM_{Bz} (the center of mass of Bz) ··C_{HCF₃} distance (one would obtain meaningless large imaginary values). Vice versa, the r_s located position of the C_{CHF₃} carbon can be reliably obtained in the principle axis systems of Bz-HCF₃ and Bz-DCF₃, separately. The a -coordinate of the C_{HCF₃} carbon atom is easily obtained from the equation for the substitution of an atom along the symmetry axes of a symmetric top. The a and b -coordinate of a C_{Bz} carbon atom

can be calculated by Kraitchman's equations for a symmetric/asymmetric top combination. We used for this purpose KRA Kisiel's program.^[123] The obtained results, which uncertainties include the Constrain errors, are shown In Table 5.17 and there compared to the values calculated with a rigid rotor model.

Table 5.17 Substitution coordinates of the carbon atoms in the complex

		Exp.	Calc.
a) In the principle axis of Bz-HCF ₃			
C _{HCF₃}	<i>a</i> /Å	±1.6466(8)	1.648
C _{Bz}	<i>a</i> /Å	±1.7915(7)	-1.803
	<i>b</i> /Å	±1.4104(11)	1.370
b) In the principle axis of Bz-DCF ₃			
C _{HCF₃}	<i>a</i> /Å	±1.6407(8)	1.645
C _{Bz}	<i>a</i> /Å	±1.7936(7)	-1.807
	<i>b</i> /Å	±1.4103(11)	1.370

Since the *a*-coordinate of CM_{Bz} is the same as its six equivalent carbon atoms, the distance between the carbon atom of HCF₃ (C_{HCF₃} or C_{DCF₃}) and CM_{Bz} can be easily estimated from the substitution coordinates, leading to a shrinkage of 0.0038(30) Å of the C_{HCF₃} ··CM_{Bz} distance upon the H→D substitution. Unfortunately, the errors on the substitution coordinates are too high to calculate a net Ubbelohde effect. However, the *r*₀ shortening, calculated - according to Eq. (5.5) - in order to reproduce the reduction of the *B*+*C* value which take place upon H→D substitution, is very precise, as one can see from Table 5.18.

$$\Delta(B+C)_{\text{obs}} - \Delta(B+C)_{\text{calc}} = [\partial(B+C)/\partial r_{\text{CM(Bz)} \cdot \cdot \text{C(CHF}_3\text{)}}]_{\text{pi}=\text{cost}} \Delta r_{\text{CM(Bz)} \cdot \cdot \text{C(CHF}_3\text{)}} \quad (5.5)$$

Table 5.18 Shortening of the *r*(C_{HCF₃} ··CM_{Bz}) distance upon H→D substitution. CM=center of mass.

	<i>r</i> _s	<i>r</i> ₀
<i>r</i> (C _{HCF₃} ··CM _{Bz})/Å	3.4381(15)	3.4683(1)
<i>r</i> (C _{DCF₃} ··CM _{Bz})/Å	3.4343(15)	3.4639(1)
Δ <i>r</i> /Å	0.0038(30)	0.0044(2)

5.7 Conclusions

The MW spectrum of $\text{CH}_2\text{F}_2\text{-CH}_2\text{Cl}_2$ represents an investigation by rotational spectroscopy of an unprecedented type of an intermolecular complex. This cluster consists of the combination of two asymmetric molecules, containing two heavy quadrupolar nuclei (^{35}Cl or ^{37}Cl) with high nuclear spin quantum numbers and large electric nuclear quadrupolar moments. The consequent complex hyperfine structure of each transition has been successfully analyzed and interpreted in terms of five or ten quadrupole coupling parameters, depending on the equivalence ($^{35}\text{Cl}/^{35}\text{Cl}$) or not ($^{35}\text{Cl}/^{37}\text{Cl}$) of the two Cl atoms. The complex has a plane of symmetry with two equivalent Cl atoms, as proved by the key available experimental data: (i) the existence of only one $^{35}\text{Cl}/^{37}\text{Cl}$ isotopologue with intensity 2/3 of that of the parent species; (ii) values of the Cl substitution coordinates; (iii) the number and the values of the quadrupole coupling constants. The detection of conformer **I**, where the two subunits are linked to each other by two C-H \cdots Cl-C and one C-H \cdots F-C WHBs, rather than conformer **II**, with two C-H \cdots F-C and one C-H \cdots Cl-C interactions, suggests that C-H \cdots Cl-C is a linkage stronger than C-H \cdots F-C.

The FTMW investigation of the rotational spectra of $\text{CF}_3\text{Cl-CH}_3\text{F}$ and of its isotopologues allowed to point out irrefutably that its more stable configuration is established by a Cl \cdots F HaB. This is, to our knowledge, the first time that this interaction is observed and described through a rotational study in an adduct made of two freon molecules. CF_3Cl can be considered as a prototype halogen donor, and we could structurally, conformationally and energetically analyze the Cl \cdots O,¹⁰ Cl \cdots N¹² and Cl \cdots F (this work) HaBs that it forms with H_2O , NH_3 and CH_3F . In addition, we could discover and interpret the effects of the two free or near-free internal rotations of the two constituent subunits, and show how dramatically they change the values of the A rotational constant.

The configuration and structures of the most stable conformer of the 1:1 complex of $\text{CH}_2\text{F}_2\cdots\text{H}_2\text{CO}$ have been determined. All atoms, except the two methylenic hydrogens of CH_2F_2 , are coplanar. The two subunits are held together through a C-H \cdots F-C and a bifurcated $\text{CH}_2\cdots\text{O}$ WHB. The tunneling splitting of each rotational transition into two component lines, with an intensity ratio of ca. 1:3, allowed determining the barrier to the internal rotation of the H_2CO subunit, $V_2 = 180(10)\text{ cm}^{-1}$.

With the present study on the tri-deuterated isotopologues of the benzene-trifluoromethane adduct, we shown that the Ubbelohde effect takes place also within WHB, such as this C-H \cdots π one. In addition, we supply a precise value of the shortening of the C \cdots CM_{Bz} distance upon H \rightarrow D

substitution. The determined shrinkage, $0.0044(2) \text{ \AA}$ is slightly smaller than that observed in dimers of alcohols, or in adducts of alcohols with ethers ($\Delta r = 5\text{-}7 \text{ m\AA}$). When replacing Bz with a rather heavy and rigid cage amine quinuclidine, the complex turns out to be a symmetric top, however no observable change in the distance C \cdots N upon the H \rightarrow D isotopic substitution is evidenced. It seems that the Ubbelohde effect vanishes within the C-H \cdots N WHB, nevertheless it appears difficult to extract a general law since these are only two subunits held together through a WHB, in which the Ubbelohde effect could be observable.

Chapter 6

Pyridine-CF_nH_{n-4}

6.1 Introduction

Pyridine (PYR from now on), is the best-known heterocyclic aromatic molecule extensively used as a ligand in coordination^[146-147] and surface chemistry.^[148] Some tens of its molecular adducts have been investigated by high resolution spectroscopy. Depending on the nature of the chemical species linked to PYR, π or σ type complexes have been observed, in relation to the PYR interaction sites, that is the π system of the aromatic ring, or the n orbital of the nitrogen atom. PYR-Metal (metal=Li, Ca, and Sc) complexes, produced with laser-vaporization, have been studied by ZEKE spectroscopy.^[149] It has been found that Li and Ca complexes prefer a σ bonding mode, whereas the Sc complex favors a π mode, with bond energies of 27.0, 49.1 and 110.6 kJ mol⁻¹, respectively.

Plenty of information on the typology and strengths of the non-bonding interactions of PYR with its partners have been obtained also by rotational spectroscopy. PYR is the only aromatic molecule for which, thanks to its permanent dipole moment, the rotational spectra of all complexes with RG (except radon) have been reported. In all cases, π -type complexes have been observed,^[33-39] even for complexes with two RG atoms, which have a “double” π arrangement, with one atom above and the other below the ring.^[38, 150-151] The interaction energies of this kind of complexes are in the range 0.5-5 kJ mol⁻¹.

MW studies of molecular complexes of PYR with other molecules, apart from RGs, revealed always, to our knowledge, a σ -type arrangement. Four investigations are available, indeed, describing this kind of interaction, on the complexes of PYR with simple molecules, such as CO, CO₂, SO₂ and SO₃. All of them are linked to the n orbital of PYR, through formal C \cdots N or S \cdots N contacts.^[152-154] In the complex with SO₃, PYR acts as a Lewis base, donating its pair of electron to the sulfur trioxide Lewis acid. The S-N bond becomes in this case a covalent bond, with unusually high bond energy, of about 120 kJ mol⁻¹.^[154]

PYR with CF₄ also has a σ -type arrangement, where the two subunits are held together by a CF₃ \cdots N HaB, with the top undergoing a free rotation with respect to PYR.^[113] In PYR-CHF₃, two kind of WHB, C-H \cdots N and C-H \cdots F, have been found to connect the two constituent units.^[155] The barrier to internal rotation of the CHF₃ group has been determined from the *A-E* splittings of the rotational transitions. To complete the family PYR-CF_nH_{n-4}, we continued the rotational studies of the complex of PYR with CH₃F, CH₂F₂ and CH₄, respectively.

The PJ-FT rotational spectra of 4 isotopologues have been measured for the most stable conformation of the molecular cluster PYR-CH₃F. Two weak C-H \cdots N and C-H \cdots F hydrogen bonds link the two subunits of the complex. Structural information on the hydrogen bridges has been obtained. The internal rotation of the CH₃F subunit around its symmetry axis splits all rotational transitions into two (*A* and *E*) well resolved component lines, leading to a *V*₃ barrier height of 1.55(1) kJ mol⁻¹.^[156]

The observed conformer of PYR-CH₂F₂ is stabilized by a small net of WHBs, that is a bifurcated CH₂ \cdots N and a CH \cdots F links.^[157] Similar interactions have been found in PYR-CHF₃, and PYR-CH₃F, but the symmetric top conformation of CHF₃ and CH₃F weak allowed the determination, in the two latter cases, of their *V*₃ barriers to internal rotation, which represented extra data to size the strengths of the WHBs. It is possible, however, to set a strength order of the CH \cdots N and a CH \cdots F weak interactions within this small family of complexes of PYR with freons.

Which one will be the absolute minimum conformation of the complex between PYR and CH₄? The methane hydrogen atoms are much less acidic than the freon's hydrogen. Will they interact with the *n* or with the π electronic system? Will the high symmetry of methane still generate splittings of the rotational transitions also in a complex such heavy as PYR-CH₄?

In this chapter, these questions will be answered with the rotational characterization of a molecular complex made by an alkane (although the simplest one) and an aromatic ring, namely, the 1:1 complex PYR-CH₄.

6.2 Experimental

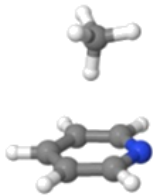

Molecular clusters were generated in a supersonic expansion, under conditions optimized for the complex formation.

A gas mixture of ca. 5% of CH₄ in Helium at a stagnation pressure of \sim 0.6 MPa was passed over a sample of pyridine (commercial sample, cooled to 0 °C) and expanded into the Fabry-Pérot cavity.

6.3 Theoretical Calculations

One can assume, by chemical intuition, a stable conformer of PYR- CH_4 to be based on a C-H $\cdots\pi$ or on a C-H $\cdots n$ link. Full *ab initio* geometry optimization (MP2/6-311++G(d,p) calculations), performed by using the Gaussian03 program package^[13] confirmed this hypothesis. The obtained relative energies and spectroscopic parameters are collected in Table 6.1. In order to have a better estimate of the relative energy of the two conformers, all intermolecular binding energy values were counterpoise corrected for BSSE.^[12] It appears, at the very end, that the C-H $\cdots\pi$ interaction is stronger than the C-H $\cdots n$ one.

Table 6.1 MP2/6-311++G(d,p) shapes and spectroscopic parameters of the two forms predicted to be the most stable of PYR- CH_4 . These structures are stabilized by a C-H $\cdots\pi$ (form **I**) or a C-H $\cdots N$ (form **II**) WHB.

	I	II
		
$A/B/C/\text{MHz}$	2901/1895/1873	5793/1128/950
$\chi_{aa}/\chi_{bb}/\chi_{cc}/\text{MHz}$	3.29/-6.28	-4.86/-1.95
$\mu_a/\mu_b/\mu_c/\text{D}$	0.4/2.3/0.0	2.7/0.2/0.0
$\Delta E/\Delta E_{\text{BSSE}}/\text{cm}^{-1}$	0/0 ^[a]	346/19

[a] Absolute energies: -287.992494 and -287.990053 E_h , respectively.

6.4 Rotational spectra

Following the theoretical indications, which suggest the π -complex to be the most stable one and its μ_b -spectrum the strongest one, we searched for the most intense μ_b -type transitions. We could assign three transitions of the family $(J+1)_{1,J+1} \leftarrow J_{0,J}$, with $J = 1$ to 3. Then, several more μ_b -transitions and some very weak μ_a -transitions have been also measured. Each transition (see, for example, the $2_{12} \leftarrow 1_{01}$ one in Figure 6.1) appeared as a multiplet of lines due to the ^{14}N quadrupolar effects.

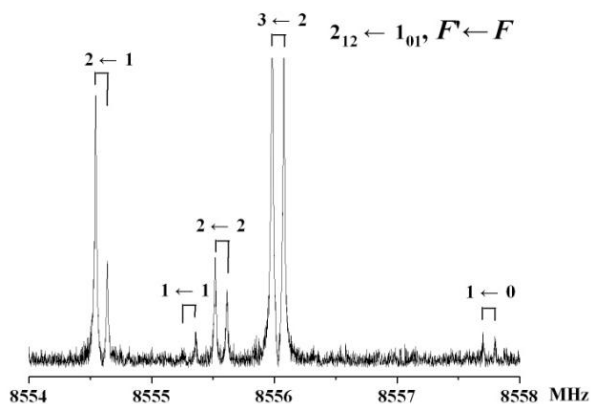


Figure 6.1 Recorded $2_{12} \leftarrow 1_{01}$ transition of the observed conformer of PYR-CH₄ showing the ¹⁴N hyperfine structure. Each component line exhibits the instrumental Doppler doubling.

The transition frequencies were fitted with Pickett’s SPFIT computer program,^[95] according to the Hamiltonian described in Chapter 4 (Eq. (4.1)). The centrifugal distortion contributions were analyzed using the *S* reduction and *I*’ representation.^[8] The obtained spectroscopic parameters are summarized in the first column of Table 6.2.

Table 6.2 Spectroscopic constants of the two measured isotopologues of PYR-CH₄

	[¹⁴ N]PYR-CH ₄	[¹⁵ N]PYR-CH ₄
<i>A</i> /MHz	2995.7148(9) ^[a]	2961.1510(6)
<i>B</i> /MHz	1873.3363(6)	1872.2691(6)
<i>C</i> /MHz	1853.4941(6)	1838.9538(5)
<i>D_y</i> /kHz	5.46(1)	5.33(2)
<i>D_{JK}</i> /kHz	53.70(6)	[53.70] ^[b]
<i>D_K</i> /kHz	-56.59(8)	[-56.59]
<i>d₁</i> /kHz	-0.23(2)	[-0.23]
<i>χ_{aa}</i> /MHz	3.251(5)	-
<i>χ_{bb}-χ_{cc}</i> /MHz	-6.137(7)	-
<i>N</i> ^[c]	55	18
<i>σ</i> /kHz ^[d]	2.6	2.2

[a] Uncertainties (in parentheses) are expressed in units of the last digit. [b] Fixed to the values of the normal species. [c] Number of transitions in the fit. [d] Standard deviation of the fit.

After the empirical correction of the rotational constants, the spectrum, without quadrupole hyperfine structure, of the ¹⁵N (*I* = 1/2) isotopologue was searched and assigned. The measured transition frequencies were fitted as described above, and the spectroscopic parameters are also shown in Table 6.2.

Comparing the experimental values of the rotational and quadrupole coupling constants of Table 6.2 to the theoretical values of Table 6.1, one can see that the match is acceptable only for conformer I. The high values of *D*_{JK} and *D*_K indicate a rather flat potential energy function of the bending motions of methane with respect to the ring rotation, a feature often encountered in rotational analysis of the spectra of aromatic ring with RGs.^[158]

In the previous investigations of adducts of CH₄ with very small molecules (H₂O, HCl, HF, HCN), many of the rotational transitions appeared as triplets, according to its three nuclear-spin modifications, denoted as *A*, *F*, and *E*.^[159-163] In the complexes with slightly heavier molecules, such as OCS and ozone, only doublets were observed, and the splittings among the observed *A* and *F* component lines were quite smaller.^[164-165] For PYR-CH₄, we observed only a single spin line for each transition. We think that for such a heavy complex, all nuclear spin components are overlapped to each other.

Further spectral searching has been dedicated to the second conformer of Table 6.1, but without success. Probably this form is relaxing to the most stable conformer upon supersonic expansion.^[104]

6.5 Molecular structure

By combining the rotational constants of the two isotopologues, we could calculate the substitution coordinates^[16] of the N atom.

Table 6.3 *r*_s coordinates (Å) of the N atom in the principal axes system of the parent species. *c* has been fixed to zero by symmetry.

	<i>a</i>	<i>b</i>
Exptl.	±0.411(4) ^[a]	±1.424(1)
Calc.	-0.441	1.427

[a] Uncertainties (in parentheses) are expressed in units of the last digit.

The obtained values are shown in Table 6.3 in the principal axes system of the parent

species. The c coordinate would have had a slightly imaginary value, but we fixed it to zero to obtain the a and b coordinates of Table 6.3.

6.6 Dissociation energy

Upon the formation of the complex, the three translational motions of the isolated spherical CH₄ are replaced by three low energy vibrational modes. The low energy and large amplitude of these motions bring Coriolis coupling contributes to the moments of inertia, leading the usual methods for structure determination supply poor results. Here we will apply a method taking into account these effects which has been successfully used in the van der Waals complexes such as PYR with Ne, Ar and Xe.^[152-154] One of the motions can be considered the stretching between the two centers of mass of the two constituent molecules, while the remaining ones can be thought as two internal rotation of CH₄ around PYR.

The stretching can be, in a first approximation, isolated from the other motions. For such a kind of asymmetric top complex in which the stretching motion between the two subunits is almost parallel to the a -axis of the complex, the stretching force constant (k_s) can be roughly estimated to be 2.73 N/m, corresponding to the harmonic stretching fundamental $\nu_s = 59.0 \text{ cm}^{-1}$, with pseudo-diatomic approximation through the equation (Eq. (1.8)).^[17] R_{CM} is 3.664 Å from *ab initio* calculation.

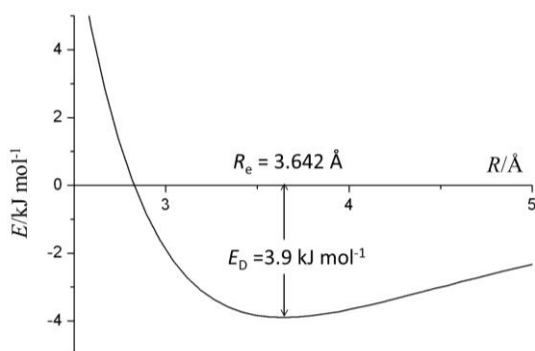


Figure 6.2 Lennard-Jones potential energy diagrams for the dissociation of PYR-CH₄.

A one-dimensional flexible model^[166] has been used to calculate the rotational and vibrational energy levels to adjust the values of dissociation energy E_D and equilibrium distance between the two CMs of the two moieties R_e within a Lennard-Jones type potential, in such a way to reproduce ν_s and $(B+C)_0$. Figure 6.2 shows the Lennard-Jones potential energy curves for PYR-CH₄. The values of E_D and R , resolving the range $(-2.0 \text{ Å}, +2.0 \text{ Å})$ into 41 mesh points^[166]

has been adjusted to $3.9(1) \text{ kJ mol}^{-1}$ and $3.642(1) \text{ \AA}$, respectively.

6.7 Internal Dynamics

As described in Chapter 1, the planar moments of inertia represent the mass extension along each principal axis (Eq. (1.3) and (1.4)). In going from isolated PYR to PYR- CH_4 , the principal axes are switched as shown in Figure 6.3, but we consider the x , y , z directions to be almost the same for the monomer and the complex. The corresponding changes of the planar moments of inertia are listed in Table 6.4. The negative values of ΔP_{xx} and ΔP_{yy} are surprising at the first sight. Similar changes in going from pyrimidine to pyrimidine-Ar, has been interpreted as a combination of mass dispersion and vibrational Coriolis coupling associated with the two bendings.^[158]

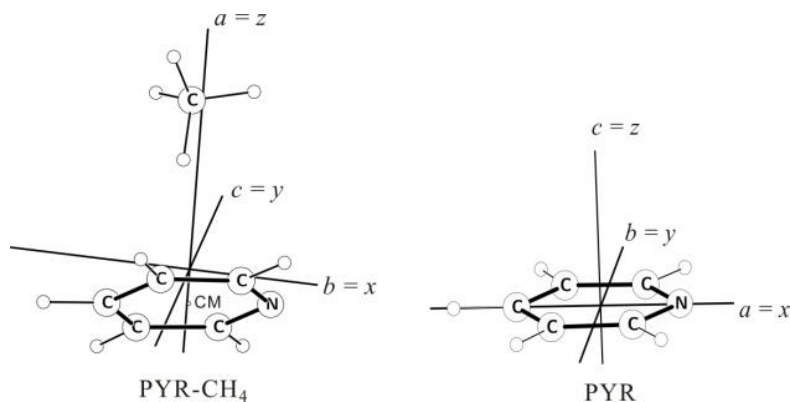


Figure 6.3 Geometry and principal axis system in PYR- CH_4 and PYR. CM is the center of mass of PYR.

In PYR- CH_4 the problem is slightly different, because CH_4 is not an atom and also the four hydrogen atoms contribute to the I_g ($g = a, b, c$) values. However, assuming CH_4 to freely rotate with respect to PYR in the $m = 0$ torsional ground state, it will not contribute to the I_a value, while its contributions to I_b and I_c are about the same. As a consequence, the P_{bb} and P_{cc} values do not include the contributions of the four hydrogen atoms. We can apply then the same method used for pyrimidine-Ar to evaluate the force constants of the bending motions of CH_4 with respect to PYR. The two motions are considered local harmonic oscillations, on one side of the aromatic plane, by a model that describes—notation according to the C_s symmetry of the complex—the A' type mode in the xz plane by the displacement X and the A'' type displacement in the y direction by Y ,

$$V(X, Y) = (1/2)[k_x Y^2 + k_y (X - X_e)^2] \quad (6.1)$$

where X_e is the displacement, within the symmetry plane, of the CM of CH₄ from the z -axis of PYR at equilibrium. The calculation has been done within two-dimensional flexible model, resolving the range (-2.0 Å, +2.0 Å) into 21 mesh points for each of the X and Y displacements.^[166]

Since only two data, ΔP_{xx} and ΔP_{yy} , two of the three parameters X_e , k_x and k_y , can be allowed to estimate. Thus we assumed $k_x = k_y$, a condition nearly fulfilled for the van der Waals complex with the same shape as PYR-CH₄. At the meantime, ΔP_{zz} was used to estimate the z -coordinate of CM of CH₄, Z_0 . The best agreement with the experimental data was obtained and listed in Table 3. It indicates that, at equilibrium position, the CM of CH₄ is 3.544 Å above the ring, and about 6.0° from the CM of PYR towards the nitrogen atom.

Table 6.4 The values of P_{gg} of PYR and PYR-CH₄ and ΔP_{gg} upon complexion, and the flexible model results corresponding to the parameters determined.

(a) Experimental and calculated data				
	$P_{gg}(\text{u}\text{\AA})$		$\Delta P_{gg}(\text{u}\text{\AA})$	
	PYR	PYR-CH ₄	Exptl.	Calc.
x	87.738(P_{aa})	85.794(P_{bb})	-1.944	-1.944
y	83.974(P_{bb})	82.906(P_{cc})	-1.068	-1.069
z	0(P_{cc})	186.888(P_{aa})	186.888	186.842
(b) Determined parameters				
	$k_x = k_y = 0.36(1) \text{ N m}^{-1}$	$X_e = 0.375(1) \text{ \AA}$	$Z_0 = 3.544(1) \text{ \AA}$	

6.8 Conclusions

The rotational spectrum of PYR-CH₄ represents an unprecedented investigation of a complex of an alkane with an aromatic molecule. The obtained results point out that CH₄ prefers to locate above the ring and link to PYR through a C-H... π WHB, rather than C-H... n interaction. This behavior, typical of complexes of PYR with RGs, would suggest classifying CH₄, in relation to his ability to form molecular complexes with aromatic molecules, as a pseudo rare gas. In this sense, and taking into account the dissociation energy of PYR-CH₄, the “rare gas” methane is very similar to Kr, as shown in Figure 6.4.

In Figure 6.4, also the dissociation energies of the complexes of PYR with two families of

partners, CF_nH_{4-n} ($n = 0$ to 4) and Rare Gases (He to Xe) are reported. The intermediate members of the CF_nH_{4-n} group ($n = 1-3$) are linked to PYR through C-H \cdots N and C-H \cdots F WHBs and have higher interaction energies than the members at the extremes. CF_4 ($n = 4$) is linked through a HaB to the N atom, and CH_4 ($n = 0$) similarly to a rare gas, and displays the lowest interaction energy of the group. It is also interesting to note a sort of linearity of the dissociation energy of the complexes of RG with the increase of the atomic number: actually such a linearity was found for a plot of the dissociation (E_D) against the RG polarization, as described in the rotational study of PYR-Xe.^[39]

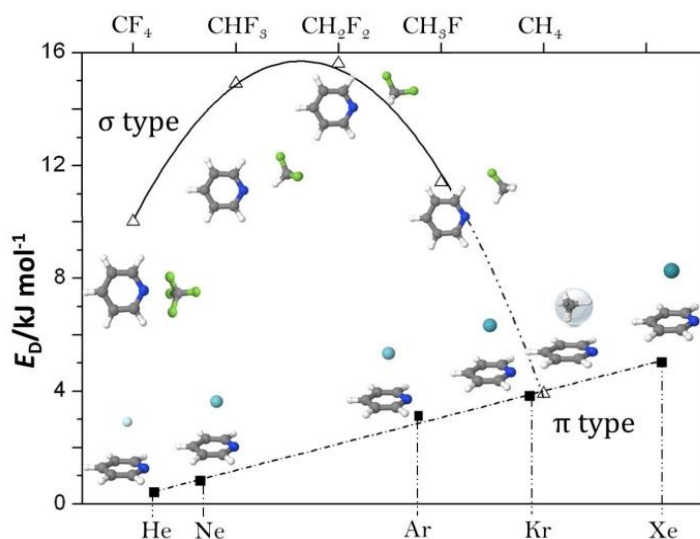


Figure 6.4 The dissociation energies and the typology of the complexes that the CF_nH_{4-n} family ($n = 0$ to 4) and the full set of rare gases form with PYR are graphically shown. The member CH_4 behaves similarly to Kr.

CH_4 seems to be one-leg connected to the π system of PYR, and to freely rotate around it, as suggested by the rotational constants A , which is larger than the rotational constant C of isolated PYR (2995.715 against 2959.21 MHz).

It seems, in addition, that in such a large complex, a coalescing of the CH_4 spin states takes place.

The internal dynamics in PYR- CH_4 is comparable to that of the van der Waals complexes involving aromatic molecules with rare gases. The effects of the CH_4 's large amplitude motions on the rotational spectrum have been used to obtain the equilibrium location of the CH_4 moiety and the PESs describing its dynamics.

Chapter 7

Bi-molecules of Carboxylic Acids

7.1 Introduction

The dimers of carboxylic acids are characterized by an eight-membered ring motif, which includes two relatively strong OH...O HBs. The corresponding dimerization energy is higher than 60 kJ mol^{-1} , and for this reason a considerable portion of dimers is found in the gas phase, even at room temperature. It was possible, indeed, to observe the low resolution MW spectra in a standing cell of some carboxylic acid bimolecules already by Costain in 1961^[135] and Bellot and Wilson in 1975.^[167]

This kind of adducts is interesting because a double proton transfers takes easily place, connecting either two equivalent, or two non-equivalent molecular conformations. In the first case tunneling effects are expected, which can lead to the determination of the PES for the tunneling motion. In the second case, we expect a conformational equilibrium to characterize the molecular system.

Various spectroscopic techniques, such as femtosecond degenerate four-wave mixing and Raman spectroscopy, have been applied to determine the tunneling splittings in dimers of carboxylic acids. Most of them have been focused on the proton transfer rate in homodimers, and mainly on the simplest carboxylic acid dimer of the series, the formic acid dimer.^[168-174] Interesting results have been obtaining on the ground and first electronic excited states of the benzoic acid dimer^[175] by rotationally resolved laser induced fluorescence.

MW spectroscopy is particularly suitable to structurally and energetically characterize the molecular interaction, and to reveal the internal dynamics. However, limited by the requirement of permanent dipole moment, the microwave investigations of acids dimers are mostly focusing on heterodimers. PJ-FTMW spectroscopy should allow obtaining precise details on the chemical and spectroscopic properties of this kind of molecular system. Bauder and co-workers reported PJ-FTMW analyses for the adducts of trifluoroacetic acid with formic and with acetic acids^[176] and

Antolinez et al. reported the MW spectrum of the trifluoroacetic acid-cyclopropanecarboxylic acid bi-molecule.^[177] In none of these cases, splitting attributed to a double proton transfer tunneling was observed. The failure to observe the tunneling splittings is due to the high values of the reduced mass of CF₃ which, in order to connect equivalent minima, has to rotate by 60°. And as a consequence, splittings are too small to be detected. A few years ago, the tunneling caused by the double proton transfer has also been observed by FTMW spectroscopy on formic acid-propionic acid^[178] and formic acid-acetic acid.^[179] Very recently, the double proton transfer dynamics in the homodimer of acrylic acid^[180] and the heterodimer benzoic acid-formic acid^[181] has been successfully described by the tunneling splittings of several isotopologues obtained from the PJ-FTMW spectra.

As to the different case, where the double proton transfer connects to different conformers, it was only available in literature since the rotational study concerning the heterodimer acrylic acid-formic acid^[136] which adopts two different conformational shapes, according to the *cis* or *trans* forms of the acrylic acid moiety.

Another interesting experimental evidence related to the investigation of carboxylic acids dimers is the Ubbelohde effect,^[24] an increase of the O...O distances upon H→D substitution of the hydrogen atoms involved in the HB. This effect was already outlined in the first MW study of this kind of bi-molecule.^[135] It is interesting to note that, in contrast to the *r*_{O...O} increase observed in carboxylic dimers, a shrinking of the O...O distance is observed (reverse Ubbelohde effect) for complexes with the two subunits held together by a single OH...O HB.^[138-140]

We focused our attention of the bi-molecules of carboxylic acids mainly on the conformational equilibria. In this chapter, three rotational studies of carboxylic acid heterodimers constituted among fluoroacetic acid (FAA), difluoroacetic acid (DFA), trifluoroacetic acid (TFA), formic acid (FA) and acrylic acid (AA) will be discussed: *i.e.* AA-TFA,^[182] DFA-FA^[183] and FAA-AA.^[184]

7.2 Experimental

Molecular clusters were generated in a supersonic expansion, under conditions optimized for the dimer formation.

Helium at a stagnation pressure of ~0.25 MPa was passed over a mixture sample of the carboxylic acids under studied with almost 1:1 ratio (commercial sample bought from Apollo or Aldrich, and used without further purification) and expanded into the Fabry-Pérot cavity.

The deuterated species in the HBs have been derived from the proton exchange by directly

mixing with deuterated water.

7.3 Acrylic acid···Trifluoroacetic acid

7.3.1 Theoretical calculation

The configurations of the complex were obtained from *ab initio* calculations at the MP2/6-311++G(d,p) level.^[13] There are two plausible conformers distinguished by the orientation of the allyl group of acrylic acid. Here the configuration with *zusammen* (*Z*) oriented allyl group with respect to carbonylic C=O bond is counted as *cis*-form, while the other *entgegen* (*E*) as *trans*-form. Draws of these two conformers as well as the calculated rotational constants, electric dipole moment and relative energies were listed in Table 7.1.

Table 7.1 MP2/6-311++G(d, p) calculated energies and spectroscopic parameters of the plausible conformers of AA-TFA

	<i>cis</i>	<i>trans</i>
$\Delta E, \Delta E_{\text{BSSE}}/\text{cm}^{-1}$	0 ^[a] , 0 ^[b]	98, 80
A, B, C/MHz	2604, 334, 312	2728, 329, 310
$\mu_a, \mu_b/\text{D}$	3.7, 0.2	3.8, 0.2

[a] Absolute energy: -792.3754723 E_h. [b] Absolute energy is -792.3700013 E_h.

In order to have a better estimate of the energy differences, all intermolecular binding energy values were counterpoise corrected for BSSE.^[12] It indicated the *trans*-form has a little higher energy than the global minimum, *cis*-form. So both conformers were expected to be observed in microwave spectroscopy with much stronger *a*-type and weaker *b*-type transitions.

7.3.2 Rotational spectra

According to the small calculated rotational constants *B* and *C*, the *a*-type *R*-branch transitions were expected to appear in narrow frequency regions separated by *B*+*C*. The individual

transitions were readily observed as the initial search for rotational transitions was restricted to those regions. Several μ_a -*R*-type lines, with *J* ranging from 11 to 15, were initially assigned for *cis*- conformer. Then some μ_b -*R*-type lines were also measured. All measured transitions have been fitted with Watson's semi-rigid Hamiltonian, within the *S*-reduction and the *I'*-representation.^[8]

Table 7.2 Spectroscopic parameters of the measured isotopologues of *cis*-AA-TFA^[a]

	AA-TFA	AA-TFA(OD)	AA(OD)-TFA	AA(OD)-TFA(OD)
<i>A</i> /MHz	2630.921(1) ^[b]	2616.5(3)	2605.5(3)	2591.4(3)
<i>B</i> /MHz	337.3895(2)	336.5472(2)	336.7495(2)	335.9544(2)
<i>C</i> /MHz	315.9790(2)	315.0353(2)	315.0486(2)	314.1463(2)
$\sigma^{[c]}$ /kHz	3.28	1.93	1.18	0.98
<i>N</i> ^[d]	50	9	9	9

[a] The quartic centrifugal distortion parameter $D_J = 0.009(1)$ kHz and $D_{JK} = 0.098(3)$ kHz have been determined for the normal species. These two parameters have been fixed to these values for the other 3 isotopologues. [b] Error in parentheses in units of the last digit. [c] RMS error of the fit. [d] Number of lines in the fit.

Three rotational constants and two centrifugal distortion constants were fitted to the measured transition frequencies. Later, the spectra of three more isotopologues with deuterium atoms involved in the HBs were assigned. Due to the smaller number of lines measured for the deuterated species, their centrifugal distortion constants couldn't be determined and were fixed to the values of the normal species. The obtained spectroscopic parameters are shown in Table 7.2.

Table 7.3 Spectroscopic parameters of the measured isotopologues of *trans*-AA-TFA^[a]

	AA-TFA	AA-TFA(OD)	AA(OD)-TFA	AA(OD)-TFA(OD)
<i>A</i> /MHz	2734.620(1) ^[b]	2713.30(1)	2719.3(3)	2697.98(1)
<i>B</i> /MHz	333.3434(2)	332.4836(2)	332.5805(2)	331.7763(2)
<i>C</i> /MHz	313.8593(2)	312.8162(2)	312.9820(2)	311.9862(2)
$\sigma^{[c]}$ /kHz	3.6	0.8	1.4	0.7
<i>N</i> ^[d]	45	10	9	10

[a] The quartic centrifugal distortion parameter $D_J = 0.008(1)$ kHz and $D_{JK} = 0.126(5)$ kHz have been determined for the normal species. These two parameters have been fixed to these values for the other 3 isotopologues. [b] Error in parentheses in units of the last digit. [c] RMS error of the fit. [d] Number of lines in the fit.

After that the assignment of the *cis*- conformer was completed, relatively strong lines were still available in the spectrum. They were easily assigned to the *trans*-conformer. The analysis of the experimental transition frequencies was performed as described for the most abundant conformer, and extended to three OD deuterated species. The determined spectroscopic parameters of are shown in Table 7.3.

7.3.3 Sizing the Ubbelohde effect

From the rotational constants it is easy to calculate, for each species, the values of the P_{aa} planar moments of inertia (see Eq. (1.3) and (1.4)). These quantities give a measure of the mass extension along the a -axis. In Table 7.4 the P_{aa} values, along with the model calculated and experimental values of their shifts upon OD deuteration are summarized.

Table 7.4 P_{aa} values ($\text{u}\text{\AA}^2$) for the various isotopologues of the *cis* and *trans* conformers of AA-FAA, and calculated and experimental values of their shifts upon OD deuteration. The largest error on the P_{aa} values is $0.01 \text{ u}\text{\AA}^2$.

	<i>cis</i>			<i>trans</i>		
	P_{aa}	ΔP_{aa}		P_{aa}	ΔP_{aa}	
		exptl.	calc.		exptl.	calc.
AA-TFA	1452.61			1470.75		
AA(OD)-TFA	1455.46	2.85	1.47	1474.22	3.47	1.94
AA-TFA(OD)	1456.35	3.74	0.28	1474.66	3.91	0.16
AA(OD)-TFA(OD)	1459.01	6.40	1.74	1477.91	7.16	2.09

One can note that the experimental ΔP_{aa} values are considerably larger than the calculated one, according to the Ubbelohde effect previously described.² Correspondingly, the substitution coordinates of the carboxylic hydrogens loses the structural meaning for fully “rigid” molecules.

Table 7.5 Increases of the carboxylic groups C-C distances (Δr_{C-C}) upon H→D substitution

	<i>Cis</i>	<i>trans</i>
AA(OD)-TFA	0.0074(3)	0.0033(3)
AA-TFA(OD)	0.0029(3)	0.0082(3)
AA(OD)-TFA(OD)	0.0099(3)	0.0110(3)

To reproduce the experimental ΔP_{aa} values originated by the H → D substitutions, it has been

necessary to slight elongate the $r_{C..C}$ distances between the two carboxylic carbon atoms, according to the values shown in Table 7.5.

7.3.4 Information on the dissociation energy

The intermolecular stretching motion which leads to the dissociation is almost parallel to the a -axis for all conformers of the complex. In this case, the pseudo diatomic approximation can be used to roughly estimate the force constant of the stretching mode leading to the dissociation and the zero point dissociation energy of the complex.^[17-18] The results are listed in Table 7.6. The dissociation energies of the two conformers have similar values, in accord with *ab initio* calculations results.

Table 7.6 Dissociation energy for both conformers of AA-TFA

	<i>Cis</i>	<i>trans</i>
$R_{CM}/\text{Å}$	5.24	5.27
k_S/Nm^{-1}	35	34
$E_D/\text{kJ mol}^{-1}$	81	80

7.4 Difluoroacetic acid...Formic acid

7.4.1 Theoretical calculations

Two rotamers have been identified in the rotational spectrum of DFA, with the difluoromethyl hydrogen atom *trans* or *gauche* with respect to the C–O bond.^[185] When forming the complex with FA, these two conformations are expected to be preserved, as shown in Figure 7.1.

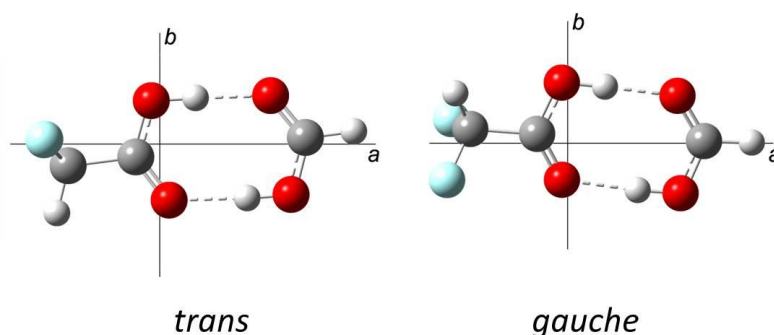


Figure 7.1 *Trans* and *gauche* conformers of DFA-FA, with their principal axes systems.

Full geometry optimization of the monomers and dimers were carried out at the MP2/6-311++G(d,p) level using the Gaussian03 program package.^[13] In order to have a better estimate of the energy differences, all intermolecular binding energy values were counterpoise corrected for BSSE.^[12] The calculation results suggest that the two conformers have more or less the same energy level. So the spectra for both conformers were expected to be observed. The estimated values of the spectroscopic constants as well as the dipole moment were listed in Table 7.7, and used as a guide in the assignment of the rotational spectra for both conformers.

Table 7.7 MP2/6-311++G(d,p) calculated spectroscopic parameters, Relative energies and dissociation energies of *trans* and *gauche* DFA-FA

	<i>Trans</i>	<i>gauche</i>
<i>A</i> /MHz	3751	3578
<i>B</i> /MHz	674	695
<i>C</i> /MHz	638	634
μ_a /D	1.7	1.6
μ_b /D	1.3	1.0
μ_c /D	0.0	1.0
ΔE /cm ⁻¹	0 ^[a]	8
ΔE_{BSSE} /cm ⁻¹	0 ^[b]	15
E_D ^[c] /kJmol ⁻¹	61.7	63.3
$E_{D-\text{BSSE}}$ ^[d] /kJmol ⁻¹	49.0	50.5

[a] Absolute energy is -616.101758 E_h. [b] Absolute energy is -616.096927 E_h. [c] Dissociation energy. [d] BSSE corrected dissociation energy.

7.4.2 Rotational spectra

Following the predictions from the model calculations, the trial assignment started with the *trans* conformer, which was expected to be the more stable one. Two frequency scans of a few hundred MHz each were carried out in the region of the $J = 7 \leftarrow 6$ and $J = 8 \leftarrow 7$ μ_a -type *R* bands. The corresponding $K_{-1} = 0, 1$ transitions were easily identified, and after some preliminary fittings, the assignment of the spectrum was extended to transitions with higher J and with K_{-1} up to 4. Some μ_b -type *R* and *Q* branch transitions have been measured later. No μ_c -type transitions have been detected, in agreement with the plane of symmetry of this form of the adduct.

Since *trans* DFA-FA is a near prolate asymmetric top, the *S*-reduction and the *I'*-representation have been chosen.^[8] The transitions were fitted with Pickett's SPFIT computer

program.^[95] Three rotational constants and four centrifugal distortion constants were determined from the 45 measured transition frequencies, as shown in the first column of Table 7.8. Later on, the spectra of three more isotopologues with the deuterium in the HB network have been assigned. Due to the smaller number of lines measured for the deuterated species, their centrifugal distortion constants were fixed to the values of the parent species. The determined spectroscopic parameters were also reported in Table 7.8.

Table 7.8 Spectroscopic parameters for the *trans* form of DFA-FA

	DFA-FA	DFA-FA(OD)	DFA(OD)-FA	DFA(OD)-FA(OD)
<i>A</i> /MHz	3756.8120(2) ^[a]	3723.217(2)	3724.703(2)	3690.960(2)
<i>B</i> /MHz	684.7062(1)	680.4802(1)	682.7161(1)	678.6128(1)
<i>C</i> /MHz	647.2307(1)	642.4528(1)	644.4905(1)	639.8197(1)
<i>D_y</i> /kHz	0.1042(7)	[0.1042] ^[b]	[0.1042]	[0.1042]
<i>D_{JK}</i> /kHz	0.924(5)	[0.924]	[0.924]	[0.924]
<i>d₁</i> /kHz	-0.0034(5)	[-0.0034]	[-0.0034]	[-0.0034]
<i>d₂</i> /kHz	0.0302(4)	[0.0302]	[0.0302]	[0.0302]
$\sigma^{[c]}$ /kHz	1.15	1.92	1.18	2.87
<i>N</i> ^[d]	45	11	11	11

[a] Error in parentheses in units of the last digit. [b] Values in bracket fixed to the value of the parent species. [c] Root-mean-square deviation of the fit. [d] Number of lines in the fit.

Several transitions remained unassigned in the spectrum, most of them showing two component lines. They were easily assigned to the *gauche* conformer. In this case also several interstate μ_c -type transitions, full split by about the double of the vibrational splitting between the $\nu = 0$ and $\nu = 1$ sublevels were measured and assigned. The energy difference between the two sublevels is so small that the μ_a -type transitions display very small splittings (of the order of a few tens of kHz) as shown in Figure 7.2, where the recorded $8_{0,8} \leftarrow 7_{0,7}$ transition is given.

Such a doubling could be attributable either the tunneling of $-\text{CHF}_2$ between its two equivalent *gauche* minima, or the proton transfer with a simultaneous internal rotation of the $-\text{CHF}_2$ group to reach an equivalent potential energy minimum. A crystal clear indication is given from the assignment of the deuterated species. Monodeuteration makes the two HBs no longer equivalent, and it quenching the tunneling, when due to the proton transfer. Since the splittings were observed, more or less unchanged, in all three deuterated isotopologues, we can attribute the transition doubling to the internal rotation of $-\text{CHF}_2$.

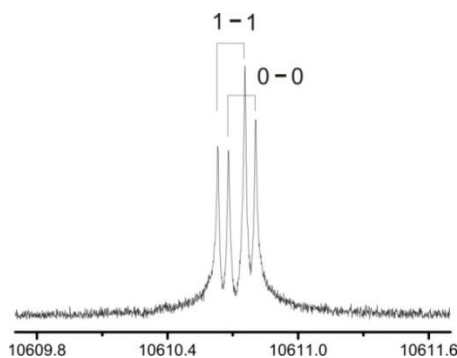


Figure 7.2 Recorded $8_{0,8} \leftarrow 7_{0,7}$ transition, split into two tunneling component lines. Each line appears as a doublet (□) due to the Doppler effect.

For the *gauche* conformer, the transitions frequencies of all four isotopologues have been fitted according to the simple coupled Hamiltonian:

$$H = H_R + H_{CD} + \Delta E_{01} \quad (7.1)$$

where H_R and H_{CD} are the rotational and centrifugal distortion contributions, common to both $\nu = 0$ and $\nu = 1$ state and ΔE_{01} is the energy splitting between the two states. All determined spectroscopic constants are reported in Table 7.9. The centrifugal distortion constants of deuterated species were also fixed to the values of the parent species.

Table 7.9 Spectroscopic parameters for the *gauche* form of DFA-FA

	DFA-FA		DFA-FA(OD)		DFA(OD)-FA		DFA(OD)-FA(OD)	
	0	1	0	1	0	1	0	1
A/MHz	3638.830(3) ^[a]	3637.294(3)	3604.112(5)	3602.785(4)	3599.368(4)	3597.898(4)	3564.696(4)	3563.416(4)
B/MHz	711.7877(2)	711.7879(2)	707.9592(3)	707.9601(3)	709.4035(3)	709.4040(3)	705.7043(3)	705.7047(3)
C/MHz	631.1527(2)	631.1536(2)	627.0917(2)	627.0923(2)	628.2371(2)	628.2379(2)	624.2782(2)	624.2790(2)
D_J/kHz		0.069(1)		[0.069] ^[b]		[0.069]		[0.069]
D_{JK}/kHz		0.39(1)		[0.39]		[0.39]		[0.39]
d_1/kHz		-0.002(1)		[-0.002]		[-0.002]		[-0.002]
d_2/kHz		-0.008(1)		[-0.008]		[-0.008]		[-0.008]
$\Delta E_{01}/\text{MHz}$		3.148(4)		2.762(7)		3.081(7)		2.714(7)
$\sigma^{[c]}/\text{kHz}$		4.98		3.13		2.87		1.94
$N^{[d]}$		84		25		26		26

[a] Error in parentheses in units of the last digit. [b] Values in bracket fixed to the value of the parent species. [c] Root-mean-square deviation of the fit. [d] Number of lines in the fit.

7.4.3 Structural analysis

By comparing the experimental and calculated values of the rotational constants (Tables 7.7-7.9) there is a general good agreement, with the exception of the rotational constant A of the *gauche* conformer, which experimental value is larger by ~ 80 MHz. This discrepancy could be partially adjusted by a considerable rotation of the $-\text{CHF}_2$ group with respect to the plane containing the two carboxylic groups. It is easier, however, to see the effects of the variation of this dihedral angle on the inertial properties considering the values of the P_{cc} planar moments of inertia and easily obtained from the rotational constants through the relation P_{cc} . For the *gauche* conformer, the experimental value of P_{cc} ($24.087 \text{ u}\text{\AA}^2$) is much smaller than the theoretical one ($35.588 \text{ u}\text{\AA}^2$). The discrepancy is reduced to zero by rotating the $-\text{CHF}_2$ group by about 18° ; that is changing the dihedral angle $\text{HC}-\text{CO}_{\text{OH}}$ from 27.0 (*ab initio* value) to 45.1° (as shown in Figure 7.3).

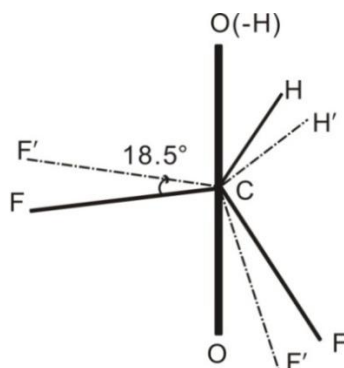


Figure 7.3 The $-\text{CHF}_2$ group of *gauche* conformer rotated 18.5° from *ab initio* to experimental result according to the inertia defect changes. $-\text{CHF}_2$ is the calculated structure while $-\text{CHF}'_2$ is the experimental structure.

7.4.4 Dissociation energy

One can see, in Figure 7.1, the intermolecular stretching motion leading to dissociation is almost parallel to the a -axis of the complex. Through the equations (Eq. (1.18) to (1.21)),^[17] the zero point dissociation energy of the complex can be derived to be $E_D = 25.6$ and 39.3 kJ mol^{-1} for *trans* and *gauche*, respectively.^[18] Both values are quite lower (up to 50% of discrepancy) than those from the calculations, probably because the pseudo diatomic approximation is too crude for this complex.

7.4.5 Ubbelohde effect

The deuteration at the HBs, produces a decrease of the B and C rotational constants larger than expected. The experimental ΔP_{aa} values (the shifts of P_{aa} upon OD deuteration) are considerably

larger than the calculated ones, according to the Ubbelohde effect previously described. To reproduce the experimental ΔP_{aa} values originated by the H→D substitutions, it has been necessary to slightly elongate the $r_{C..C}$ distances between the carboxylic carbon atoms of the two units by the $\Delta r_{C..C}$ quantities. The ΔP_{aa} and $\Delta r_{C..C}$ values are shown in Table 7.10 for all OD isotopologues of the two conformers.

Table 7.10 Experimental and calculated ΔP_{aa} values ($\text{u}\text{\AA}^2$) for the various isotopologues of the *trans* and *gauche* conformers of DFA-FA, and shifts ($\Delta r_{C..C}$) of the distances between the two carboxylic carbon atoms upon OD deuteration.

	<i>trans</i>			<i>gauche</i>		
	$\Delta P_{aa}^{[a]}/\text{u}\text{\AA}^2$		$\Delta r_{C..C}/\text{\AA}$	$\Delta P_{aa}^{[a]}/\text{u}\text{\AA}^2$		$\Delta r_{C..C}/\text{\AA}$
	exptl.	calc.		exptl.	calc.	
	DFA(OD)-FA	2.156	0.612	0.0060(3) ^[b]	2.290	0.971
DFA-FA(OD)	4.589	3.822	0.0030(3)	3.845	3.006	0.0031(3)
DFA(OD)-FA(OD)	6.636	4.407	0.0087(3)	6.050	3.945	0.0077(3)

[a] The P_{aa} values of the parent species are 692.203 and 685.926 $\text{u}\text{\AA}^2$ for *trans* and *gauche*, respectively. [b] Error in parentheses in units of the last digit.

7.4.7 One-dimensional flexible model calculation

After showing that the small vibrational splitting between the 0 and 1 sub-states is due to the $-\text{CHF}_2$ internal rotation connecting the two equivalent *gauche* form, we proceed in this section to the determination of the B_2 barrier along this pathway. First of all, we calculated the potential energy function along the CHF_2 internal rotation at the MP2/6-311++G(d,p) level using Gaussian03 program package, obtaining the results shown graphically in Figure 7.4. Since the barrier between the *gauche* and *trans* conformers is considerably higher than that connecting the two *gauche* forms, we assumed the splitting as due to the tunneling through the smaller (G-G') barrier. We used then the ΔE_{01} splitting to determine the local B_2 barrier by using Meyer's one-dimensional flexible model.^[166] We described the potential energy pathway with this following equation:

$$V(\tau) = B_2[(1 - (\tau/\tau_e)^2)^2] \quad (7.2)$$

where B_2 is the torsional barrier, and τ (\equiv HC-CO_{OH} dihedral angle) is the torsional angle of the -CHF₂ group, assumed to be zero when “*cis*-orientated”, that is the transition state between the two equilibrium minima ($\pm\tau_e$).

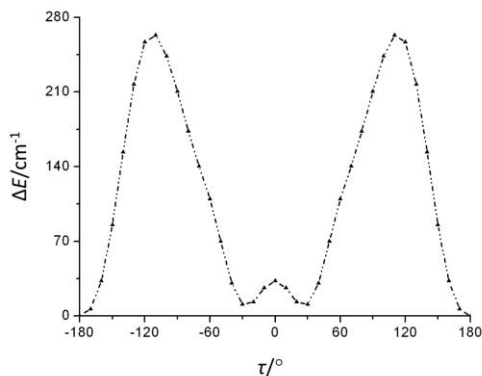


Figure 7.4 *Ab initio* potential energy function for the internal rotation of the -CHF₂ group in DFA-FA.

The structural relaxations of the bond lengths and valence angles of the two fluorine atoms as a function of τ were also taken into account by the expression:

$$S(\tau) = S_0 + \Delta S(\tau/\tau_e) \quad (7.3)$$

For a given parameter S , S_0 is the value at $\tau = 0$ while ΔS is its variation in going from $\tau = 0$ to $\tau = \tau_e$. All these values have been obtained comparing the *ab initio* geometries of the minimum to those of the transition state.

Table 7.11 Flexible model results for the B_2 barrier connecting the two *gauche* forms of DFA-FA

1) Experimental and calculated data		
	exptl.	calc.
$P_{\text{ex}}/\text{u}\text{\AA}^2$	24.090	24.094
$\Delta A/\text{MHz}$	-1.54	-1.45
$\Delta E/\text{MHz}$	3.15	3.14
2) Determined parameters		
B_2/cm^{-1}		101.8(3)
$\tau_e/^\circ$		45.2(3)

In the flexible model calculations, the range -85 to $+85$ has been resolved into 41 mesh points.^[136] The obtained results are listed in Table 7.11. A barrier $B_2 = 101.8(3) \text{ cm}^{-1}$ has been

determined, about five times larger than the *ab initio* value (22 cm^{-1}), but similar to the barrier obtained for the complex acrylic acid - difluoroacetic acid.^[186]

7.5 Acrylic acid...Fluoroacetic acid

7.3.1 Theoretical calculations

Full geometry optimization of the four more stable configurations of the dimer were carried out at the MP2/6-311++G(d,p) level.^[13] The corresponding draws, as well as the calculated rotational constants, electric dipole moment and relative energies are listed in Table 7.12.

Table 7.12. MP2/6-311++G(d,p) calculated parameters of the plausible conformers of FAA-AA bimolecule.

	<i>Tc</i>	<i>Tt</i>	<i>Cc</i>	<i>Ct</i>
$\Delta E/\text{cm}^{-1}$	0 ^[a]	85	169	266
$\Delta E_{\text{bsse}}/\text{cm}^{-1}$	0 ^[b]	70	178	261
<i>A</i> /MHz	4285	4025	3977	4704
<i>B</i> /MHz	464	468	471	456
<i>C</i> /MHz	420	421	422	416
$ \mu_a , \mu_b /\text{D}$	1.9, 1.8	1.7, 1.2	1.7, 1.0	2.0, 1.6

[a] Absolute energy is $-594.201813 E_h$. [b] Absolute energy is $-594.196566 E_h$.

We label the four species with acronyms of the type Xx , where X indicates the configurations of FAA (T for *trans*, C for *cis*), while x indicates the configurations of AA (t for *trans*, c for *cis*). In order to have a better estimate of the energy differences, all intermolecular binding energy values were counterpoise corrected for BSSE.^[12] These calculations suggest configurations with *trans* FAA to lie at lower energies. According to the calculated rotational constants, the μ_a -type R branch bands, which is more intense, were expected to appear in narrow frequency regions, separated by a $B+C$ spacing.

7.3.2. Rotational spectra

We searched first for the μ_a -type transitions of the global minimum Tc , which are expected to be the most intense lines. Transitions with $J = 9$ to 12 and with K_{-1} 0 to 4 could be measured. Then some

μ_b -type *R* and *Q* branch lines were also identified.

Once conformer *Tc* was excluded from the spectrum, a number of less intense transitions could be easily assigned to conformer *Tt*. With further signal accumulation, some much weaker lines were found which were assigned to the *Cc* transitions.

It is interesting to note that *cis*-FAA, which appears in the *Cc* form of the dimer, was not observed in the MW spectrum of the monomer (a second conformer was observed, but with a *cis* configuration of the COOH group),^[187] probably because of the very small values of its dipole moment components. So, acrylic acid acts as an electrophore for *cis*-FAA, leading to its indirect observation.

It was not possible to assign the spectrum of the fourth conformer (*Ct*).

Table 7.13 Experimental spectroscopic parameters of the observed conformers of FAA-AA bimolecule (*S*-reduction, *I*^r representation)

	<i>Tc</i>	<i>Tt</i>	<i>Cc</i>
<i>A</i> /MHz	4350.3931(7) ^[a]	4046.0566(8)	3997.401(1)
<i>B</i> /MHz	470.1161(2)	475.4679(2)	477.7362(2)
<i>C</i> /MHz	425.7949(2)	426.9990(2)	428.2972(2)
<i>D_J</i> /kHz	0.017(1)	0.018(1)	0.017(1)
<i>D_{JK}</i> /kHz	-0.014(2)	-0.091(2)	-0.064(2)
σ ^[b] /kHz	2.1	2.4	2.0
<i>N</i> ^[c]	48	48	35

[a] Error in parentheses in units of the last digit. [b] RMS error of the fit. [c] Number of lines in the fit.

All measured transitions could be fit, independently for each conformer, with Watson's semi-rigid Hamiltonian (*S*-reduction; *I*^r-representation),^[8] obtaining the rotational and two first order centrifugal distortion constants reported in Table 7.13. The comparison between the experimental and predicted rotational constants (see Tables 7.12 and 7.13) gives unequivocal conformational assignments of conformers *Tc*, *Tt*, and *Cc*. The spectroscopic rotational constants of the three detected conformers agree almost perfectly with the calculated values. The deviations are all less than 2%. Therefore, no further structural fitting has been done for the geometric structures.

Then, we analyzed the rotational spectra of the OD deuterated species, obtained by mixing the acids with D₂O. The spectra of these species resulted quite weak, probably due to the presence of adducts of the carboxylic acids with water. For this reason, only five OD isotopologues have

been observed (3 for the Tc and 2 for the Tt species, respectively). A few transitions have been measured for each deuterated species, and for this reason the centrifugal distortion constants have been fixed, in the fits, to the values of the corresponding parent species. The determined spectroscopic parameters of all deuterated isotopologues are listed in Table 7.14.

Table 7.14 Experimental spectroscopic parameters for the deuterated species of FAA-AA. (S-reduction, I' representation). The D_J and D_{JK} centrifugal distortion parameters have been fixed to the values of the corresponding parent species.

	Tc			Tt	
	FAA(OD)-AA	FAA-AA(OD)	FAA(OD)-AA(OD)	FAA(OD)-AA	FAA-AA(OD)
A/MHz	4295.258(5) ^[a]	4292.946(5)	4238.737(5)	3983.443(5)	4019.761(5)
B/MHz	469.4828(2)	469.3397(2)	468.7634(2)	474.5850(2)	474.6199(2)
C/MHz	424.7434(2)	424.6039(2)	423.5976(2)	425.5827(2)	426.0249(2)
$\sigma^{[b]}/\text{kHz}$	1.3	1.7	3.3	3.1	2.6
$N^{[c]}$	11	11	11	11	11

[a] Error in parentheses in units of the last digit. [b] RMS error of the fit. [c] Number of lines in the fit.

7.4.3 Sizing the Ubbelohde effect

From the rotational constants it is easy to calculate, for each species, the values of the P_{aa} . We report in Table 7.15 the P_{aa} values, along with the calculated and experimental values of their shifts upon OD deuteration.

Table 7.15 P_{aa} values ($\text{u}\text{\AA}^2$) for the various isotopologues of the Tc and Tt conformers of FAA-AA, and calculated and experimental values of their shifts upon OD deuteration.

	Tc				Tt		
	P_{aa}	ΔP_{aa}		P_{aa}	ΔP_{aa}		
		exptl.	calc.		exptl.	calc.	
FAA-AA	1072.874			1060.781			
FAA(OD)-AA	1074.323	1.449	0.009	1062.757	1.976	0.073	
FAA-AA(OD)	1074.650	1.777	0.173	1062.675	1.894	0.318	
FAA(OD)-AA(OD)	1075.964	3.091	0.183	-	-	-	

The experimental ΔP_{aa} values are considerably larger than the calculated one, according to the Ubbelohde effect previously described.^[135-136] To reproduce the experimental ΔP_{aa} values

expected originated by the H→D substitutions, it has been necessary to slight elongate the r_{C-C} distances of the carboxylic carbon atoms, according to the values shown in Table 7.16.

Table 7.16 Increases of the C-C distances (r_{C-C}) upon H→D substitution

	$r_{C-C}/\text{Å}$	
	T_c	T_t
FAA(OD)-AA	0.0040(3)	0.0053(3)
FAA-AA(OD)	0.0045(3)	0.0044(3)
FAA(OD)-AA(OD)	0.0082(3)	-

7.5.4 Information on the dissociation energy

The intermolecular stretching motion which leads to the dissociation is almost parallel to the a -axis for all conformers of the complex. In this case, a pseudo diatomic approximation can be used to roughly estimate the force constant of the stretching mode leading to the dissociation through Eq. (1.18),^[17] and then the zero point dissociation energy of the complex can be derived applying the approximate expression (Eq. (1.21)).^[18]

The results are listed in Table 7.17. The dissociation energies of the three conformers have similar values, in accord with *ab initio* calculations results.

Table 7.17 Dissociation energy data (see text)

	T_c	T_t	C_c
k_s/Nm^{-1}	40	39	42
ν/cm^{-1}	134	132	137
$R_{CM}/\text{Å}$	4.81	4.81	4.80
$E_D^{[a]}/\text{kJ mol}^{-1}$	77	75	80
$E_{D0}^{[b]}/\text{kJmol}^{-1}$	67	67	67
$E_{DBSSE}^{[c]}/\text{kJmol}^{-1}$	53	54	53

[a] Pseudo diatomic approximation. [b] MP2/6-311++G(d,p) values. [c] Counterpoise corrected MP2/6-311++G(d,p) values.

7.6 Relative population of the conformers in the jet

Relative intensity measurements of some pairs of nearby μ_a -type lines, allowed the estimation of the relative population of the conformers in the jet for the three above carboxylic acid

bimolecules. We obtained for AA-TFA $N_{cis}/N_{trans} \approx 6/1$, for DFA-FA $N_{trans}/N_{gauche} \approx 1/1$, and for AA-FAA $N_{Tc}/N_{Tt}/N_{Cc} \approx 7/4/1$. As outlined in other papers,^[188] in the jet plume there is not an equilibrium situation, and the relative concentration of the dimer conformers depend also on the concentrations of the conformers of the monomers, so that is difficult to give the relative energies. The relative populations are, however, qualitatively in agreement with the order of the calculated *ab initio* relative energies.

7.7 Conclusions

In summary, with FTMW technique, we assigned the rotational spectra of TFA-AA, DFA-FA and FAA-AA carboxylic acid dimers including their deuterated species. Two or three conformers were identified. The concerted double proton transfer in these three complexes connects different conformers, differently with respect to the cases of AA-AA or benzoic acid-formic acid, where this motion connects equivalent minima, generating tunneling splitting. The increase of the HB length upon H→D isotopic substitution (Ubbelohde effect) has been deduced from the elongation of the carboxylic carbons C··C distance.

What deserves to be mentioned is the successful assignment of the conformer *Cc* involving *cis*-FAA evinced the existence of *cis*-FAA in the supersonic jet, in spite of the failure of observing it in isolation.

For DFA-FA, experimental values of the ΔE_{01} splitting allowed determining the barrier to the inversion of the two *gauche* forms. The value of the planar moment of inertia P_{cc} shows that for this form its experimental geometry requires a rotation of $-\text{CHF}_2$ about 18° with respect to the theoretical value.

Chapter 8

Complex of Rare Gas

8.1 Introduction

As mentioned in Chapter 3, complexes with aromatic molecules have the RG atom firmly linked to one side of the ring and the vdW motions do not generate any observable inversion splittings. Vice versa, when a RG atom is linked to an open chain molecule, all the complexes display rotational transitions characterized by inversion splittings. Aliphatic ring organic molecules are intermediate between aromatic molecules and open chain molecules as far as tunneling splittings are concerned.

Tetrahydrofuran (THF) is a fully aliphatic cyclic non-planar molecule, which undergoes a pseudo-rotation motion, with a consequent splitting in four pseudo-rotation sub-states of the ground vibrational state.^[11, 189] Its complex with Ar (THF-Ar) displayed a systematic doubling of the rotational lines.^[190] According to the observed Coriolis coupling constants, the observed tunneling splitting was mainly attributed to the residual pseudo-rotation effects of the THF subunit in the complex.

In this chapter, in order to check if the interpretation of the doubling in THF-Ar was correct, to investigate the influence of the RG atomic weight and polarizability on the tunneling effects, and to model the potential energy function of the tunneling motion, the rotational study of the THF- Kr complex with PJ-FTMW technique has been discussed in detail.^[191]

8.2 Experimental

Molecular clusters were generated in a supersonic expansion, under conditions optimized for the dimer formation.

A gas mixture of ca. 11% of Kr in Helium at a stagnation pressure of ~ 0.25 MPa was passed over a sample of THF (commercial sample bought from Aldrich, and used without further

purification) and expanded into the Fabry-Pérot cavity.

8.3 Theoretical Calculations

THF-Kr is schematically shown in Figure 8.1, together with the parameters defining the position of the Kr atom, which will be used through the text. In going from the molecule to the complex, an inversion of the principal axis of inertia takes place with respect to the ring skeleton. The position of Kr in the complex can be described with spherical coordinates R_{cm} , θ and ϕ . R_{cm} is the distance of the Kr atom from the center of mass of the monomer, θ is the angle that R_{cm} makes with the c principle axis of THF, and ϕ is the angle between the projection of R_{cm} in the ab plane and the a principle axis of THF.

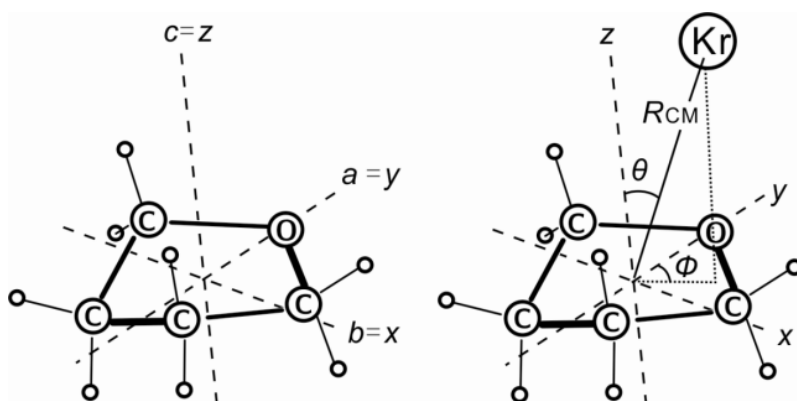


Figure 8.1 Sketch of THF-Kr. the spherical coordinates locating the position of Kr, used in the DPM calculation are defined. The principal axis of the complex are, in a first approximation, linked to the x , y , z coordinates according to $x \approx b$, $y \approx c$, $z \approx a$.

First we applied the distributed polarizability model (DPM),^[192-193] using the computer program RGDMIN with full minimization of the structural vdW parameters,^[123] which is very simple and fast, while very efficient to find the possible minima on the vdW PES.^[194] Later on we better characterized the global minimum found with RGDMIN by *ab initio* calculations (MP2/6-311++G(d,p)).^[13] The calculated rotational constants and electric dipole moments are listed in Table 8.1, whilst the three spherical coordinates are given in a subsequent section. According to the calculated electric dipole moment components, we expected to observe an asymmetric rotor spectrum with weak a -type, b -type and stronger c -type transitions.

Table 8.1. MP2/6-311++G(d,p) and DPM calculated rotational constants and components of the electric dipole moment of THF-Kr

	MP2/6-311++G(d, p)	DPM
<i>A, B, C</i> /MHz	4371, 784, 773	4240, 755, 747
$ \mu_a , \mu_b , \mu_c $ /D	0.9, 0.8, 1.5	-

8.4 Rotational Spectra

The spectrum of the most abundant isotopic species (^{84}Kr , *ca.* 57% of natural abundance) has been investigated first. Since THF-Kr is an almost prolate symmetric top, the *S*-reduction and the I^r -representation have been chosen.^[8] The frequencies were fitted with a Pickett SPFIT computer program,^[95, 195] according to the reduced axis Hamiltonian,

$$H = \sum_i H_i + H_{0+0^-} \quad (i = 0^+, 0^-) \quad (8.1)$$

where

$$\begin{aligned} H_i = & A(i)P_a^2 + B(i)P_b^2 + C(i)P_c^2 - D_J P^4 \\ & - D_{JK} P_a^2 P^2 + d_1 P^2 \times (P_+^2 + P_-^2) \\ & + d_2 P^2 \times (P_+^2 + P_-^2) \end{aligned} \quad (8.2)$$

and

$$\begin{aligned} H_{0^+0^-} = & [F_{bc} + F'_{bc} J(J+1)] \times (P_b P_c + P_c P_b) \\ & + F_{ab} \times (P_a P_b + P_b P_a) + \Delta E_{0^+0^-} \end{aligned} \quad (8.3)$$

Several μ_a -R-type lines, with *J* ranging from 5 to 11, were initially assigned. Then some μ_c -R-type lines were measured. Both μ_a - and μ_c -type are split into two nearby component lines, as shown in Figure 8.2 for the $6_{1,5} \leftarrow 5_{1,5}$ transition. Below we will show that they are intrastate transitions due to a tunneling motion in THF-Kr.

Later, the vibration-rotation transitions $5_{1,5}(0^-) \leftarrow 4_{1,3}(0^+)$ and $5_{1,4}(0^+) \leftarrow 4_{1,4}(0^-)$, in principle forbidden, were observed at 7743.889 MHz ($\nu_{\text{obs}} - \nu_{\text{calc}} = 0.67$ kHz) and 7786.077 MHz ($\nu_{\text{obs}} - \nu_{\text{calc}} = 0.03$ kHz), respectively. These transitions have μ_a -type character due to the strong mixing between the pairs of states $5_{1,5}(0^-) - 5_{1,4}(0^+)$ and $4_{1,4}(0^-) - 4_{1,3}(0^+)$ produced by Coriolis

interactions.

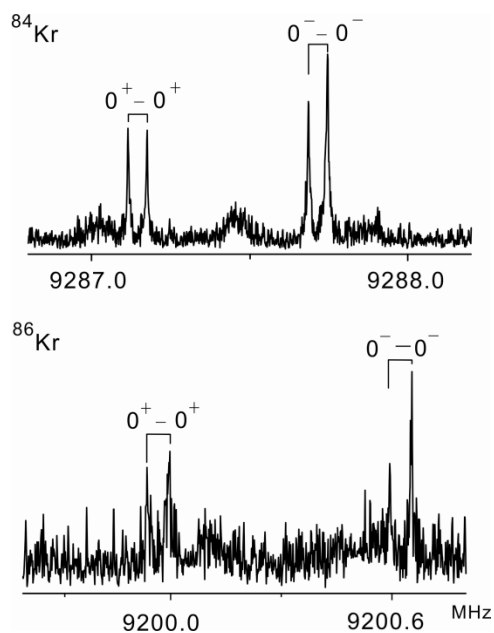


Figure 8.2 Recorded $6_{1,6} \leftarrow 5_{1,5}$ transitions, split into two tunneling component lines, for the ^{84}Kr (top) and ^{86}Kr (bottom) isotopologues. Each line appears as a doublet (\square) due to the Doppler effect.

Finally, several interstate μ_b -type transitions, fully split by about the double of the vibrational splitting between the 0^+ and 0^- sublevels, were assigned and measured.

The determined 14 spectroscopic parameters are listed in Table 8.2. They are three rotational constants for each of the coupled states, four quartic centrifugal distortion constants (set to a common value for the two states), their energy difference ($\Delta E_{0^+0^-}$), the interaction constants F_{ab} and F_{bc} , and J -dependence F'_{bc} , as defined in the interaction Hamiltonian ($H_{0^+0^-}$).

The spectrum of the second most intense isotopologue (^{86}Kr , *ca.* 17% of natural abundance) has also been measured in the same way. The vibration-rotation transitions $5_{1,5}(0^-) \leftarrow 4_{1,3}(0^+)$ and $5_{1,4}(0^+) \leftarrow 4_{1,4}(0^-)$ at 7671.3488 MHz ($\nu_{\text{obs}} - \nu_{\text{calc}} = -1.50$ kHz) and 7712.2631 MHz ($\nu_{\text{obs}} - \nu_{\text{calc}} = 0.39$ kHz) were observed likewise, respectively.

The F_{ab} coefficient is larger than F_{bc} although the latter is better determined due to the small energy separation ($\Delta E_{0^+0^-}$) which is of the same order of magnitude of the rotational spacing between many of the observed K_a asymmetry doublets. These data help to understand which kind of motion is responsible for the tunneling splitting which evidently indicates a double minimum potential owing to a large amplitude motion of the complex. This motion could be: (i) the residual pseudo-rotation of the ring in the complex, or (ii) the transfer of Kr from above to below

the THF ring (see Figure 8.1). In the first case, the angular momentum vector oriented along the a -principle axis of isolated THF should have components mainly along a - and c -axes of THF-Kr. Orienting along the a -axis of THF, a larger projection along the c -axis than a -axis of THF-Kr is expected. As in the principle inertial axes system, the Coriolis coupling could be interpreted in terms of the angular momentum operator^[195]. It's in good agreement with the facts that the a - and c -type coupling terms, F_{bc} and F_{ab} , are observed between the tunneling states of THF-Kr, being larger the c -type coupling. In addition, the μ_b dipole moment component should invert when going from one minimum to the equivalent one, and correspondingly μ_b type transitions should be interstate transitions. Contrastively, in the second case, μ_c type transitions should be the interstate ones. Therefore, the kinds of the observed Coriolis coupling terms and the kind of interstate transitions, allow us to conclude that the observed tunneling splitting should be in connection with a residual pseudo-rotation of the THF subunit. Similar behaviors have also been observed for some HB complexes involving THF like THF-HCl^[196] and THF-HF^[197] whose rotational spectrum present doublets owing to the pseudo-rotation tunneling of THF.

Table 8.2 Experimental spectroscopic constants of THF-Kr (S reduction, F representation)

	THF- ⁸⁴ Kr		THF- ⁸⁶ Kr	
	0 ⁺	0 ⁺	0 ⁺	0 ⁺
A /MHz	4369.442(6) ^[a]	4369.569(6)	4369.261(1)	4369.385(1)
B /MHz	784.394(6)	784.387(6)	776.829(1)	776.821(1)
C /MHz	773.3362(3)	773.3173(2)	766.0845(2)	766.0604(2)
D_J /kHz	1.4044(4)		1.3799(9)	
D_{JK} /kHz	4.46(1)		4.24(6)	
d_1 /kHz	0.120(2)		[0.120] ^[b]	
d_2 /Hz	0.4(1)		[0.4]	
$\Delta E_{0^+0^-}$ /MHz	87.462(2)		87.070(2)	
F_{ab} /MHz	127.01(9)		124.57(9)	
F_{bc} /MHz	-4.3642(2)		-4.2789(1)	
F'_{bc} /kHz	0.172(4)		[0.172]	
N ^[c]	60		36	
σ ^[d] /kHz	1.10		1.60	

[a] Error in parenthesis is expressed in units of the last digit; [b] Values in square brackets fixed to the values of the THF-⁸⁴Kr;

[c] Number of transitions in the fit; [d] Standard deviation of the fit.

8.5 Location of the Kr atom in the complex

Four different sets (r_0 , r_s , r_{DPM} and r_c) of the vdW structural parameters of the complex are shown in Table 8.3.

The partial r_0 structure was obtained by fitting the distance R_{cm} and the angles θ and ϕ indicated in Figure 8.1 to the available rotational constants, and starting from the *ab initio* structure. The r_s coordinates^[16] of the krypton atom can be obtained in the principal axes system of THF by a hypothetical substitution of an atom of zero mass with a Kr in going from THF to THF ··Kr, or in the principal axes system of THF ··⁸⁴Kr when substituting ⁸⁴Kr with ⁸⁶Kr. However, these values are quite approximate because of vdW vibrations, which take place only in the complex. The r_e and r_{DPM} geometries are from *ab initio* and DPM calculations, respectively.

The r_0 values are very similar to the r_e ones, so that just a slight adjustment of the vdW parameters has been required.

Table 8.3 Experimental (r_s and r_0) and theoretical (r_e and r_{DPM}) vdW structural parameters of THF ··Kr.

	r_0	r_s	r_e	r_{DPM}
<i>1) Kr coordinates in the principal axes system of THF ··Kr.</i>				
$ a /\text{Å}$	1.774	1.766(1) ^[a]	1.775	1.812
$ b /\text{Å}$	0.004	0.13(1)	0.004	0.003
$ c /\text{Å}$	0.067	0.0 ^[b]	0.067	0.060
<i>2) Kr coordinates in the principal axes system of THF</i>				
$ a /\text{Å}$	1.377	1.62(1)	1.430	1.245
$ b /\text{Å}$	0.750	0.2(1)	0.652	0.668
$ c /\text{Å}$	3.508	3.488(1)	3.508	3.661
<i>3) Kr vdW parameters</i>				
$R_{\text{cm}}/\text{Å}$	3.843(1)	3.841	3.845	3.924
$\theta/^\circ$	24.1(1)	24.8	24.1	21.1
$\phi/^\circ$	29(4)	5.7	24.5	28.2

[a] Error in parenthesis is expressed in units of the last digit; [b] Imaginary value: set to zero

8.6 VdW vibrations

8.6.1 VdW Stretching

Upon complexation with THF, the three translational degrees of freedom of the isolated krypton atom are replaced by three vdW vibrational modes: the THF-Kr stretching, and two bendings. First we assumed the Kr stretching motion to be isolated from the other motions. So the stretching force constant (k_s) can be estimated with pseudo diatomic approximation (Eq.

(1.18)).^[17] We obtained $k_s = 3.0 \text{ N m}^{-1}$, and corresponding to a harmonic stretching fundamental 36 cm^{-1} . The dissociation energy, according to Eq. (1.21), has been estimated to be 3.7 kJ mol^{-1} .^[18]

The dissociation energy of THF-Kr is higher than that of THF-Ar ($E_D = 2.6 \text{ kJ mol}^{-1}$),^[190] in agreement with the higher polarizability of Kr with respect to Ar. The same parameters of the complexes involving THF, 2,5-dihydrofuran, pyridine and oxirane with Kr are listed in Table 8.4.

Table 8.4 Force constant and dissociation energy of the vdW stretching in some complexes of Kr with ring molecules.

	$k_s/\text{N m}^{-1}$	$E_D/\text{kJ mol}^{-1}$	Ref.
THF-Kr	3.02	3.7	present work
2,5-dihydrofuran-Kr	3.26	3.5	[24]
pyridine-Kr	3.51	3.8	[4a]
oxirane-Kr	2.69	3.1	[25]

8.6.2 Tunneling Motion Described by One-Dimensional Flexible Model Calculation

Meyer's one-dimensional flexible model^[166] has been used to determine the potential energy barrier between the two equivalent minima due to the bending motions of C5 and C6 up and down to the plane C3D2C4 in Figure 8.3 where the notation D is for "dummy" atoms referencing points in the molecule not corresponding to real atoms.

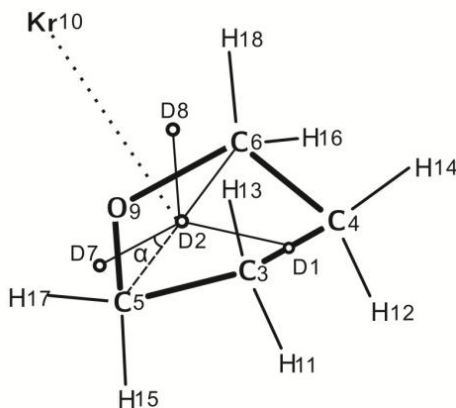


Figure 8.3 Ring-puckering in THF-Kr. α denotes the inversion angle of C5 or C6. D_i ($i = 1, 2, 7, 8$) denotes dummy points.

This model allows the numerical calculation of the rotational and vibrational wave functions and eigenvalues (and then the vibrational spacings), but needs a description of the pathway and a potential energy function. For this purpose, the geometry of the transient states of THF-Ar were obtained from *ab initio* calculations at the MP2/6-311++G(d,p) level. The experimental value for the barrier has been obtained from the ΔE_{0+0} -splitting (see in table 8.2). The following potential energy function has been adopted:

$$V(\alpha) = B_2[1 - (\alpha/\alpha_e)^2]^2, \quad (8.4)$$

where the inversion coordinate α is the twisting angle (with respect to the planarity of the four carbon atoms) of the C5 and C6 atoms (see Figure 8.3). B_2 is the barrier to inversion and α_e is the equilibrium value of the inversion angle. The main relaxations of other structural parameters have been accounted for according to:

$$S(\alpha) = S_0 + \Delta S(\alpha/\alpha_e)^2, \quad (8.5)$$

for symmetric variations with respect to α (most parameters), or according to:

$$A(\alpha) = A_0 + \Delta A(\alpha/\alpha_e), \quad (8.6)$$

for asymmetric changes. For a given parameter S (or A), S_0 (or A_0) is the value at $\alpha = 0$ while ΔS (or ΔA) is its variation in going from $\alpha = 0$ to $\alpha = \alpha_e$. All these values have been obtained from the *ab initio* geometries of the minimum and of the transition state.

Table 8.5 Results of the flexible model calculations

1) Tunneling Splittings		
	Obs	Calc
$\Delta E_{0+0}({}^{84}\text{Kr})$ / MHz	87.462(2) ^[a]	87.51
$\Delta E_{0+0}({}^{86}\text{Kr})$ / MHz	87.070(2)	87.12
2) Determined parameters		
	$B_2 = 67(1) \text{ cm}^{-1}$	$\tau_0 = 25.3^\circ$ ^[b]
3) Structural relaxation parameters		
$\Delta S(r_{\text{C5-C6}}) = 0.090 \text{ \AA}$	$\Delta S(r_{\text{D1-D2}}) = -0.085 \text{ \AA}$	$\Delta S(r_{\text{O9-D2}}) = -0.084 \text{ \AA}$
$\Delta S(r_{\text{Kr-D2}}) = -0.192 \text{ \AA}$	$\Delta S(\text{O9D2D7}) = 40.8^\circ$	$\Delta S(\text{KrD2D1}) = 27.1^\circ$
$\Delta A(\text{O9D2-D7D8}) = 0.1^\circ$	$\Delta A(\text{KrD2-D1C5}) = 3.4^\circ$	$\Delta A(\text{H11C3-C5D2}) = 27.5^\circ$ ^[c]

[a] Error in parenthesis is expressed in units of the last digit; [b] Fixed at the *ab initio* values; [c] The structural relaxation for the dihedral angle H11C3-C5D2 holds also for the corresponding dihedral angles of H12, H13, H14.

The results of the flexible model calculations are showed in Table 8.5. α_0 was fixed at the *ab initio* value, 25.3° , because there were not enough data to fit also this parameter. The determined potential energy function is shown in Figure 8.4. The B_2 value, 67 cm^{-1} , is about the double of that suggested by the *ab initio* calculations (34 cm^{-1}). The excellent reproduction of the shift of ΔE_{0+0} in going from THF- ^{84}Kr to THF- ^{86}Kr , justify the reliability of flexible model.

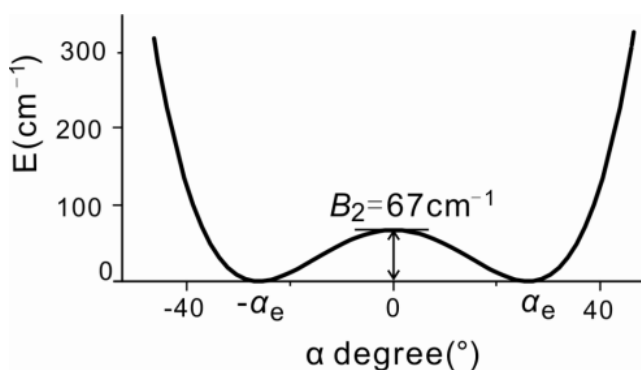


Figure 8.4 Pseudo-rotation potential energy pathway in THF-Kr according to the flexible model analysis.

In the flexible model calculations the α coordinate has been considered in the $\pm 50^\circ$ range and solved into 61 mesh points.^[166]

8.7 Conclusions

In this chapter, the rotational spectrum of the van der Waals complex THF-Kr investigated by PJ-FTMW spectroscopic techniques shows that the systematic doubling of the rotational lines has been attributed to the residual pseudo-rotation of THF in the complex, based on the values of the Coriolis coupling constants, and on the type (μ_b) of the interstate transitions. Meyer's one-dimensional flexible model analysis proved the potential energy function for the pseudo-rotation motion.

The strength of the THF-Kr "chemical" bond ($\sim 3.7\text{ kJ mol}^{-1}$) is higher than that of the related THF-Ar, in accord with the higher polarizability of krypton.

References

- [1] W. Gordy, R. L. Cook, *Microwave Molecular Spectra*, 3rd ed., Wiley, New York, **1984**.
- [2] C. H. Townes, A. L. Schawlow, *Microwave Spectroscopy*, McGraw-Hill, Inc., New York, **1955**.
- [3] H. W. Kroto, *Molecular Rotation Spectra*, John Wiley & Sons, London, **1975**.
- [4] W. Caminati, J.-U. Grabow, *Microwave Spectroscopy in Molecular Systems in Frontiers of Molecular Spectroscopy* (Ed.: J. Laane), Elsevier, **2009**.
- [5] E. Hirota, *Ann. Rev. phys. Chem.* **1991**, 42, 1-23.
- [6] D. W. Pratt, *Ann. Rev. phys. Chem.* **1998**, 49, 481-530.
- [7] L. Evangelisti, W. Caminati, *Phys.Chem. Chem. Phys.* **2010**, 12, 14433-14441.
- [8] J. K. G. Watson, *Vibrational Spectra and Structure*, Vol. 6, ELSEVIER, New York/Amsterdam, **1977**.
- [9] J. W. Simmons, W. E. Anderson, W. Gordy, *Phys. Rev.* **1950**, 77, 77-79.
- [10] R. Chang, *Basic Principles of Spectroscopy*, McGraw-Hill, **1971**.
- [11] R. Meyer, J. C. Lopez, J. L. Alonso, S. Melandri, P. G. Favero, W. Caminati, *J. Chem. Phys.* **1999**, 111, 7871-7880.
- [12] S. F. Boys, F. Bernardi, *Mol. Phys.* **1970**, 19.
- [13] M. J. T. Frisch, G. W.; Schlegel, H. B.; Scuseria, G. E.; Robb, M. A.; Cheeseman, J. R.; Montgomery, Jr., J. A.; Vreven, T.; Kudin, K. N.; Burant, J. C.; Millam, J. M.; Iyengar, S. S.; Tomasi, J.; Barone, V.; Mennucci, B.; Cossi, M.; Scalmani, G.; Rega, N.; Petersson, G. A.; Nakatsuji, H.; Hada, M.; Ehara, M.; Toyota, K.; Fukuda, R.; Hasegawa, J.; Ishida, M.; Nakajima, T.; Honda, Y.; Kitao, O.; Nakai, H.; Klene, M.; Li, X.; Knox, J. E.; Hratchian, H. P.; Cross, J. B.; Adamo, C.; Jaramillo, J.; Gomperts, R.; Stratmann, R. E.; Yazyev, O.; Austin, A. J.; Cammi, R.; Pomelli, C.; Ochterski, J. W.; Ayala, P. Y.; Morokuma, K.; Voth, G. A.; Salvador, P.; Dannenberg, J. J.; Zakrzewski, V. G.; Dapprich, S.; Daniels, A. D.; Strain, M. C.; Farkas, O.; Malick, D. K.; Rabuck, A. D.; Raghavachari, K.; Foresman, J. B.; Ortiz, J. V.; Cui, Q.; Baboul, A. G.; Clifford, S.; Cioslowski, J.; Stefanov, B. B.; Liu, G.; Liashenko, A.; Piskorz, P.; Komaromi, I.; Martin, R. L.; Fox, D. J.; Keith, T.; Al-Laham, M. A.; Peng, C. Y.; Nanayakkara, A.; Challacombe, M.; Gill, P. M. W.; Johnson, B.; Chen, W.; Wong, M. W.; Gonzalez, C.; Pople, J. A. , *Gaussian 03* (Revision B.01) ed., Gaussian, Inc., Pittsburgh PA, **2003**.
- [14] M. J. Frisch, G. W. Trucks, H. B. Schlegel, G. E. Scuseria, M. A. Robb, J. R. Cheeseman, G. Scalmani, V. Barone, B. Mennucci, G. A. Petersson, H. Nakatsuji, M. L. Caricato, X.; Hratchian, H. P.; Izmaylov, A. F.; Bloino, J.; Zheng, G.; Sonnenberg, J. L.; Hada, M.; Ehara, M.; Toyota, K.; Fukuda, R.; Hasegawa, J.; Ishida, M.; Nakajima, T.; Honda, Y.; Kitao, O.; Nakai, H.; Vreven, T.; Montgomery, J. A.; J. E. J. Peralta, F. B. Ogliaro, M.; Heyd, J. J.; Brothers, E.; Kudin, K. N.; Staroverov, V. N.; Kobayashi, R.; Normand, J.; Raghavachari, K.; Rendell, A.; Burant, J. C.; Iyengar,

References

- S. S.; Tomasi, J.; Cossi, M.; Rega, N.; Millam, J. M.; Klene, M.; Knox, J. E.; , J. B. Cross, V. A. Bakken, C.; Jaramillo, J.; Gomperts, R.; Stratmann, R. E.; Yazyev, O.; Austin, A. J.; Cammi, R.; Pomelli, C.; Ochterski, J. W.; Martin, R. L.; Morokuma, K.; Zakrzewski, V. G.; Voth, G. A.; Salvador, P.; Dannenberg, J. J.; Dapprich, S.; , A. D. Daniels, Ö. F. Farkas, J. B.; Ortiz, J. V.; Cioslowski, J.; Fox, D. J., Gaussian, Inc., Wallingford CT, **2009**.
- [15] Maestro, version 9.2 ed., Schrödinger, LLC, New York, **2012**.
- [16] J. Kraitchman, *Am. J. Phys.* **1953**, *21*.
- [17] D. J. Millen, *Can. J. Chem.* **1985**, *63*, 1477-1479.
- [18] S. E. Novick, S. J. Harris, K. C. Janda, W. Klemperer, *Can. J. Phys.* **1975**, *53*, 2007-2015.
- [19] J. P. Klinman, *Pure Appl. Chem.* **2003**, *75*, 601-608.
- [20] J. Bigeleisen, M. W. Lee, F. Mandel, *Ann. Rev. phys. Chem.* **1973**, *24*, 407-440.
- [21] J. Szydlowski, *J. Mol. Struct.* **1994**, *321*, 101-113.
- [22] R. E. Wasylshen, S. Peiris, D. R. Arnold, *Chem. Phys. Lett.* **1985**, *114*, 31-34.
- [23] M. Ichikawa, *J. Mol. Struct.* **2000**, *552*, 63-70.
- [24] A. R. Ubbelohde, K. J. Gallagher, *Acta Crystallogr.* **1955**, *8*, 71-83.
- [25] H.-H. Limbach, M. Pietrzak, H. Benedict, P. M. Tolstoy, N. S. Golubev, G. S. Denisov, *J. Mol. Struct.* **2004**, *706*, 115-119.
- [26] X.-Z. Li, B. Walker, A. Michaelides, *Proc. Natl. Acad. Sci.* **2011**, *108*, 6369-6373.
- [27] B. M. Giuliano, W. Caminati, *Angew. Chem. Int. Ed.* **2005**, *44*, 603-606.
- [28] W. Caminati, A. Millemaggi, J. L. Alonso, A. Lesarri, J. C. Lopez, S. Mata, *Chem. Phys. Lett.* **2004**, *392*, 1-6.
- [29] U. Andresen, H. Dreizler, J. U. Grabow, W. Stahl, *Rev. Sci. Instrum.* **1990**, *61*, 3694-3699.
- [30] J. U. Grabow, W. Stahl, H. Dreizler, *Rev. Sci. Instrum.* **1996**, *67*, 4072-4084.
- [31] J. Alonso, F. J. Lorenzo, J. C. López, A. Lesarri, S. Mata, H. Dreizler, *Chem. Phys.* **1997**, *218*, 267-275.
- [32] J. Ross, *Molecular Beams*, John Wiley & Sons, New York, **1966**.
- [33] C. Tanjaroon, W. Jager, *J. Chem. Phys.* **2007**, *127*.
- [34] A. Maris, W. Caminati, P. G. Favero, *Chem. Commun.* **1998**, 2625-2626.
- [35] B. Velino, W. Caminati, *J. Mol. Spectrosc.* **2008**, *251*, 176-179.
- [36] T. D. Klots, T. Emilsson, R. S. Ruoff, H. S. Gutowsky, *J. Phys. Chem.* **1989**, *93*, 1255-1261.
- [37] R. M. Spycher, D. Petitprez, F. L. Bettens, A. Bauder, *J. Phys. Chem.* **1994**, *98*, 11863-11869.
- [38] S. Melandri, G. Maccaferri, A. Maris, A. Millemaggi, W. Caminati, P. G. Favero, *Chem. Phys. Lett.* **1996**, *261*, 267-271.
- [39] S. Y. Tang, L. Evangelisti, B. Velino, W. Caminati, *J. Chem. Phys.* **2008**, *129*.
- [40] A. Maris, W. Caminati, *J. Chem. Phys.* **2003**, *118*, 1649-1652.
- [41] P. Ottaviani, A. Maris, W. Caminati, Y. Tatamitani, Y. Suzuki, T. Ogata, J. L. Alonso, *Chem. Phys. Lett.* **2002**, *361*, 341-348.
- [42] Y. Morita, N. Ohashi, Y. Kawashima, E. Hirota, *J. Chem. Phys.* **2006**, *124*.
- [43] A. Costantini, A. Lagana, F. Pirani, A. Maris, W. Caminati, *Lect. Notes. Comput. Sci.* **2005**, *3480*, 1046-1053.
- [44] A. Maris, P. Ottaviani, S. Melandri, W. Caminati, A. Costantini, A. Lagana, F. Pirani, *J. Mol. Spectrosc.* **2009**, *257*, 29-33.
- [45] B. Velino, S. Melandri, W. Caminati, *J. Phys. Chem. A* **2004**, *108*, 4224-4227.

References

- [46] L. B. Favero, B. Velino, A. Millemaggi, W. Caminati, *ChemPhysChem* **2003**, *4*, 881-884.
- [47] E. Arunan, G. R. Desiraju, R. A. Klein, J. Sadlej, S. Scheiner, I. Alkorta, D. C. Clary, R. H. Crabtree, J. J. Dannenberg, P. Hobza, H. G. Kjaergaard, A. C. Legon, B. Mennucci, D. J. Nesbitt, *Pure Appl. Chem.*, **2011**, *8*, 1619-1636.
- [48] in *The weak hydrogen bond in structural chemistry and biology*, Vol. IX (Ed.: G. R. S. Desiraju, T.), Oxford University Press, Oxford, **2001**.
- [49] S. N. Delanoye, W. A. Herrebout, B. J. van der Veken, *J. Am. Chem. Soc.* **2002**, *124*, 11854-11855.
- [50] E. Cubero, M. Orozco, P. Hobza, F. J. Luque, *J. Phys. Chem. A* **1999**, *103*, 6394-6401.
- [51] P. Hobza, Z. Havlas, *Chem. Rev.* **2000**, *100*, 4253-4264.
- [52] G. R. Desiraju, P. S. Kloo, A. C. Legon, R. Marquardt, P. Metrangolo, P. Politzer, G. Resnati, K. Rissanen, *Pure Appl. Chem.* **2013**, *85*, 1711-1713.
- [53] P. Metrangolo, G. Resnati, T. Pilati, R. Liantonio, F. Meyer, *J. Polym. Sci., Part A: Polym. Chem.* **2007**, *45*, 1-15.
- [54] P. Politzer, P. Lane, M. Concha, Y. Ma, J. Murray, *J. Mol. Model.* **2007**, *13*, 305-311.
- [55] P. Metrangolo, G. Resnati, *Science* **2008**, *321*, 918-919.
- [56] D. Braga, G. R. Desiraju, J. S. Miller, A. G. Orpen, S. L. Price, *CrystEngComm.* **2002**, *4*, 500-509.
- [57] D. Hauchecorne, R. Szostak, W. A. Herrebout, B. J. van der Veken, *ChemPhysChem* **2009**, *10*, 2105-2115.
- [58] A. C. Legon, *Angew. Chem. Int. Ed.* **1999**, *38*, 2686-2714.
- [59] A. C. Legon, *Phys. Chem. Chem. Phys.* **2010**, *12*, 7736-7747.
- [60] E. Vohringer-Martinez, B. Hansmann, H. Hernandez-Soto, J. S. Francisco, J. Troe, B. Abel, *Science* **2007**, *315*, 497-501.
- [61] M. L. Chabinyc, S. L. Craig, C. K. Regan, J. I. Brauman, *Science* **1998**, *279*, 1882-1886.
- [62] B. C. Garrett, *Science* **2004**, *303*, 1146-1147.
- [63] M. J. Tait, F. Franks, *Nature* **1971**, *230*, 91-94.
- [64] W. Caminati, A. Dell'Erba, S. Melandri, P. G. Favero, *J. Am. Chem. Soc.* **1998**, *120*, 5555-5558.
- [65] U. Spoerel, W. Stahl, W. Caminati, P. G. Favero, *Chem-Eur. J.* **1998**, *4*, 1974-1981.
- [66] P. Ottaviani, M. Giuliano, B. Velino, W. Caminati, *Chem-Eur. J.* **2004**, *10*, 538-543.
- [67] W. Caminati, P. Moreschini, I. Rossi, P. G. Favero, *J. Am. Chem. Soc.* **1998**, *120*, 11144-11148.
- [68] W. Caminati, A. Dell'Erba, G. Maccaferri, P. G. Favero, *J. Am. Chem. Soc.* **1998**, *120*, 2616-2621.
- [69] W. Caminati, L. B. Favero, P. G. Favero, A. Maris, S. Melandri, *Angew. Chem. Int. Ed.* **1998**, *37*, 792-795.
- [70] W. Caminati, P. Moreschini, P. G. Favero, *J. Phys. Chem. A* **1998**, *102*, 8097-8100.
- [71] S. Melandri, M. E. Sanz, W. Caminati, P. G. Favero, Z. Kisiel, *J. Am. Chem. Soc.* **1998**, *120*, 11504-11509.
- [72] A. R. Conrad, N. H. Teumelsan, P. E. Wang, M. J. Tubergen, *J. Phys. Chem. A* **2010**, *114*, 336-342.
- [73] S. Melandri, A. Maris, P. G. Favero, W. Caminati, *Chem. Phys.* **2002**, *283*, 185-192.
- [74] S. Blanco, J. C. Lopez, J. L. Alonso, P. Ottaviani, W. Caminati, *J. Chem. Phys.* **2003**, *119*, 880-886.
- [75] S. Blanco, J. C. Lopez, A. Lesarri, J. L. Alonso, *J. Am. Chem. Soc.* **2006**, *128*, 12111-12121.
- [76] J. L. Alonso, E. J. Cocinero, A. Lesarri, M. E. Sanz, J. C. Lopez, *Angew. Chem. Int. Ed.* **2006**, *45*, 3471-3474.
- [77] W. Caminati, S. Melandri, A. Maris, P. Ottaviani, *Angew. Chem. Int. Ed.* **2006**, *45*, 2438-2442.
- [78] G. Feng, L. Evangelisti, L. B. Favero, J. U. Grabow, Z. N. Xia, W. Caminati, *Phys. Chem. Chem. Phys.* **2011**, *13*, 14092-14096.

References

- [79] W. Caminati, S. Melandri, I. Rossi, P. G. Favero, *J. Am. Chem. Soc.* **1999**, *121*, 10098-10101.
- [80] W. Caminati, S. Melandri, M. Schnell, D. Banser, J. U. Grabow, J. L. Alonso, *J. Mol. Struct.* **2005**, *742*, 87-90.
- [81] W. Caminati, A. Maris, A. Dell'Erba, P. G. Favero, *Angew. Chem. Int. Ed.* **2006**, *45*, 6711-6714.
- [82] L. Evangelisti, G. Feng, P. Ecija, E. J. Cocinero, F. Castano, W. Caminati, *Angew. Chem. Int. Ed.* **2011**, *50*, 7807-7810.
- [83] Q. Gou, G. Feng, L. Evangelisti, W. Caminati, *Angew. Chem. Int. Ed.* **2013**, *52*, 11888-11891.
- [84] Q. Gou, G. Feng, L. Evangelisti, M. Vallejo - López, L. Spada, A. Lesarri, E. J. Cocinero, W. Caminati, *Chem.-Eur. J.* **2014**, *20*, 1980-1984.
- [85] Q. Gou, L. Spada, M. Vallejo López, L. Kang, S. E. Novick, W. Caminati, *J. Phys. Chem. A* **2014**, *118*, 1047-1051.
- [86] A. Reyes, L. Fomina, L. Rumsh, S. Fomine, *Int. J. Quantum Chem.* **2005**, *104*, 335-341.
- [87] I. Rozas, I. Alkorta, J. Elguero, *J. Phys. Chem. A* **1997**, *101*, 9457-9463.
- [88] H. S. Gutowsky, T. Emilsson, E. Arunan, *J. Chem. Phys.* **1993**, *99*, 4883-4893.
- [89] B. R. Prasad, M. S. Krishnan, E. Arunan, *J. Mol. Spectrosc.* **2005**, *232*, 308-314.
- [90] M. Egli, S. Sarkhel, *Acc. Chem. Res.* **2007**, *40*, 197-205.
- [91] J. P. Gullivan, D. A. Dougherty, *Org. Lett.* **1999**, *1*, 103-105.
- [92] K. I. Peterson, W. Klemperer, *J. Chem. Phys.* **1984**, *81*, 3842.
- [93] A. M. Andrews, R. L. Kuczjowski, *J. Chem. Phys.* **1993**, *98*, 791.
- [94] K. W. Hillig II, E. R. Bittner, R. L. Kuczjowski, *J. Mol. Spectrosc.* **1988**, *148*, 371.
- [95] H. M. Pickett, *J. Mol. Spectrosc.* **1991**, *148*, 371-377.
- [96] J. S. Murray, P. Lane, T. Clark, K. E. Riley, P. Politzer, *J. Mol. Model.* **2012**, *18*, 541-548.
- [97] N. P. Franks, W. R. Lieb, *Nature* **1994**, *367*, 607-614.
- [98] A. S. Evers, C. M. Crowder, J. R. Balsler, *Foodman & Gilman's The Pharmacological Basis of Therapeutics, 11th ed*, McGraw-Hill, New York, **2006**.
- [99] A. A. Bhattacharya, S. Curry, N. P. Franks, *J. Biol. Chem.* **2000**, *275*, 38731-38738.
- [100] A. Lesarri, A. Vega-Toribio, R. D. Suenram, D. J. Brugh, D. Nori-Shargh, J. E. Boggs, J.-U. Grabow, *Phys. Chem. Chem. Phys.* **2011**, *13*, 6610-6618.
- [101] J. Murray, P. Lane, T. Clark, P. Politzer, *J. Mol. Model.* **2007**, *13*, 1033-1038.
- [102] M. Onda, A. Toda, S. Mori, I. Yamaguchi, *J. Mol. Struct.* **1986**, *144*, 47-51.
- [103] D. Federsel, A. Herrmann, D. Christen, S. Sander, H. Willner, H. Oberhammer, *J. Mol. Struct.* **2001**, *567-568*, 127-136.
- [104] R. Ruoff, T. Klots, T. Emilsson, H. Gutowsky, *J. Chem. Phys.* **1990**, *93*, 3142.
- [105] B. M. Giuliano, S. Melandri, A. Maris, L. B. Favero, W. Caminati, *Angew. Chem. Int. Ed.* **2009**, *48*, 1102-1105.
- [106] B. M. Giuliano, A. Maris, S. Melandri, W. Caminati, *J. Phys. Chem. A* **2009**, *113*, 14277-14280.
- [107] K. Brendel, H. Mäder, Y. Xu, W. Jäger, *J. Mol. Spectrosc.* **2011**, *268*, 47-52.
- [108] L. Evangelisti, G. Feng, Q. Gou, G. Guidetti, W. Caminati, *Spectrochim. Acta Part A* **2014**, <http://dx.doi.org/10.1016/j.saa.2013.08.116>.
- [109] L. Evangelisti, G. Feng, Q. Gou, G. Guidetti, W. Caminati, *J. Mol. Spectrosc.* **2012**, *282*, 39-41.
- [110] V. Vaida, H. G. Kjaergaard, K. J. Feierabend, *Inter. Rev. Phys. Chem.* **2003**, *22*, 203-219.
- [111] Q. Gou, G. Feng, L. Evangelisti, M. Vallejo-Lopez, A. Lesarri, E. J. Cocinero, W. Caminati, *Phys. Chem. Chem.*

References

- Phys.* **2013**, *15*, 6714-6718.
- [112] G. Feng, L. Evangelisti, N. Gasparini, W. Caminati, *Chem-Eur J* **2012**, *18*, 1364-1368.
- [113] A. Maris, L. B. Favero, B. Velino, W. Caminati, *J. Phys. Chem. A* **2013**, *117*, 11289-11292.
- [114] Q. Gou, G. Feng, L. Evangelisti, D. Loru, J. L. Alonso, J. C. López, W. Caminati, *J. Phys. Chem. A* **2013**, *117*, 13531-13534.
- [115] W. Caminati, S. Melandri, P. Moreschini, P. G. Favero, *Angew. Chem. Int. Ed.* **1999**, *38*, 2924-2925.
- [116] S. Blanco, S. Melandri, P. Ottaviani, W. Caminati, *J. Am. Chem. Soc.* **2007**, *129*, 2700-2703.
- [117] G. Feng, L. Evangelisti, I. Cacelli, L. Carbonaro, G. Prampolini, W. Caminati, *Chem Commun* **2014**, *50*, 171-173.
- [118] W. Caminati, J. C. Lopez, J. L. Alonso, J. U. Grabow, *Angew. Chem. Int. Ed.* **2005**, *44*, 3840-3844.
- [119] C. L. Christenholz, D. A. Obenchain, S. A. Peebles, R. A. Peebles, *J. Mol. Spectrosc.* **2012**, *280*, 61-67.
- [120] Z. Kisiel, L. Pszczolkowski, W. Caminati, P. G. Favero, *J. Chem. Phys.* **1996**, *105*, 1778-1785.
- [121] Z. Kisiel, L. Pszczolkowski, L. B. Favero, W. Caminati, *J. Mol. Spectrosc.* **1998**, *189*, 283-290.
- [122] Z. Kisiel, E. Białkowska-Jaworska, L. Pszczółkowski, *J. Chem. Phys.* **1998**, *109*, 10263-10272.
- [123] PROSPE, <http://www.ifpan.edu.pl/~kisiel/prospe.htm>.
- [124] Z. Kisiel, *Spectroscopy from space*, Kluwer Academic Publishers, Dordrecht, **2001**.
- [125] L. Evangelisti, G. Feng, Q. Gou, J.-U. Grabow, W. Caminati, *J. Phys. Chem. A* **2014**.
- [126] D. Hauchecorne, W. A. Herrebout, *J. Phys. Chem. A* **2013**, *117*, 11548-11557.
- [127] D. R. Herschbach, *J. Chem. Phys.* **1959**, *31*, 91-108.
- [128] S. Blanco, J. C. Lopez, A. Lesarri, W. Caminati, J. L. Alonso, *ChemPhysChem* **2004**, *5*, 1779-1782.
- [129] M. M. Serafin, S. A. Peebles, *J. Phys. Chem. A* **2008**, *112*, 12616-12621.
- [130] J. L. Alonso, S. Antolinez, S. Blanco, A. Lesarri, J. C. Lopez, W. Caminati, *J. Am. Chem. Soc.* **2004**, *126*, 3244-3249.
- [131] P. Ottaviani, W. Caminati, L. B. Favero, S. Blanco, J. C. Lopez, J. L. Alonso, *Chem-Eur J* **2006**, *12*, 915-920.
- [132] L. B. Favero, B. M. Giuliano, S. Melandri, A. Maris, P. Ottaviani, B. Velino, W. Caminati, *J. Phys. Chem. A* **2005**, *109*, 7402-7404.
- [133] A. C. Lopez, W. Caminati, J. L. Alonso, *Angew. Chem. Int. Ed.* **2006**, *45*, 290-293.
- [134] E. Hirota, *J. Mol. Spectrosc.* **1978**, *71*.
- [135] C. C. Costain, G. P. Srivastava, *J. Chem. Phys.* **1961**, *35*, 1903-1904.
- [136] G. Feng, Q. Gou, L. Evangelisti, Z. N. Xia, W. Caminati, *Phys. Chem. Chem. Phys.* **2013**, *15*, 2917-2922.
- [137] R. E. Penn, R. J. Olsen, *J. Mol. Spectrosc.* **1976**, *62*, 423-428.
- [138] S. Y. Tang, I. Majerz, W. Caminati, *Phys. Chem. Chem. Phys.* **2011**, *13*, 9137-9139.
- [139] M. S. Snow, B. J. Howard, L. Evangelisti, W. Caminati, *J. Phys. Chem. A* **2011**, *115*, 47-51.
- [140] L. Evangelisti, G. Feng, R. Rizzato, W. Caminati, *ChemPhysChem* **2011**, *12*, 1916-1920.
- [141] L. Evangelisti, F. Pesci, W. Caminati, *J. Phys. Chem. A* **2011**, *115*, 9510-9513.
- [142] L. Evangelisti, W. Caminati, *Chem. Phys. Lett.* **2011**, *514*, 244-246.
- [143] L. Evangelisti, W. Caminati, *J. Mol. Spectrosc.* **2011**, *270*, 120-122.
- [144] W. H. Kirchhoff, D. R. Lide, *J. Chem. Phys.* **1965**, *43*, 2203-2212.
- [145] S. E. Forest, R. L. Kuczkowski, *Chem. Phys. Lett.* **1994**, *218*, 349-352.
- [146] R. Kempe, *Eur. J. Inorgan. Chem.* **2003**, *2003*, 791-803.

References

- [147] J. Ashmore, J. C. Green, M. L. Green, M. L. Smith, C. Mehnert, E. J. Wucherer, *J. Chem. Soc., Dalton Trans.* **1995**, 1873-1877.
- [148] S. Haq, D. King, *J. Phys. Chem.* **1996**, *100*, 16957-16965.
- [149] S. A. Krasnokutski, D.-S. Yang, *J. Chem. Phys.* **2009**, *130*, 134313.
- [150] L. Evangelisti, L. B. Favero, B. M. Giuliano, S. Y. Tang, S. Melandri, W. Caminati, *J. Phys. Chem. A* **2009**, *113*, 14227-14230.
- [151] S. Melandri, B. M. Giuliano, A. Maris, L. Evangelisti, B. Velino, W. Caminati, *ChemPhysChem* **2009**, *10*, 2503-2507.
- [152] R. P. A. Bettens, A. Bauder, *J. Chem. Phys.* **1995**, *102*, 1501-1509.
- [153] J. L. Doran, B. Hon, K. R. Leopold, *J Mol Struct* **2012**, *1019*, 191-195.
- [154] S. W. Hunt, K. R. Leopold, *J. Phys. Chem. A* **2001**, *105*, 5498-5506.
- [155] L. B. Favero, B. M. Giuliano, A. Maris, S. Melandri, P. Ottaviani, B. Velino, W. Caminati, *Chem-Eur J* **2010**, *16*, 1761-1764.
- [156] L. Spada, Q. Gou, M. Vallejo-Lopez, A. Lesarri, E. J. Cocinero, W. Caminati, *Phys. Chem. Chem. Phys.* **2014**, *16*, 2149-2153.
- [157] M. Vallejo-López, L. Spada, Q. Gou, A. Lesarri, E. J. Cocinero, W. Caminati, *Chem. Phys. Lett.* **2014**, *591*, 216-219.
- [158] W. Caminati, P. G. Favero, S. Melandri, R. Meyer, *Chem. Phys. Lett.* **1997**, *268*, 393-400.
- [159] R. Suenram, G. Fraser, F. Lovas, Y. Kawashima, *J. Chem. Phys.* **1994**, *101*, 7230-7240.
- [160] L. Dore, R. Cohen, C. Schmuttenmaer, K. Busarow, M. Elrod, J. Loeser, R. Saykally, *J. Chem. Phys.* **1994**, *100*, 863.
- [161] A. Legon, B. Roberts, A. Wallwork, *Chem Phys Lett* **1990**, *173*, 107-114.
- [162] A. Legon, A. Wallwork, *J. Chem. Soc., Chem. Commun.* **1989**, 588-590.
- [163] Y. Ohshima, Y. Endo, *J. Chem. Phys.* **1990**, *93*, 6256.
- [164] J. P. I. Hearn, B. J. Howard, *Mol Phys* **2002**, *100*, 2679-2687.
- [165] A. R. Hight Walker, G. T. Fraser, R. D. Suenram, F. J. Lovas, *J. Chem. Phys.* **2000**, *113*, 2139-2144.
- [166] M. Meyer, *J Mol Spectrosc* **1979**, *76*, 266-300.
- [167] E. M. Bellott Jr, E. B. Wilson, *Tetrahedron* **1975**, *31*, 2896-2898.
- [168] V. V. Matylitsky, C. Riehn, M. F. Gelin, B. Brutschy, *J. Chem. Phys.* **2003**, *119*, 10553-10562.
- [169] R. Georges, M. Freytes, D. Hurtmans, I. Kleiner, J. Vander Auwera, M. Herman, *Chem. Phys.* **2004**, *305*, 187-196.
- [170] Z. Xue, M. A. Suhm, *J. Chem. Phys.* **2009**, *131*, -.
- [171] F. Madeja, M. Havenith, *J. Chem. Phys.* **2002**, *117*, 7162-7168.
- [172] M. Ortlieb, M. Havenith, *J. Phys. Chem. A* **2007**, *111*, 7355-7363.
- [173] A. Gutberlet, G. W. Schwaab, M. Havenith, *Chem. Phys.* **2008**, *343*, 158-167.
- [174] Ö. Birer, M. Havenith, *Ann. Rev. phys. Chem.* **2009**, *60*, 263-275.
- [175] I. Kalkman, C. Vu, M. Schmitt, W. L. Meerts, *ChemPhysChem* **2008**, *9*, 1788-1797.
- [176] L. Martinache, W. Kresa, M. Wegener, U. Vonmont, A. Bauder, *Chem. Phys.* **1990**, *148*, 129-140.
- [177] S. Antolínez, H. Dreizler, V. Storm, D. H. Sutter, J. L. Alonso, *Z. Naturforsch.* **1997**, *52a*, 803-806.
- [178] A. M. Daly, K. O. Douglass, L. C. Sarkozy, J. L. Neill, M. T. Muckle, D. P. Zaleski, B. H. Pate, S. G. Kukolich, *J. Chem. Phys.* **2011**, *135*, -.

References

- [179] M. C. D. Tayler, B. Ouyang, B. J. Howard, *J. Chem. Phys.* **2011**, *134*, -.
- [180] G. Feng, L. B. Favero, A. Maris, A. Vigorito, W. Caminati, R. Meyer, *J. Am. Chem. Soc.* **2012**, *134*, 19281-19286.
- [181] L. Evangelisti, P. Eciija, E. J. Cocinero, F. Castano, A. Lesarri, W. Caminati, R. Meyer, *J. Phys. Chem. Lett.* **2012**, *3*, 3770-3775.
- [182] Q. Gou, G. Feng, L. Evangelisti, W. Caminati, *J. Phys. Chem. A* **2013**, *117*, 13500-13503.
- [183] Q. Gou, G. Feng, L. Evangelisti, W. Caminati, *Chem. Phys. Lett.* **2014**, *591*, 301-305.
- [184] Q. Gou, G. Feng, L. Evangelisti, W. Caminati, *J. Phys. Chem. Lett.* **2013**, *4*, 2838-2842.
- [185] B. P. van Eijck, A. A. J. Maagdenberg, G. Janssen, T. J. van Goethem-Wiersma, *J. Mol. Spectrosc.* **1983**, *98*, 282-303.
- [186] G. Feng, Q. Gou, L. Evangelisti, W. Caminati, *Angew. Chem. Int. Ed.* **2013**.
- [187] B. P. Van Eijck, P. Brandts, J. P. M. Maas, *J. Mol. Struct.* **1978**, *44*, 1-13.
- [188] K. Bolton, D. G. Lister, J. Sheridan, *J. Chem. Soc., Perkin Trans. 2* **1974**, *70*, 113-123.
- [189] D. G. Melnik, S. Gopalakrishnan, T. A. Miller, F. C. De Lucia, *J. Chem. Phys.* **2003**, *118*, 3589-3599.
- [190] S. Melandri, J. C. Lopez, P. G. Favero, W. Caminati, J. L. Alonso, *Chem. Phys.* **1998**, *239*, 229-234.
- [191] Q. Gou, G. Feng, L. Evangelisti, A. Maris, M. Marchini, B. Velino, W. Caminati, *ChemPhysChem* **2012**, *13*, 221-225.
- [192] Z. Kisiel, *J. Phys. Chem.* **1991**, *95*, 7605-7612.
- [193] Z. Kisiel, P. W. Fowler, A. C. Legon, *J. Chem. Phys.* **1991**, *95*, 2283-2291.
- [194] S. Blanco, S. Melandri, A. Maris, W. Caminati, B. Velino, Z. Kisiel, *Phys. Chem. Chem. Phys.* **2003**, *5*, 1359-1364.
- [195] H. M. Pickett, *J. Chem. Phys.* **1972**, *56*, 1715-1723.
- [196] J. C. Lopez, J. L. Alonso, F. J. Lorenzo, V. M. Rayon, J. A. Sordo, *J. Chem. Phys.* **1999**, *111*, 6363-6374.
- [197] J. L. Alonso, J. C. Lopez, S. Blanco, A. Lesarri, F. J. Lorenzo, *J. Chem. Phys.* **2000**, *113*, 2760-2767.

Acknowledgement

First and foremost, I would like to show my deepest gratitude to my supervisor, Prof. Walther Caminati, a respectable, responsible and resourceful scholar. Without his enlightening instruction, impressive kindness and patience, I could not have completed this dissertation. His keen and vigorous academic activities enlighten me not only in this dissertation but also in my future study. The hospitality of Prof. Caminati and his family makes a foreign student like me to find a home from home in Bologna. I shall extend my thanks to every colleague who is or was working with me in this group, Prof. Sonia Melandri, Dr. Assimo Maris, Dr. Biagio Velino, Dr. Laura B. Favero, Dr. Luca Evangelisti, Dr. Gang Feng, Dr. Cristóbal Pérez, Ms. Montserrat Vallejo-López, Ms. Camilla Calabrese, Mr. Lorenzo Spada and Ms. Annalisa Vigorito, for all their kindness and help. I would also like to thank all the helps and suggestions from the other groups. I also wish to thank all my friends in Bologna, who bring me a lot of laughter, affection and courage. I'm grateful for the scholarship from China Scholarships Council (CSC). Last but for sure not least, many many thanks to all my family for their encouragement and support.

Qian Gou
January 2014

Appendices

Publications

1. Q. Gou, G. Feng, L. Evangelisti, A. Maris, M. Marcini, B. Velino, W. Caminati. Rotational Spectrum and Internal Dynamics of Tetrahydrofuran-Krypton. *ChemPhysChem* **2012**, *13*, 221-225.
2. L. Evangelisti, G. Feng, Q. Gou, W. Caminati. Rotational Spectrum of 2,5-Difluorobenzyl Alcohol. *J. Mol. Struct.* **2012**, *1023*, 15-17.
3. L. Evangelisti, G. Feng, Q. Gou, G. Gloria, W. Caminati. Orientation of The Water Moiety in CF₄-H₂O. *J. Mol. Spectrosc.* **2012**, *282*, 39-41.
4. L. Evangelisti, Q. Gou, L. Spada, G. Feng, W. Caminati. Conformational Analysis of 1,4-Butanediol: A Microwave Spectroscopy Study. *Chem. Phys. Lett.* **2013**, *556*, 55-58.
5. G. Feng, Q. Gou, L. Evangelisti, Z. Xia, W. Caminati. Conformational Equilibria in Carboxylic Acid Bimolecules: A Rotational Study of Acrylic Acid-Formic Acid. *Phys. Chem. Chem. Phys.* **2013**, *15*, 2917-2922.
6. Q. Gou, G. Feng, L. Evangelisti, M. Vallejo López, A. Lesarri, E. J. Cocinero, W. Caminati. Non Bonding Interactions and internal dynamics in CH₂F₂···H₂CO. A rotational and model calculations study. *Phys. Chem. Chem. Phys.* **2013**, *15*, 6714-6718.
7. Q. Gou, G. Feng, L. Evangelisti, W. Caminati. Conformational Equilibria in Bimolecules of Carboxylic Acids: A Rotational Study of Fluoroacetic Acid–Acrylic Acid. *J. Phys. Chem. Lett.* **2013**, *4*, 2838–2842.
8. L. Evangelisti, Q. Gou, G. Feng, W. Caminati. Effects of ring fluorination on the transient atropisomerism of benzyl alcohol: the rotational spectrum of 3,4-difluorobenzyl alcohol. *Mol.*

- Phys.* **2013**, *111*, 1994-1998.
9. Q. Gou, G. Feng, L. Evangelisti, W. Caminati. Lone-Pair $\cdots\pi$ Interaction: A Rotational Study of the Chlorotrifluoroethylene–Water Adduct, *Angew. Chem. Int. Ed.* **2013**, *52*, 11888-11891.
 10. Q. Gou, G. Feng, L. Evangelisti, W. Caminati. A Rotational Study of *cis* and *trans* Acrylic Acid-Trifluoroacetic Acid. *J. Phys. Chem. A* **2013**, *117*, 13500-13503.
 11. Q. Gou, G. Feng, L. Evangelisti, D. Loru, J. L. Alonso, J. C. López, W. Caminati. Ubbelohde Effect within Weak C–H $\cdots\pi$ Hydrogen Bonds: the Rotational Spectrum of Benzene–DCF₃. *J. Phys. Chem. A* **2013**, *117*, 13531-13534.
 12. M. Vallejo-López, L. Spada, Q. Gou, A. Lesarri, E. J. Cocinero, W. Caminati. Interactions between freons and aromatic molecules: the rotational spectrum of pyridine-difluoromethane, *Chem. Phys. Lett.* **2014**, *591*, 216-219.
 13. Q. Gou, G. Feng, L. Evangelisti, W. Caminati. Conformers of dimers of carboxylic acids in the gas phase: A rotational study of difluoroacetic acid-formic acid. *Chem. Phys. Lett.* **2014**, *591*, 301-305.
 14. L. Spada, Q. Gou, M. Vallejo-López, A. Lesarri, E. J. Cocinero, W. Caminati. Weak C–H \cdots N and C–H \cdots F hydrogen bonds and internal rotation in pyridine-CH₃F. *Phys. Chem. Chem. Phys.* **2014**, *16*, 2149-2153.
 15. G. Feng, Q. Gou, L. Evangelisti, W. Caminati. Frontiers in Rotational Spectroscopy: Shapes and Tunneling Dynamics of the Four Conformers of the Acrylic Acid-Difluoroacetic Acid Addct. *Angew. Chem. Int. Ed.* **2014**, *53*, 530-534.
 16. L. Evangelisti, G. Feng, Q. Gou, J.-U. Grabow, W. Caminati. Halogen Bond and Free Internal Rotation: The Microwave Spectrum of CF₃Cl-Dimethylether. *J. Phys. Chem. A* **2014**, *118*, 579–582.
 17. Q. Gou, G. Feng, L. Evangelisti, W. Caminati. Interaction between Freons and Amines: The C–H \cdots N Weak Hydrogen Bond in Quinuclidine–Trifluoromethane. *J. Phys. Chem. A* **2014**, *118*, 737-740.
 18. Q. Gou, G. Feng, L. Evangelisti, M. Vallejo-López, L. Spada, A. Lesarri, E. J. Cocinero, W. Caminati. How water interacts with halogenated anesthetics: the rotational spectrum of isoflurane-water. *Chem. Eur. J.* **2014**, *20*, 1980-1984.
 19. L. Kang, S. E. Novick, Q. Gou, L. Spada, M. Vallejo-López, W. Caminati. The shape of

- trifluoromethoxybenzene. *J. Mol. Spectrosc.* **2014**, 297, 32-34.
20. Q. Gou, L. Spada, M. Vallejo-López, L. Kang, S. E. Novick, W. Caminati. Fluorination Effects on the Shapes of Complexes of Water with Ethers: A Rotational Study of Trifluoroanisole-Water. *J. Phys. Chem. A* **2014**, 118, 1047-1051.
21. L. Evangelisti, G. Feng, Q. Gou, G. Guidetti, W. Caminati. Average orientation of water in $\text{CH}_2\text{F}_2 \cdot \text{H}_2\text{O}$ from the ^{17}O quadrupole effects in the rotational spectrum of $\text{CH}_2\text{F}_2 \cdot \text{H}_2^{17}\text{O}$, *Spectrochim. Acta Part A* **2014**, <http://dx.doi.org/10.1016/j.saa.2013.08.116>.
22. Q. Gou, L. Spada, M. Vallejo-López, Z. Kisiel, W. Caminati. Interactions between freons: a rotational study of $\text{CH}_2\text{F}_2\text{-CH}_2\text{Cl}_2$, *Chem. Asian. J.*, DOI: 10.1002/asia.201301722.
23. Q. Gou, L. Spada, M. Vallejo-López, A. Lesarri, E. J. Cocinero, W. Caminati. Interactions between alkanes and aromatic molecules: a rotational study of pyridine – methane. *Phys. Chem. Chem. Phys.*, DOI: 10.1039/C4CP00204K.
24. Q. Gou, L. Evangelisti, G. Feng, G. Guidetti, W. Caminati. Effective orientation of water in 1,4-dioxane ·water: the rotational spectrum of the H_2^{17}O isotopologue. *Mol. Phys.*, accepted.
25. Q. Gou, L. Spada, E. J. Cocinero, W. Caminati. Halogen-halogen links and internal dynamics in adducts of freons, submitted.

Academic Congresses

1. XXIV CONGRESSO NAZIONALE DELLA SOCIETÀ CHIMICA ITALIANA, 11-16, September, 2011, Lecce, Puglia, Italy. I presented an poster contribution on “**ROTATIONAL SPECTRUM AND INTERNAL DYNAMICS OF TETRAHYDROFURAN-KRYPTON**”;
2. IMAMPC2012 INTERNATIONAL MEETING ON ATOMIC AND MOLECULAR PHYSICS AND CHEMISTRY, 12-14 September 2012, Scuola Normale Superiore, Pisa, Italy. I presented an oral contribution on “**FOURIER TRANSFORM MICROWAVE STUDIES ON DIMERS OF CARBOXYLIC ACIDS**”;
3. THEORY, EXPERIMENTS AND MODELLING OF CHEMICAL PROCESSES, DYNAMICS AND MOLECULAR INTERACTIONS (INTERNATIONAL CONFERENCE), 29 November 2012, Sala Ulisse, Accademia delle Scienze, Bologna, Italy.

- I presented an oral contribution on “**WEAK HYDROGEN BOND: REVEALED BY ROTATIONAL SPECTROSCOPY**”;
4. XII GIORNATA DI CHIMICA DELL'EMILIA ROMAGNA, 17 December 2012, Sala Acquario, Polo Chimico Bio Medico, Unicersit à di Ferrara, Ferrara, Italy. I presented an oral contribution on “**FOURIER TRANSFORM MICROWAVE SPECTRA OF SEVERAL ISOTOPOLOGUES OF ISOFLURANE-WATER COMPLEX**”.
 5. INTERNATIONAL SYMPOSIUM ON MOLECULAR SPECTROSCOPY (68TH MEETING), 17th-21st June, 2013. The Ohio state university, Columbus, Ohio, USA. I presented an oral contribution on “**ROTATIONAL SPECTRA OF THE ADDUCTS OF FORMALDEHYDE WITH FREONS**”.
 6. CHIRALITÀ E AUTOASSEMBLAGGIO: DALLE MOLECOLE AI SISTEMI COMPLESSI. GIORNATA SCIENTIFICA IN RICORDO DEL PROFESSOR GIAN PIERO SPADA. I presented an oral contribution on “**NON-COVALENT INTERACTIONS: REVEALED BY ROTATIONAL SPECTROSCOPY**”.

Award

SPADA AWARD: To whom that his/her researches have distinguished themselves for productivity, innovation and scientific maturity.